REPEATED NUCLEATION OF PRECIPITATES ON DISLOCATIONS IN ALUMINUM-COPPER

By

THOMAS JEFFREY HEADLEY

A DISSERTATION PRESENTED TO THE GRADUATE COUNCIL OF
THE UNIVERSITY OF FLORIDA
IN PARTIAL FULFILLMENT OF THE REQUIREMENTS FOR THE
DEGREE OF DOCTOR OF PHILOSOPHY

UNIVERSITY OF FLORIDA

1974

Dedicated to my wife, Lynn

ACKNOWLEDGMENTS

The author is deeply indebted to his Advisory Chairman, Dr. John J. Hren, who contributed unselfishly of his time, and provided advice, encouragement, and stimulating discussion during the course of this research. He is indebted to his advisory committee for assistance, and to Dr. R. T. DeHoff for many helpful discussions.

Thanks are due to Dr. R. W. Gould for providing alloy materials; to the Sandia Corporation, Albuquerque, New Mexico, for chemical analysis; to the Japan Electron Optics Laboratory, Boston, Massachusetts, for use of the JEOL 100B Electron Microscope; to Mr. E. J. Jenkins for assistance in the laboratory; to Mr. Paul Smith for assistance in the darkroom; and to Mrs. Elizabeth Godey for typing this manuscript.

The author's wife, Lynn, is acknowledged for her constant inspiration and support. His mother is acknowledged for her lifelong encouragement.

Finally, the financial support of the Atomic Energy Commission was deeply appreciated.

TABLE OF CONTENTS

TABLE OF CONTENTS - Continued

Abstract of Dissertation Presented to the Graduate Council of the University of Florida in Partial Fulfillment of the Requirements for the Degree of Doctor of Philosophy

REPEATED NUCLEATION OF PRECIPITATES ON DISLOCATIONS IN ALUMINUM-COPPER

By

Thomas Jeffrey Headley

August, 1974

Chairman: John J. Hren
Major Department: Materials Science and Engineering

Results are presented of an investigation of a newly discovered propagation mechanism for the $\alpha \rightarrow \theta'$ transformation in Al-Cu: repeated nucleation on climbing dislocations. It was found that during the quench, dislocations are generated and climb by the annihilation of quenched-in vacancies. Densely populated colonies of θ' precipitates nucleate in the stress fields of the climbing dislocations. In this way, the distribution of the entire volume fraction of θ' is established during the quench.

The climbing dislocations were found to be a/2<110> type, falling into three categories according to origin: (1) pure-edge loops on {110} habits nucleated at dislocation climb sources, (2) glide dislocations initially on {111}, and (3) pure-edge loops on {110} formed by the collapse of vacancy clusters.

The effects of solution treatment temperature, aging temperature, quench rate, and solute concentration on the

repeated nucleation process were determined. It was found that repeated nucleation occurs during quenching from all temperatures within the solid solution range, to all temperatures in the range room temperature to 300°C. It occurs during slow and fast quenching as well, but does not occur in alloys with concentration ≤ 1 wt.% Cu.

Mechanisms of repeated nucleation proposed earlier for other alloys are not applicable to Al-Cu. Dislocation climb and precipitation were found to be independently controlled processes. The relevant criteria for repeated nucleation in this system are:

(1) a precipitate phase which nucleates easily on dislocations,

(2) a source of dislocations during quenching,

(3) a driving force for dislocation climb which is independent of the precipitation process, and

(4) a climb rate slow enough to permit nucleation but rapid enough to avoid pinning.

It is suggested that pipe diffusion along the moving dislocation provides the necessary solute enhancement for successive nucleations.

CHAPTER 1

INTRODUCTION

Some of the most important strengthening mechanisms in alloys result from the precipitation of a second solid phase from a supersaturated solid solution. The age-hardening phenomenon in many aluminum alloys is a well-known example. A precipitation reaction is a nucleation-and-growth transformation. Hence, the rate of the reaction is dependent upon (1) the nucleation rate of precipitates, and (2) the rate of their growth. If either or both of these rates is low the reaction rate will be low. Consequently, it is important to understand how and where precipitate reactions nucleate, apart from the problem of growth. Much is known about the kinetics of growth, but not about nucleation, especially heterogeneous nucleation.

Precipitate reactions nucleate either homogeneously or heterogeneously within the matrix. If both the volume misfit and interfacial energy between precipitate and matrix are small, the reaction can nucleate homogeneously at random sites throughout the lattice. Homogeneous nucleation is known to occur in only a few alloy systems, e.g., the precipitation of cobalt particles from dilute solutions of cobalt in copper (Servi and Turnbull, 1966). In most

precipitate reactions, either the volume misfit or interfacial energy, or both, is sufficiently large so that only heterogeneous nucleation occurs at preferred sites within the lattice. These sites are lattice defects such as grain boundaries, dislocations, stacking faults, point defects, and other particles. Presumably, a portion of the energy associated with the defect is supplied to help reduce the activation energy for formation of the critical nucleus, resulting in a nucleation event which is otherwise energetically unfavorable.

In the case of heterogeneous nucleation at dislocations, it is the dislocation strain energy in the matrix which helps overcome the barrier to nucleation. If the misfit strain caused by the precipitate is large, dislocation-nucleation may be the only method of decomposition of the supersaturated solid solution. Kelly and Nicholson (1963) and Nicholson (1970), have given excellent reviews of the evidence for nucleation on dislocations in a number of alloy systems. A well-known example of heterogeneous nucleation on dislocations is that of the metastable θ' phase in Al-Cu alloys.

For a precipitate reaction which is dislocation-nucleated, the following problem arises whenever the initial dislocation density is low, as is often the case following quenching. How can the reaction propagate once the available nucleation sites on dislocations have been saturated, i.e., what is the mechanism for propagation of the nucleation? Currently there are two known mechanisms whereby the reaction

may propagate. One mechanism is autocatalytic nucleation, first proposed by Lorimer (1968), and similar to the way in which martensite propagates. The initial precipitates nucleate on dislocations and grow into the matrix. In so doing, they generate stress fields in the matrix which aid in the nucleation of new precipitates. Thus, the reaction propagates in bands spreading out from the original dislocations to fill the lattice. Lorimer showed that the $\alpha \rightarrow \theta'$ reaction in Al-Cu could propagate by autocatalytic nucleation. Before the present work, this was the only reported mechanism whereby the θ' reaction propagates from a low initial dislocation density.

Secondly, nucleation of the reaction can be propagated if the dislocation can somehow free itself from the initial precipitates and move away under a chemical or mechanical stress. It then presents fresh sites for the nucleation of more precipitates. Nicholson (1970) was the first to use the term "repeated precipitation on dislocations" to describe this process. Repeated nucleation on climbing dislocations was first observed for carbide precipitation in austenitic stainless steel (Silcock and Tunstall, 1964). Since that time it has been reported for only a few other alloy systems. Very recently, Nes (1974) published a paper on the mechanism for repeated precipitation on dislocations which he implied was universal with the statement that his model "can be applied to repeated precipitation (or colony growth) in any alloy system."

During experiments in which Al-Cu alloys were quenched directly to aging temperatures, this author observed that precipitation of the θ' phase occurred exclusively by repeated nucleation on climbing dislocations. Further examination revealed that the repeated nucleation in this system could not be explained by the mechanism proposed by Nes (1974). Therefore, the primary purpose of this research was to establish the mechanism for repeated nucleation of θ' on climbing dislocations in Al-Cu, and in so doing, to determine if there are aspects of the mechanism which might apply to precipitation in other alloy systems.

CHAPTER 2

REVIEW OF THEORY AND PREVIOUS WORK

2.1. Theory of Heterogeneous Nucleation at Dislocations

Nucleation theory employs the concepts of a critical nucleus and an activation energy for nucleation. An assumption of the theory is that random thermal fluctuations lead to the formation of small embryos of the transformed phase. Embryos having a size and shape smaller than some critical size and shape will on the average disappear, and those with a larger size will grow and become stable. This critical size and shape is defined as the critical nucleus. The activation energy is the minimum energy barrier which must be overcome before nucleation can occur and turns out to be the free energy of the critical nucleus. This energy barrier is a maximum with respect to size and a minimum with respect to all other variables. The importance of the free energy of the critical nucleus can be recognized from its appearance in the equation for the steady state nucleation rate, which is written in general form as

$$J = Z\beta \frac{N_s}{c_s} \exp\left[\frac{-\Delta G^*}{kT}\right] \tag{2.1}$$

where J = nucleation rate,

Z = the Zeldovich factor,

β = frequency which atoms add to the nucleus,

N_s = number of available nucleation sites,

c_s = composition of the nucleus,

ΔG^* = free energy of the critical nucleus,

k = the Boltzmann constant, and

T = temperature.

ΔG^* has the form

$$\Delta G^* = \frac{K(\sigma_{surf})^3}{(\Delta G^{drive})^2} \tag{2.2}$$

where K = a shape factor,

σ_{surf} = particle/matrix interfacial energy, and

ΔG^{drive} = driving force for the reaction.

For homogeneous nucleation, N_s is high assuring reasonable nucleation rates. For heterogeneous nucleation, N_s is low and the nucleation rate is usually dominated by the exponential dependence on the free energy of the critical nucleus.

For precipitation in solids, there is a chemical free energy change per unit volume tending to drive the transformation to the new phase. If the atomic volumes in the matrix and particle are different, there is a misfit strain energy associated with formation of the new phase. Thus the free energy of the critical nucleus can be written

$$\Delta G^* = \frac{K(\sigma_{surf})^3}{[\Delta G(chem)+\Delta G(strain)]^2} .$$

$\Delta G(chem)$ is negative whereas σ_{surf} and $\Delta G(strain)$ are positive. For a given reaction, $\Delta G(chem)$ can be calculated from thermodynamic parameters by the method of Aaronson et al. (1970). Attempts have been made to calculate σ_{surf} from atomic bond models, but in general, the binding energies are unknown. In the absence of a proven model, σ_{surf} is often taken as the measured bulk interfacial energy. The validity of this approximation is questionable. $\Delta G(strain)$ can be calculated by the method of Eshelby (1957,1961).

If a nucleus forms in the stress field of a dislocation, an additional energy term arises from the interaction of the displacement field of the precipitate with the stress field of the dislocation. We can then write ΔG^* as

$$\Delta G^* = \frac{K(\sigma_{surf})^3}{[\Delta G(chem)+\Delta G(strain)+\Delta G(int)]^2} .$$

$\Delta G(int)$ is negative and acts to reduce the positive $\Delta G(strain)$ term, so that it represents a major part of the advantage gained from nucleation at a dislocation. If $\Delta G(strain)$ is large (i.e., the precipitate misfit is large), nucleation at dislocations may be the only way the reaction can initiate. In addition to the $\Delta G(int)$ term, a second advantage for nucleation at a dislocation arises from the pre-exponential β term in Equation (2.1). This term is the frequency with which atoms join the nucleus and depends on solute diffusion to the nucleus and across the interface. Solute pipe-diffusion along a dislocation core is always faster than

bulk diffusion, so that β increases for nucleation at a dislocation. Also, solute diffusion to dislocations themselves enhances the local concentration (e.g., Bullough and Newman, 1959).

The task of calculating $\Delta G(int)$ is difficult, which is the main reason why the theory of heterogeneous nucleation at dislocations is less advanced than homogeneous nucleation theory. In fact, there have been only six published attempts to calculate ΔG^* for nucleation at a dislocation. Cahn (1957) made the first calculation. He assumed an incoherent precipitate, an isotropic material, and completely neglected any interaction term. Despite these simplifications, his model was able to predict qualitatively some experimental observations of nucleation at dislocations. Dollins (1970) calculated ΔG^* for coherent, spherical and disk-shaped nuclei at a dislocation in an isotropic matrix. His work was reexamined by Barnett (1971). Lyubov and Solov'Yev (1965) have given the most complete treatment for calculating ΔG^* for a coherent nucleus at a dislocation. Ramírez and Pound (1973) attempted to include effects of the dislocation core energy on nucleation, effects that were omitted from the other models which use linear elasticity theory. An excellent recent review of the present status of calculating ΔG^* for nucleation at dislocations has been given by Larché (1974). None of the above treatments, however, have included effects of elastic anisotropy, principally because the calculations involved are extremely difficult. It can be concluded that

the presence of the dislocation stress field aids in reducing the energy barrier to nucleation, but a rigorous calculation of the effect is not yet available to provide an explicit expression for the rate of heterogeneous nucleation at dislocations.

It is instructive, however, to examine the order of magnitude of the terms in ΔG^* to estimate the catalytic effect of the dislocation. Typical values of $\Delta G(chem)$ are in the range $1\text{-}5 \times 10^9$ ergs/cm^3 (20-100 cal/cm^3). Values of $\Delta G(strain)$ are in the same range as $\Delta G(chem)$ for particles with appreciable misfit. Values of σ_{surf} obtained from bulk measurements are almost certainly too large since they relate to incoherent interfaces, whereas critical nuclei whose sizes are of the order of 10's of Ångstroms should have coherent interfaces. Estimates of coherent interfacial energies are in the range 20-50 ergs/cm^2.

If we take $\Delta G(chem) = 2 \times 10^9$ ergs/cm^3, $\sigma_{surf} = 20$ ergs/cm^2, and $\Delta G(strain) = 2 \times 10^9$ ergs/cm^3, then a spherical nucleus with a diameter of 20Å would have a chemical free energy change and strain energy $= 8 \times 10^{-13}$ ergs each, and a surface energy $= 24 \times 10^{-13}$ ergs. Due to the problems discussed above, no calculated values are available for $\Delta G(int)$, but it is estimated that it can be of the same order of magnitude as $\Delta G(chem)$ and $\Delta G(strain)$. Then if one assumes that the surface energy is overestimated, as is likely (Barnett, 1973), the interaction energy due to the presence of the

dislocation can have an appreciable effect of lowering the total free energy of the critical nucleus, whenever $\Delta G(\text{strain})$ is large.

2.2. Precipitation in the Al-Cu System

The aluminum-rich end of the Al-Cu phase diagram is a eutectic system between the aluminum solid solution and θ-$CuAl_2$ ($\approx$53 wt.% Cu). Figure 2.1 shows the portion of the diagram containing the α-solid solution region. Upon quenching from the solid solution region and aging, the equilibrium precipitate is the b.c.t. θ-phase. The existence of three metastable, transition phases, Guinier-Preston (G.P.) zones, θ'' and θ', was established by the early x-ray work of Preston (1938a,b,c) on the 4 wt.% Cu alloy, and by Guinier (1938, 1939,1942,1950,1952) on the 4 and 5 wt.% Cu alloys. The solvus lines for these three transition phases are shown in Figure 2.1. The positions of the θ'' and θ' solvuses are due to Hornbogen (1967). That of the G.P. solvus is due to Beton and Rollason (1957).

Guinier (1938) and Preston (1938a) determined that the G.P. zones are coherent, copper-rich clusters of plate-like shape which form on {100} planes of the matrix. The most reliable lattice parameters of the θ'' and θ' phases are given by Silcock et al. (1953). θ'' is complex tetragonal with $a = 4.04$Å and $c = 7.8$Å. It is coherent with the matrix and

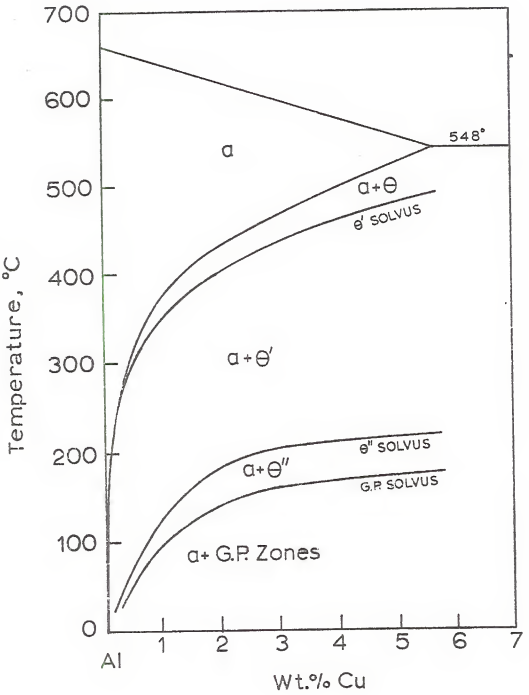

Figure 2.1. The aluminum-rich end of the Al-Cu phase diagram, including the solvus lines for G.P. zones, θ'', and θ' precipitates.

forms as platelets on {100} planes of the matrix. θ' is complex tetragonal with a = 4.04Å and c = 5.8Å. It also forms as platelets parallel to {100} matrix planes, and is initially coherent on its broad faces and semi-coherent on its edge. As it grows its broad faces become semi-coherent. The orientation relationship for both θ'' and θ' is $\{100\}_{ppt} \parallel \{100\}_{matrix}$ and $\langle 100\rangle_{ppt} \parallel \langle 100\rangle_{matrix}$.

The tetragonal unit cell of θ' is shown in Figure 2.2. There are 6 atoms/unit cell. The α-solid solution is f.c.c. with a = 4.045Å, and has 4 atoms/unit cell. When the atomic volumes are calculated for these two unit cells and compared, it is found that the α→θ' transformation involves a 3.95% volume contraction. The resulting transformation strain can be partially compensated if vacancies are generated by the growing precipitates and supplied to the matrix.

The early x-ray work established the following precipitation sequence for quenching and aging below the G.P. solvus:

$$\text{G.P. zones} \rightarrow \theta'' \rightarrow \theta' \rightarrow \theta(CuAl_2).$$

However, as suggested by the x-ray work and later confirmed by many transmission electron microscope (TEM) studies, several of the reactions can proceed concurrently depending on the quenching and aging procedures. In addition, TEM investigations have clearly established the homogeneous or heterogeneous nature of the various reactions. Nicholson and Nutting (1958) resolved G.P. zones and θ'' platelets in the 4 wt.% Cu alloy and found them to be homogeneously distributed in the matrix. It is now clear, however, that θ''

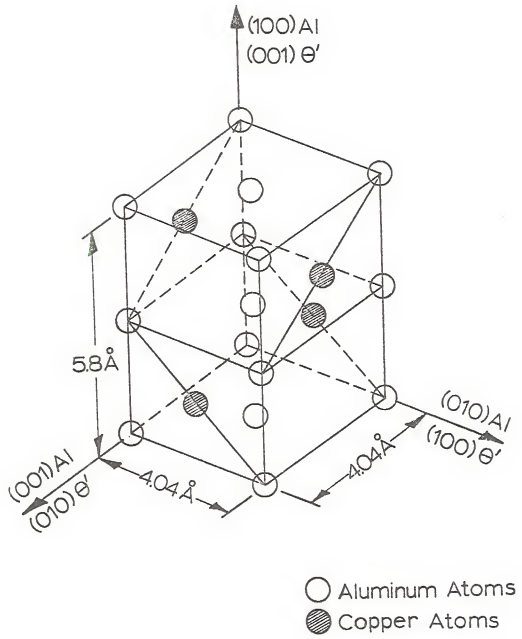

Figure 2.2. The tetragonal unit cell of θ' (after Silcock, Heal, and Hardy, 1953).

must be nucleated on G.P. zones (Lorimer and Nicholson, 1969; Lorimer, 1970). If a sample is direct-quenched into the region below the θ" solvus but above the G.P. solvus (Figure 2.1), no θ" forms. However, if a sample is direct-quenched below the G.P. solvus and then up-quenched into this region and aged, θ" forms and its distribution is a function of the size distribution of G.P. zones present before the sample was up-quenched (Lorimer, 1970). Neither G.P. zones nor θ" plays a role in the nucleation of θ'. Due to its misfit strain, θ' nucleates only heterogeneously in the presence of a stress field in the lattice. It nucleates either at dislocations (Nicholson and Nutting, 1958), in the stress fields of other θ' precipitates (Lorimer, 1968), or in the presence of a macroscopic stress applied to the sample during aging (Hosford and Agrawal, 1974).

Numerous TEM investigations have confirmed the catalytic effect of dislocations for nucleating θ'. It was suggested early (Wilsdorf and Kuhlmann-Wilsdorf, 1955; Thomas and Nutting, 1956), and later confirmed by TEM, that only certain θ' orientations will nucleate at a given dislocation. This is explained in terms of the misfit strain of the θ' platelet and the Burgers vector of the dislocation. In Figure 2.3, it is shown that the principal misfit around a θ' platelet is normal to the {100} plane of the platelet. In Figure 2.4, it is shown that a dislocation with Burgers vector a/2[110] partially relieves the misfit strain around θ' platelets on (100) and (010) whose misfits lie at 45° to the Burgers vector,

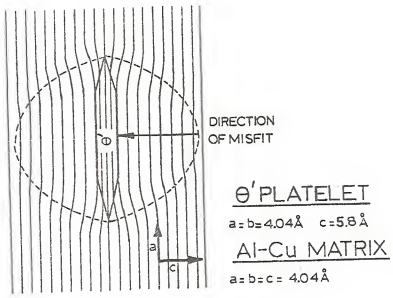

Figure 2.3. Diagram showing that the distortion of (001) planes around a θ' platelet is normal to the platelet (not to scale).

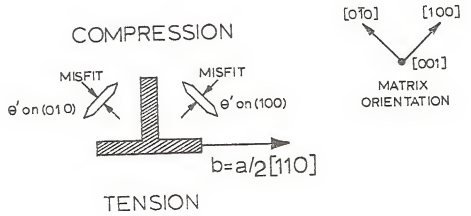

Figure 2.4. Diagram showing that a dislocation with Burgers vector a/2[110] relieves the misfit around θ' platelets lying on (100) and (010). It does not relieve the misfit around a platelet on (001).

but not for a θ' platelet on (001) whose misfit vector is perpendicular to the Burgers vector. Hence, the (001) orientation gains no advantage by nucleating in the stress field of the dislocation. Likewise for a dislocation with $\vec{b}$=a[100], only the (100) orientation of θ' should nucleate in its stress field.

Many early TEM investigations of the θ' phase were conducted after long aging treatments at high temperatures in the α+θ' field (Figure 2.1). The resulting microstructures contained a uniform distribution of large θ' platelets, and it was initially concluded that these θ' platelets were nucleated by a random distribution of pre-existing θ". However, as it became clear that θ' nucleates at dislocations and not at θ", the problem of how the random distribution of θ' could form by quenching and aging alone remained unresolved until the work of Lorimer (1968,1970). Lorimer showed that the α+θ' reaction could propagate from an initially low dislocation density, introduced during quenching, by an autocatalytic nucleation mechanism. Early during the aging period, the initial dislocations become saturated with θ'. These platelets then grow into the matrix and produce their own stress fields which aid the nucleation of more precipitates. With long aging, the reaction propagates in bands spreading out from the dislocations to fill the structure with a uniform distribution of θ' platelets on all three {100} orientations. Until the present research, this was the only

reported mechanism whereby the $\alpha \rightarrow \theta'$ reaction was found to propagate from a low initial dislocation density.

2.3. Dislocation Climb

2.3.1. Quenched-In Vacancies and the Chemical Climb Force

It is now widely accepted that vacancies can exist in crystals in thermal equilibrium with the lattice. The equilibrium concentration of vacancies increases exponentially with temperature according to the Arrhenius relation:

$$C_0 = A \exp(-E_f/kT)$$

where A = an entropy factor,

E_f = the activation energy for forming a vacancy,

k = the Boltzmann constant, and

T = temperature.

Large supersaturations of vacancies can be retained in the lattice by quenching rapidly from elevated temperatures. During and after the quench, the excess vacancies diffuse to sinks such as surfaces, grain boundaries, and dislocations, or they may cluster and collapse into vacancy disks bounded by dislocation loops. The condensation of vacancies onto a dislocation causes it to undergo positive climb. The greater the supersaturation of vacancies, the greater is the driving force for climb. A simple picture of dislocation climb by vacancy annihilation is shown in Figure 2.5(a). Dislocations

can also climb by vacancy-emission (negative climb) and this is illustrated in Figure 2.5(b).

Christian (1965) has suggested that the vacancy-annihilating climb of a/2<110> dislocations in f.c.c. lattices occurs easily only on the {111} and {110} planes. A necessary condition for climb is that the Burgers vector has a component perpendicular to the plane of climb. Therefore there are two {111} and five {110} "planes of easy climb" for an a/2[110] dislocation in f.c.c. Miekk-oja and Räty (1971) have considered the choice of climb planes in terms of the chemical climb force on each plane. This force arises from the supersaturation (or subsaturation) of vacancies (Bardeen and Herring, 1952). Its magnitude is proportional to $(\overline{b}x\overline{u})$, where $\overline{b}$ is the Burgers vector and $\overline{u}$ is the dislocation line direction. Thus, according to Miekk-oja and Räty, a dislocation with $\overline{b}$=a/2[110] is affected by the maximum climb force, $F_{c,max}$, on the {110} plane perpendicular to $\overline{b}$. It is not affected at all on the {111} and {110} planes containing $\overline{b}$. And it is affected by forces $0.82F_{c,max}$ and $0.5F_{c,max}$ on the two {111} and four {110} planes, respectively, which are inclined to $\overline{b}$.

2.3.2. Theory of Dislocation Climb

In reality, dislocation climb is more complex than the simple picture envisioned in Figure 2.5. The theory of climb has been developed by Lothe (1960), Thomson and Balluffi (1962), Balluffi and Thomson (1962), Friedel (1964), Hirth

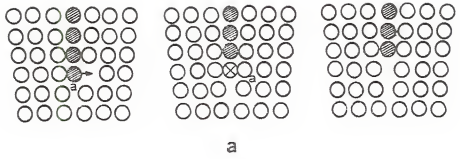

Figure 2.5. (a) Positive climb of an edge dislocation by vacancy annihilation. (b) Negative climb by vacancy emission (after Reed-Hill, 1973).

and Lothe (1968), and a general review of the mechanisms has been given by Balluffi (1969).

Briefly, dislocation climb occurs by (1) the absorption of vacancies onto the dislocation core, (2) diffusion of the vacancies along the core to jogs, and (3) subsequent movement of the jogs by destruction of the vacancies. This sequence is illustrated in Figure 2.6 for climb of an undissociated edge dislocation (a similar model applies for climb by vacancy-emission). Then, according to Balluffi (1969), the dislocation climb velocity is

$$v = \frac{2\pi D_1 b^2 [c(R) - c^0]}{[\ln(\frac{2\bar{z}}{b}) + \frac{2\bar{z}}{\lambda} \ln(\frac{R}{\lambda})]}$$

where D_1 = vacancy diffusivity in the lattice,

b = magnitude of the Burgers vector,

$c(R)$ = vacancy supersaturation at a large distance R from the dislocation,

c^0 = vacancy concentration maintained in the lattice in equilibrium with the jogs,

$\bar{z}$ = mean migration distance of a vacancy along the core before jumping off, and

λ = jog spacing.

Seidman and Balluffi (1968) surveyed the available experimental data on climb rates and concluded that, in the presence of moderate to large supersaturations, climb in aluminum appears to be highly efficient. In other words, jog production and motion is sufficiently fast that the climb rate is limited only by the diffusion of vacancies to the dislocation, and the dislocation acts as a perfect line sink.

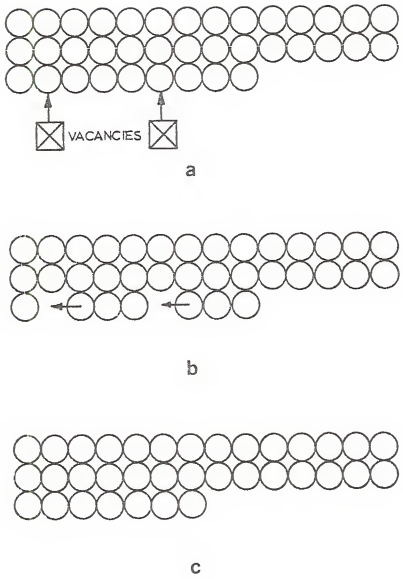

Figure 2.6. Diagram of vacancy processes associated with climb of the extra half-plane of an edge dislocation. Vacancies absorb onto the core (a), diffuse along the core (b), and annihilate at jogs (c). Subsequent motion of the jog across the page moves the extra half-plane up one atomic spacing.

2.3.3. Dislocation Climb Sources

The classical dislocation multiplication mechanism is that proposed by Frank and Read (1950), whereby a dislocation, pinned at each end, expands in its slip plane by glide. Westmacott et al. (1959) observed dislocation sources in thin foils of Al-4 wt.% Cu by transmission electron microscopy, and interpreted them to be Frank-Read sources. Gulden and Nix (1968) have observed similar sources in Al-4 wt.% Cu-3 wt.% Si. Analogous to the Frank-Read mechanism, a dislocation multiplication mechanism which operates by climb was proposed by Bardeen and Herring (1952) to act as a continuous sink for excess vacancies. The Bardeen-Herring model for a dislocation climb source is shown in Figure 2.7. Initially, a straight dislocation between A and B has its slip plane normal to the plane of the paper. Hence, it can move in the plane of the paper only by climb. Condensation of vacancies onto this line would move the dislocation out through the sequence of positions shown. When the bottom segments of the loop meet, they annihilate and rejoin as shown by the dotted lines. The segment ABC is now free to repeat the process, and there is left a vacancy loop outlined by the dislocation ring. As long as there remains a vacancy supersaturation in the region, this loop will expand, removing atoms from the lattice, and the operation can repeat removing an indefinite number of planes.

Dislocation climb source configurations were first observed by TEM in Al-Mg alloys (Westmacott et al. 1962;

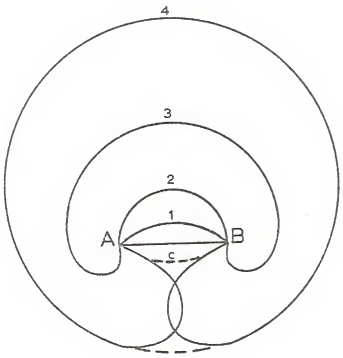

Figure 2.7. The Bardeen-Herring model of a dislocation climb source. An edge dislocation, pinned between AB, has its slip plane normal to the paper. It climbs in the plane of the paper, by vacancy annihilation, through the successive positions 1-4, rejoining at the bottom. The portion ACB can then repeat the process (after Bardeen and Herring, 1952).

Embury and Nicholson, 1963). Since then, dislocation climb sources have been identified in aluminum (Edington and West, 1966) and a number of other aluminum alloys, including Al-Ag (Edington and West, 1966), Al-Ag ternary alloys (Passoja and Ansell, 1971), and Al-Cu (Boyd and Edington, 1971). They have also been observed in other systems, including silicon (Ravi, 1971) and NiAl (Marshall and Brittain, 1974). Often the dislocation climb sources observed by TEM have small particles at the center of the source loop. An example from the present work is shown in Figure 4.2. Although the particles are usually too small to be identified, it is thought that they are insoluble particles existing at the solution treatment temperature. It is generally believed that vacancies diffusing to the particle interface activate the source which then operates to produce successive loops. The source itself is often thought to be a portion of a misfit dislocation at the particle/matrix interface.

The only reported observation of dislocation climb sources in binary Al-Cu alloys is that of Boyd and Edington (1971). They observed source densities of about 3/grain. These sources generated pure-edge loops on {110} habits with a/2<110> Burgers vectors.

2.4. Repeated Nucleation on Dislocations

The concept of repeated precipitation on climbing dislocations was first proposed by Silcock and Tunstall (1964) to explain the occurrence of planar colonies of NbC precipitates on stacking faults in austenitic stainless steels. In connection with the precipitate reaction, the stacking faults were found to grow by the climb of a/3<111> Frank partial dislocations bounding the fault. The transformation to the NbC phase involves a 23% volume expansion, so that the growing precipitates consume vacancies from the matrix in order to relieve the transformation strains. Silcock and Tunstall proposed that the Frank partial climbs by vacancy-emission in order to feed vacancies to the transformation. Thus the driving force for the dislocation climb is this need to supply vacancies for the precipitate reaction. The principles of the Silcock-Tunstall model are outlined in Figure 2.8.

Repeated precipitation on climbing dislocations by this mechanism has since been reported in a variety of systems, including different steels, an iron-vanadium alloy, a copper-silver alloy, superalloys, and semiconducting materials. The phenomenon has been observed to occur on both partial and total dislocations. For the sake of brevity, the list of reports will not be given here, and the reader is referred to the complete list in the recent paper by Nes (1974). In every reported case to date, the precipitate phase has a larger atomic volume than the matrix, thereby consuming

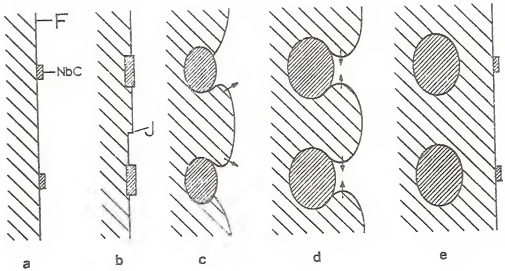

Figure 2.8. The Silcock-Tunstall model for repeated precipitation of NbC in austenitic stainless steel. The precipitates nucleate on Frank partials (a). Movement of jogs, J, provides vacancies for the precipitates to grow (b) with the consequent climb of the dislocation (c). The dislocation pinches off (d) and the process repeats (e) (after Silcock and Tunstall, 1964).

vacancies during the transformation. In every case the dislocation climb has been reported to be vacancy-emitting in order to supply the necessary vacancies.

Nes (1974) has expanded the original model of Silcock and Tunstall (1964) into a more quantitative theory, which was intended to account for the various features of repeated precipitation in all the systems reported since 1964. The fundamentals of the Nes theory are:

(1) Vacancies must be supplied to the transforming particles in order to reduce the particle/matrix mismatch.

(2) The subsequent particle growth causes vacancy-emitting climb of the dislocation in order to feed the transformation.

(3) The particle growth/dislocation climb sequence between conservative nucleations is controlled by balancing the rate at which vacancies must be supplied to the precipitates with the climb rate of the dislocation.

(4) The particle is dragged some distance by the dislocation before unpinning occurs.

(5) The rate controlling parameters in the kinetics of colony growth are either (a) the atomic diffusion of the precipitating atoms, or (b) the core (interface) self-diffusion, depending on which has the highest activation energy.

Nes implied that this mechanism is applicable to repeated precipitation on climbing dislocations in all systems, whereas in reality, it probably applies only when there is required a mass balance of vacancies between growing precipitates and climbing dislocations.

There is one report of repeated precipitation on climbing dislocations which has not been attributed to the above mechanism. Embury (1963) observed that dislocations in Al-Mg alloys were drawn around Mg_2Al_3 precipitate particles, pinched off leaving loops, and climbed away under the chemical force of a quenched-in vacancy supersaturation where the process repeated. However, this process is reported to occur only to a small extent.

2.5. Pertinent Electron Microscopy Theory

2.5.1. Two-Beam Diffraction Contrast Theory

In the transmission electron microscope, contrast arises from differences in intensity scattered out of the incident electron beam by Bragg diffraction from the crystal planes. The best contrast from defects occurs under so-called "two-beam" conditions. Owing to the large amount of tilt available in commercial goniometer stages, the crystal can be oriented so that the incident beam diffracts strongly only from one set of lattice planes. Then approximately 95% or more of the incident intensity is contained either in the

beam scattered in the forward direction (called the "transmitted" or "main" beam), or in the strong diffracted beam. The electron image is usually formed by placing an aperture around one of these beams and allowing it to pass through, while the other beam is blocked by the aperture holder (Figure 2.9). The unblocked beam is then magnified by successive lenses and projected onto the fluorescent screen. When the aperture is placed around the transmitted beam, the image formed is called a "bright-field" image. When it is placed around the diffracted beam, the image is called a "dark-field" image. Contrast at defects arises in, say, the bright-field image because the strain in the lattice around the defect causes local distortions in the atomic planes which lead to local changes in the intensity scattered into the diffracted beam. This in turn leads to local variations in intensity in the bright-field image. This is illustrated for the case of a dislocation in Figure 2.10.

When a crystal of sufficient thickness is oriented very close to the Bragg condition for one set of planes, there can be a dynamic interchange of electrons between the two beams, resulting from multiple scattering back and forth as the two beams pass through the crystal (Figure 2.11). In order to predict the intensities in the bright- or dark-field image, it is necessary to describe mathematically the physical processes which go on in this dynamic interchange. The two-beam dynamical theory of electron diffraction for a distorted crystal was developed by Howie and Whelan (1961). Their

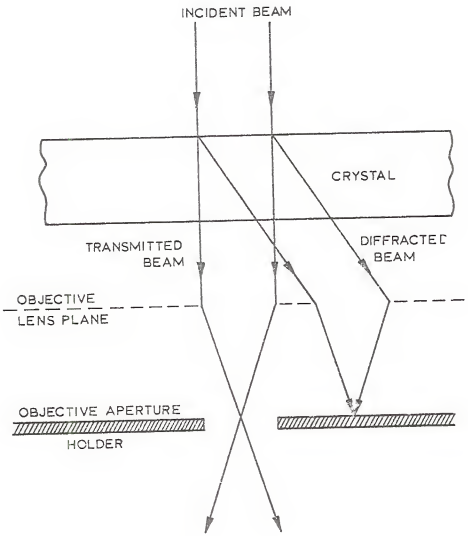

Figure 2.9. Method for forming a bright-field image under two-beam conditions. The transmitted beam is allowed to pass through the objective aperture while the diffracted beam is blocked by the aperture holder.

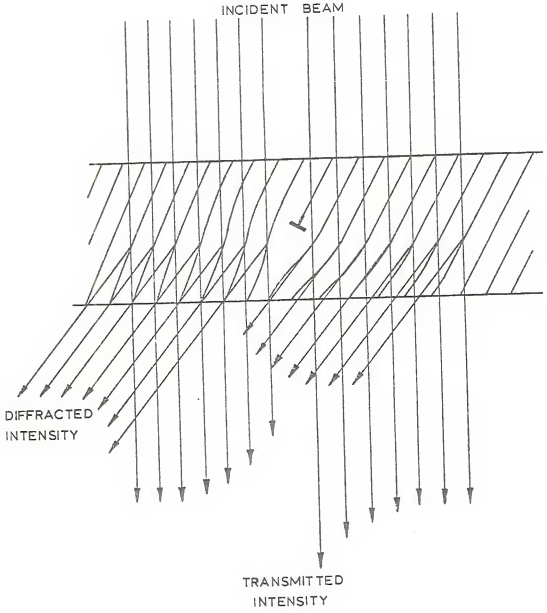

Figure 2.10. Diagram illustrating how contrast arises in the transmitted and diffracted beams from diffraction off the distorted planes around an edge dislocation. Planes to the left of the dislocation are tilted toward the Bragg angle. Planes to the right are tilted away from the Bragg angle.

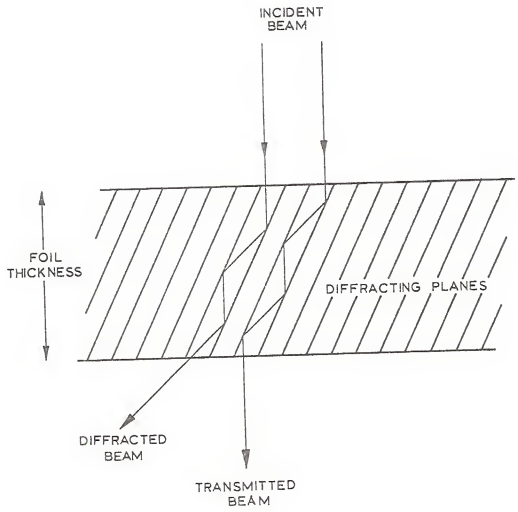

Figure 2.11. Diagram illustrating the dynamic interchange of electron intensity between the two beams resulting from multiple scattering events.

derivation is similar to the derivation of a two-beam theory for x-ray diffraction by Darwin (1914). The Howie-Whelan theory predicts the amplitudes T and S of the electron waves in the transmitted and scattered beams, respectively, at any point in the crystal. The formulation of the theory uses a column approximation, whereby the crystal is imagined to be divided up into parallel columns in the direction of the incident beam. Dynamic interchange between T and S is considered within a column, but not between neighboring columns. This is a valid approximation because the Bragg angles for high energy electron diffraction are small ($\sim 1/2°$).

The Howie-Whelan theory predicts the following coupled pair of first-order differential equations for the variations in T and S with depth in the crystal:

$$\frac{dT}{dz} = (\pi i/\xi_o)T + (\pi i/\xi_g)S \exp(2\pi isz + 2\pi i\bar{g}\cdot\bar{R})$$

$$\frac{dS}{dz} = (\pi i/\xi_o)S + (\pi i/\xi_g)T \exp(-2\pi isz - 2\pi i\bar{g}\cdot\bar{R})$$

where T = amplitude of the incident beam,

S = amplitude of the diffracted beam,

z = depth in the crystal in the direction of the incident beam,

s = parameter measuring deviation from the Bragg condition,

$\bar{g}$ = the diffracting vector,

$\bar{R}$ = the local displacement field at depth z,

ξ_o = parameter related to mean refractive index of the crystal, and

ξ_g = the extinction distance.

Each separate equation represents the variation in amplitude of the electron waves in that beam as it passes through the crystal. The first term in each equation represents the intensity scattered in the forward direction for that beam. The second term in each equation represents the intensity scattered into that beam from the other beam.

In order to account for experimentally observed effects of absorption, it is necessary to replace the quantities $1/\xi_o$ and $1/\xi_g$ in the equations by the complex quantities $(1/\xi_o+i/\xi'_o)$ and $(1/\xi_g+i/\xi'_g)$, respectively. One then obtains:

$$\frac{dT}{dz} = \pi i(1/\xi_o+i/\xi'_o)T + \pi i(1/\xi_g+i/\xi'_g)S \exp(2\pi isz+2\pi i\bar{g}\cdot\bar{R})$$

$$\frac{dS}{dz} = \pi i(1/\xi_o+i/\xi'_o)S + \pi i(1/\xi_g+i/\xi'_g)T \exp(-2\pi isz-2\pi i\bar{g}\cdot\bar{R})$$

Multiplying the amplitudes T and S by their complex conjugates gives the relative intensities in the two beams at any point in the crystal. In particular, when the intensity is calculated at the bottom of all imaginary columns in the foil, it predicts the image projected onto the viewing screen, since no interaction occurs in vacuum once the beams exit the crystal.

In the absence of any displacement field ($\bar{R}$=0), or in the presence of a fixed, rigid body displacement ($\bar{R}$=constant), the equations can be solved analytically for T or S, and the solution predicts a uniform intensity over the bottom of the crystal. When the displacement field $\bar{R}$ varies with depth, as is the case around dislocations and other defects, the equations can no longer be solved analytically, and numerical methods must be used to obtain T and S.

The validity of the Howie-Whelan equations in predicting intensities which correspond to two-beam images has been overwhelmingly demonstrated by the success of computer simulation techniques for matching defect images (Head et al., 1973). (See for example Section 4.2.1.)

2.5.2. Defect Identification from Invisibility Conditions

Although the solution of the two-beam equations is not straightforward for the case of defects with varying displacement fields, often the solution per se is not needed to identify the defect from its image. Instead, it is often possible to apply a simple criterion to identify defects in the electron microscope. This criterion is based on the fact that the term in the equations which gives rise to contrast is the product $\overline{g}\cdot\overline{R}$. The diffraction vector $\overline{g}$ is the reciprocal lattice vector normal to the diffracting planes, so that the product $\overline{g}\cdot\overline{R}$ samples the magnitude of the distortion created in the diffracting planes by the displacement field $\overline{R}$. If a defect happens to cause no distortion in the diffracting planes for a two-beam condition, then $\overline{g}\cdot\overline{R}=0$ and the two-beam equations predict uniform intensity everywhere at the bottom of the foil. In other words, there is no contrast around the defect and it is said to be "invisible" for this diffraction condition. This criterion, applied to the identification of dislocations, can be described as follows. To a first approximation, the planes parallel to the Burgers vector of a dislocation in an isotropic crystal are not

distorted. Then when the crystal is oriented so that one such set of planes is in the reflecting position, the dislocation will be "invisible" in the image. The diffracting vector is perpendicular to the diffracting planes, and therefore to the Burgers vector for this condition. Hence, the criterion for invisibility of a dislocation is the well-known relation $\bar{g}\cdot\bar{b}=0$. To identify the Burgers vector of a dislocation, it is simply a matter of tilting the foil and selecting various two-beam conditions until two diffraction vectors, $\bar{g}_1$ and $\bar{g}_2$, are found for which the dislocation is invisible in the bright-field image. The Burgers vector must be perpendicular to both $\bar{g}_1$ and $\bar{g}_2$ so that it can be determined from their cross product, i.e., $\bar{b}=(\bar{g}_1 x \bar{g}_2)$. However, this technique is not capable of determining the Burgers vector unambiguously, i.e., whether it is $+\bar{b}$ or $-\bar{b}$. Furthermore, the criterion $\bar{g}\cdot\bar{b}=0$ for invisibility applies only to screw dislocations where, in the isotropic approximation, all sets of planes parallel to the Burgers vector are undistorted. This is not so for an edge dislocation. For a set of planes to remain undistorted by an edge dislocation, not only must $\bar{g}\cdot\bar{b}=0$, but in addition, $\bar{g}$ must be parallel to the dislocation line direction. Mathematically this is written $\bar{g}\cdot(\bar{b}x\bar{u})=0$, where $\bar{u}$ is the line direction. This is a very stringent condition which is seldom obtained in the microscope. Thus, edge dislocations, or dislocations with appreciable edge orientation, often exhibit strong "residual contrast" when $\bar{g}\cdot\bar{b}=0$, due to the $(\bar{b}x\bar{u})$ term. For

this reason, practical experience in recognizing "residual contrast" is necessary in order to identify dislocations from the invisibility criterion.

The criterion $\overline{g}\cdot\overline{b}=0$ for invisibility is valid only for total dislocations, where the product $\overline{g}\cdot\overline{b}$ can be only zero or an integer (since it is the product of a reciprocal lattice vector and a real lattice vector). For partial dislocations, $\overline{g}\cdot\overline{b}$ can take on the non-integer values $\pm 1/3$, $2/3$, $4/3$, etc., in cubic lattices. Howie and Whelan (1962) determined that partial dislocations are invisible when $\overline{g}\cdot\overline{b}=0$ or $\pm 1/3$ and are visible for all other products. Silcock and Tunstall (1964) further determined that, for this to be strictly valid, the deviation from the Bragg condition cannot be too large.

The condition that a defect is "invisible" if its displacement field does not distort the reflecting planes can be applied to identify certain small precipitates. For example, in the case of θ' platelets in Al-Cu, the principal misfit in the lattice caused by the platelet is normal to the plane of the platelet (Section 2.2). If such platelets are too small to distinguish their shape, their orientation can still be determined since they will be invisible whenever $\overline{g}$ is perpendicular to the misfit vector.

2.5.3. Imaging Precipitates in the Electron Microscope

Precipitates can be imaged by one or more of several mechanisms in the electron microscope. A good description

of these mechanisms is given by Hirsch et al. (1965, p. 336). Those pertinent to this research will be outlined below.

(1) Strain contrast in the matrix. All coherent and semicoherent precipitates, and most incoherent precipitates, cause some strain in the matrix. These strain fields therefore give rise to diffraction contrast effects in the matrix. This can be the only mechanism for imaging very small precipitates whose sizes are less than the resolution limit of the microscope, but whose long-range strain fields are greater than this limit.

(2) Misfit dislocation imaging. Semicoherent precipitates have misfit dislocations over their semicoherent interfaces. The strain fields of these misfit dislocations can cause strain contrast just as for isolated dislocations in the matrix. Weatherly and Nicholson (1968) have investigated the conditions for imaging misfit dislocations. Often small platelets viewed normal to the platelets are imaged by the misfit-dislocation loops around their edges. This is referred to as "dislocation-ring" contrast.

(3) Structure factor contrast. According to Ashby and Brown (1963), this contrast arises whenever a coherent precipitate has a different structure factor from the matrix, and thus a different extinction distance. A particle of thickness Δt then increases the effective foil thickness in columns passing through the particle, giving rise to an intensity change relative to columns in the matrix. Depending on the depth of the particles in the foil and the

relative values of the extinction distances in the particle and matrix, the particles can appear either lighter or darker than the surrounding matrix. Structure factor contrast arises only within the limits of the particle boundary.

(4) Orientation contrast. This contrast mechanism arises whenever a foil is oriented such that a certain set of lattice planes in the precipitate is diffracting strongly, whereas the matrix is diffracting weakly, or vice versa. The contrast is of a uniform light and dark nature, typically dark precipitates in a light matrix. Orientation contrast can arise only when there is appreciable difference in crystal structure between the precipitate and matrix, i.e., when the precipitates are semicoherent or incoherent. For example, when the electron beam is parallel to the thin dimension of large precipitate platelets, often certain lattice planes in the precipitate will also be parallel to the beam. In this case, the precipitate diffracts strongly. If the matrix is not oriented for strong Bragg diffraction, the bright-field image will show dark precipitates in a light matrix.

(5) Displacement fringe contrast. Displacement fringe contrast arises when there is an abrupt change in the phase of the transmitted and diffracted waves as they encounter a thin sheet of precipitate which displaces the matrix planes in opposite directions on either side of it. This displacement $\vec{R}$ around a typical semicoherent precipitate platelet is normal to the plane of the platelet, and its magnitude is given by

$$|\overline{R}_n| = \Delta t\delta - n|\overline{b}_n|$$

where Δt = thickness of the platelet,

δ = precipitate misfit,

n = number of misfit dislocations at the periphery of the platelet, and

$\overline{b}$ = Burgers vector of the misfit dislocations.

When this displacement is substituted into the equations of the dynamical theory, the intensity of the transmitted beam is found to oscillate with thickness (Whelan and Hirsch, 1957). Thus, when the precipitate platelet is inclined to the electron beam, a fringe effect is observed. The so-called stacking fault fringes are the limiting case of displacement fringe contrast.

CHAPTER 3

EXPERIMENTAL PROCEDURES AND MATERIALS

3.1. Specimen Materials

The four Al-Cu alloys used in this work were obtained as rolled sheets from a previous research project. They were prepared from 99.99% aluminum and 99.99% copper by double melting in an induction furnace using a graphite mold. After solidification, the billets were alternately cold-rolled and annealed to reduce them to sheet form.

The target compositions were the 4, 2, 1, and 1/2 wt.% Cu alloys. The nominal copper concentrations of the four alloys were 3.85, 1.96, 0.99, and 0.5 wt.%, based on starting weights before melting. The impurity content in the 3.85 wt.% Cu alloy was determined by x-ray spectrographic analysis by the Sandia Corporation, Albuquerque, New Mexico. The impurity levels are given as ranges in Table 3.1. The barium level is suspect as it was determined from only one line. The impurity levels in the other three alloys were not determined. However, since all four alloys were prepared from the same starting materials, the other three probably had the same impurity levels as the 3.85 wt.% Cu alloy.

The 1 wt.% and 1/2 wt.% Cu alloys were obtained as rolled sheet, 0.038 inch and 0.034 inch, respectively. They

Table 3.1

Impurity Levels in the Al-3.85 wt.% Copper Alloy

Impurity	Weight ppm
Fe	5-25
Pb	$\leq$10
Si	1-10
Mo	$\leq$10
Mg	5-20
Ca	1-5
Ga	$\leq$10
Ba	10-40

were then cold-rolled to 0.005 inch for heat treatment. The 3.85 wt.% and 1.96 wt.% Cu alloys were obtained as rolled sheet, 0.004 inch thick. They were not reduced further before heat treatment. Samples for heat treatment were cut from the rolled foils to the approximate dimensions 1/8 x 1/2 x 0.004 inch. This was found to be a suitable size for preparing electron microscope specimens after heat treatment.

3.2. Heat Treatments

All samples were solution treated for one hour at a temperature in the α-solid solution range (Figure 2.1). Next, they were either (1) direct-quenched to an aging temperature

above the G.P. solvus, or (2) quenched to a low temperature. The samples given direct-quenches were aged for various times from approximately one second to 24 hours, and then quenched into room-temperature water. Samples quenched to low temperatures were either prepared for electron microscopy without further treatment, or they were up-quenched to a temperature above the G.P. solvus and aged for various times. They were then quenched into room-temperature water.

The solution treatments were conducted in a vertical furnace in air. The temperature in the heat zone was controlled to within ±2°C. One end of the sample was clamped in a stainless steel alligator clip attached to the bottom of a one-half inch diameter stainless steel tube, and this was inserted into the heat zone of the furnace. Before each treatment, the temperature in the heat zone was determined by inserting a thermocouple into a dummy stainless steel tube suspended in the heat zone.

Quenching was achieved by dropping the specimen-stainless steel tube assembly out of the bottom of the furnace into the quench bath. For direct-quenches to the aging temperature, the specimen was dropped into a Lauda Constant Temperature Oil Bath, maintained at the aging temperature, to within ±0.2°C. A schematic diagram of the apparatus used for solution treatment and direct-quenching is shown in Figure 3.1. For quenching to low temperatures, the specimen was dropped into one of several low temperature baths in place of the oil bath. Following the quench to low temperatures, some

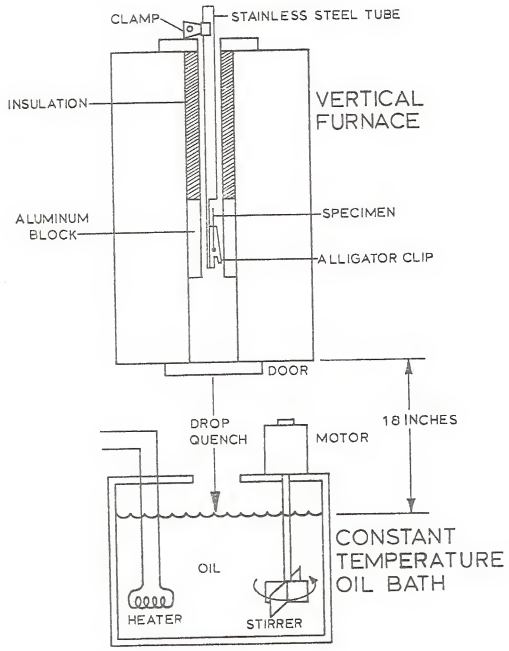

Figure 3.1. Diagram of the apparatus used for solution treatment and direct-quenching. The specimen, attached to the stainless steel tube for weight, is dropped from the solution treatment furnace into the constant temperature, aging bath.

samples were immediately up-quenched into the constant temperature oil bath maintained at the desired aging temperature. Due to the wide variety of solution treatment temperatures, aging temperatures, and aging times employed in this research, no table of heat treatments will be given here. Instead, the specific heat treatment information will be given either in the text or in the figure captions.

3.3. Electron Microscope Specimen Preparation

Electron microscope specimens were prepared from the heat treated strips by electropolishing in a solution of 5% perchloric acid in methyl alcohol. A polishing potential of 18 volts d.c. was used with a stainless steel cathode. The electropolishing setup is shown in Figure 3.2. The beaker containing the polishing solution was immersed in a bath of dry ice and acetone to slow down the polishing reaction. The solution was circulated at a slow speed with a magnetic stirrer to keep it cold. Under these conditions, the polishing bath was maintained at -45°C.

The specimen strip was held with locking tweezers and polished by dipping the bottom end (approximately 1/8-3/16 inch) into the solution at a dipping rate of about 1/second. Dipping was found to reduce edge attack and to give a relatively uniform polish. The voltage dropped to about 12 volts during immersion. Total polishing time to obtain a suitable

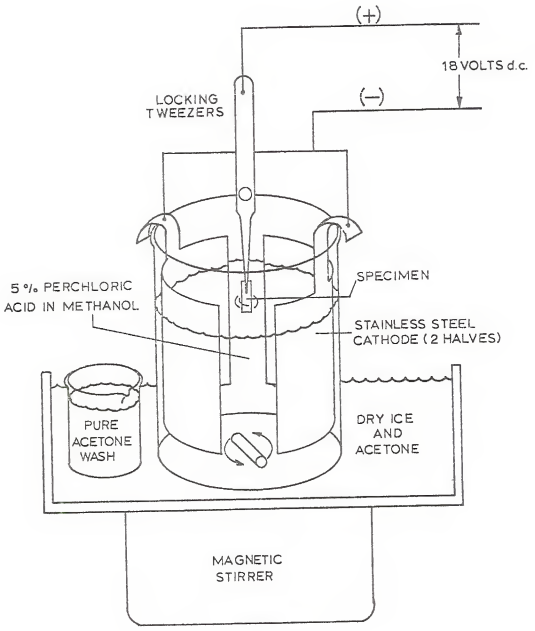

Figure 3.2. The electropolishing setup for preparing thin foils for electron microscopy. Polishing is accomplished by dipping the bottom end of the specimen into the solution.

thin area was about 15 minutes. When it was determined (by experience) that the specimen was nearly thin enough, the stirring was stopped to avoid damaging the thin area. The last 20-30 seconds of polishing was done by immersion and agitation instead of dipping, since dipping to the last was found to sometimes etch the thin foil edge. Polishing was continued until the bottom edge appeared very ragged or until small holes had broken through. Then the power was switched off and the specimen was rapidly removed and plunged into a beaker of cold acetone (99.8% pure) immersed in the dry ice-acetone cooling bath. It was agitated for about 10 seconds and then immediately placed under a stream of room-temperature acetone from a wash bottle. After washing for about 30 seconds, it was allowed to dry in air. The initial wash in cold acetone was necessary to remove most of the electrolyte which rapidly etched the polished surface if allowed to warm to room temperature.

The thinned, bottom portion of the sample strip was cut off with an X-acto razor knife and mounted in a 3 mm, 75 mesh, locking, double copper grid for viewing in the electron microscope. Several more specimens could then be polished from the same sample strip, if desired. However, the remaining bottom part of the strip was already polished quite thin. To avoid etching this polished surface, the specimen was agitated for about one minute in the small beaker of cold acetone prior to repolishing.

3.4. Electron Microscopy

The thin foils were examined in a Phillips EM 200 electron microscope operated at 100 Kv potential. A goniometer stage with ±45° and ±30° tilt on two orthogonal axes was used. Two-beam diffraction conditions were established for taking all micrographs. To obtain two-beam conditions, the foils were oriented close to one of the low index poles shown on the Kikuchi line map for an f.c.c. crystal in Figure 3.3. Use of this Kikuchi line map during specimen tilting, as described by Head et al. (1973), enabled diffraction vectors to be determined unambiguously in every case.

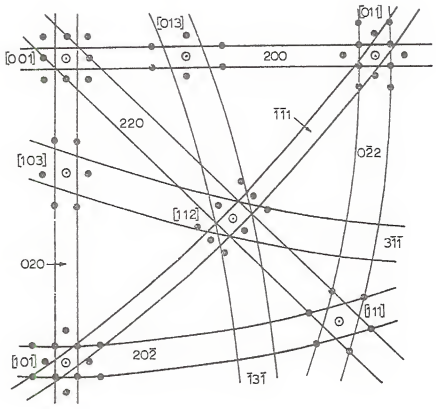

Figure 3.3. Kikuchi line map over two adjacent stereographic triangles for a face-centered cubic crystal (after Head et al., 1973).

CHAPTER 4

EXPERIMENTAL RESULTS AND ANALYSES

4.1. Introduction

Evidence for repeated nucleation of the θ' phase on dislocations was first observed in this research when the Al-3.85 wt.% Cu alloy was quenched directly to aging temperatures above the θ'' solvus. Figure 4.1 shows a typical microstructure resulting from direct-quenching and aging. A brief description of the features and evolution of this microstructure (with the facts to be established in this chapter) is as follows. Dispersed throughout the foil are densely populated colonies of small θ' precipitates. The colonies are bounded either totally or partially by dislocations, some of which are out of contrast in this image. The dislocations were generated and climbed during the quench from the solution treatment temperature. As they climbed, they nucleated and dispersed the θ' colonies in their paths. All dislocations climbed during quenching and all nucleated precipitate colonies. The precipitate colonies may (1) be planar, (2) lie on smoothly curved surfaces, or (3) lie on corrugated-shaped surfaces, depending on the climb paths of the dislocations.

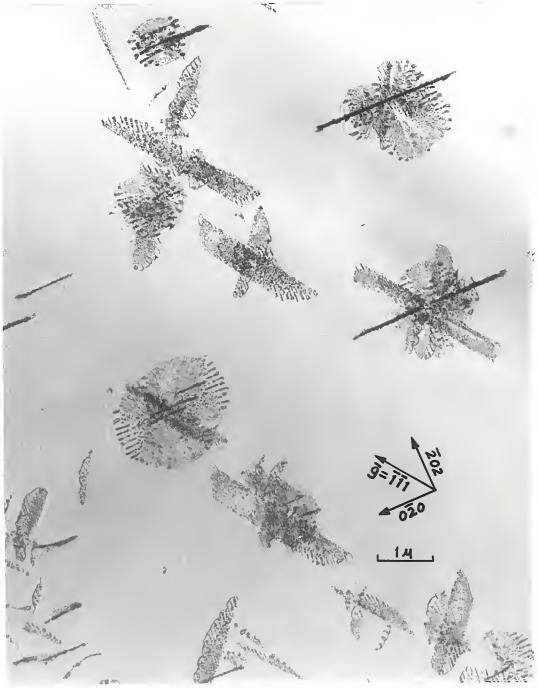

Figure 4.1. Typical microstructure resulting from quenching the Al-4 wt.% Cu alloy directly to the aging temperature. The foil contains colonies of small θ' precipitates, bounded by dislocations. (Heat treatment: S.T. 1 hour, quench to 220°C, age 5 minutes.)

The primary goal of this research was to determine the mechanism by which repeated nucleation of θ' occurs in the Al-Cu system. However, since this work is the first reported observation of the phenomenon in Al-Cu alloys, a secondary goal was to characterize thoroughly the various features of the microstructures observed. The geometrical analyses are reported in detail here.

The material in this chapter is developed much in the way in which the experimental analysis was performed. First, in Section 4.2, the nature and sources of the climbing dislocations are established. Next, in Section 4.3 the precipitate is identified as θ' and characterized as to distribution of orientations in the colonies. Section 4.4 contains descriptions of the various geometries and some of the diffraction effects. Finally, Section 4.5 describes results of experiments designed to determine the effects of different parameters on the repeated nucleation process. Most of the analyses for identification purposes were conducted on the 3.85 wt.% Cu alloy. Accordingly, all micrographs in this chapter are from this alloy, except those in Section 4.5.5. In addition, most micrographs in this chapter are from samples quenched directly to aging temperatures. For the sake of brevity, the copper concentration of the alloys is listed in the figure captions as either 4, 2, 1, or 1/2 wt.%.

4.2. Nature and Source of the Climbing Dislocations

The dislocations which climbed during quenching can be classified mainly into one of two categories according to origin: (1) those generated at dislocation climb sources, and (2) glide dislocations which subsequently climb (a third category found in alloys quenched into oil or water at room temperature will be discussed in Section 4.5.4).

4.2.1. Dislocation Climb Sources

Figure 4.2 shows micrographs from foils direct-quenched to 220°C and aged for short times before quenching to room temperature. Present in the microstructures are configurations consisting of concentric dislocation loops. When viewed edge-on, the loops are seen to be coplanar since their traces are straight lines, as at points A in Figure 4.2(c). Tilting the foil confirms that these straight lines are traces of coplanar loops. Concentric loops sectioned by the thin foil leave straight-line traces with the foil surfaces, e.g., at B-B in Figure 4.2(b) and (c). Often small particles were observed at the center of the loops as in Figure 4.2(b). The operation of dislocation sources has been discussed in Section 2.3.3 and will not be repeated here. It will now be established that these are climb sources, and the Burgers vectors and habit planes of the loops will be identified.

A typical source is shown in Figure 4.3. Several loop habits have been generated at the source. We are concerned

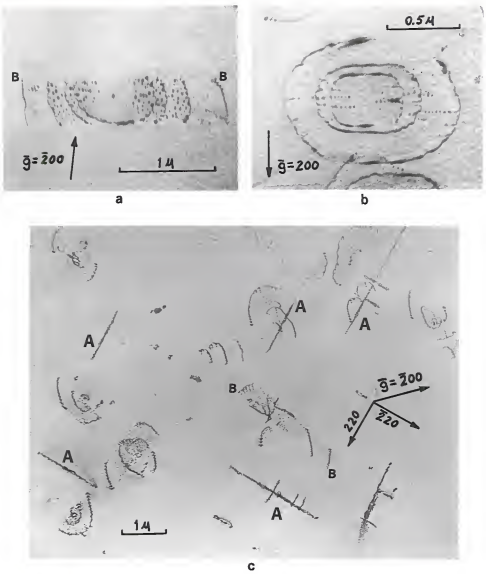

Figure 4.2. Dislocation sources in Al-4 wt.% Cu direct-quenched from 550°C to 220°C and aged for 8 seconds in (a) and (b) and one minute in (c).

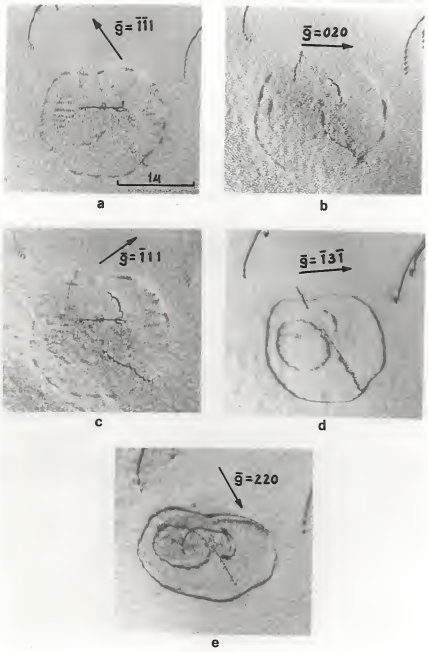

Figure 4.3. Series of micrographs for determining the geometry and Burgers vectors of the source loops. The beam direction is close to [101] in (a), (b), and (c), to [112] in (d), and to [001] in (e). (Heat treatment: S.T. 1 hour 550°C, quench to 220°C, age 8 seconds.)

in this analysis with the outermost loop and the one inner loop which lie totally within the foil. The plane of the foil was analyzed to be very close to (101) so that this loop habit must lie on or very close to (101). Consider first the three images (a), (b), and (c) taken about the [101] beam direction. In each image the source loops on (101) exhibit weak, residual contrast typical of "invisible" images of edge dislocations for which $\bar{g}\cdot\bar{b}=0$, but $\bar{g}\cdot(\bar{b}\times\bar{u})\neq 0$ (Hirsch et al., 1965, p. 261). Those loop segments lying approximately parallel to the $\bar{g}$ vectors, where $\bar{g}\cdot(\bar{b}\times\bar{u})\approx 0$, are invisible. The loops are everywhere visible for the two reflections, $\bar{g}=\bar{1}3\bar{1}$ and 220. From this analysis, the source loops are identified as pure edge-dislocation loops lying on (101) with $\bar{b}=a/2[101]$. Since the Burgers vector is normal to the plane of the loops, the loops must expand in this plane by the process of climb. The sources are therefore dislocation climb sources of the type observed by Boyd and Edington (1971) in Al-2.5 wt.% Cu.

The loop habits of climb sources in these alloys were observed always to be {110} (with one exception to be discussed in Section 4.4). The typical source produced loops on more than one {110} habit. Loops lying on as many as five of the six possible {110} habits were observed at one source. The typical source also generated more than one loop on each habit. As many as five or six loops on one habit were commonly observed, although the average number varied with the heat treatment.

When a given foil was first examined, a technique was used for rapidly determining if the dislocation sources were indeed climb sources with {110} habits, or if some or all of them might be dislocation glide sources which are known to operate on the {111} slip planes in Al-Cu alloys (Westmacott et al., 1959). This technique was to tilt the foil to {001}, {111}, and {101} orientations and, in each orientation, to determine the number of different source habits viewed edge-on together with the angles between these habits. For example, when a foil was tilted to the (001) orientation, two edge-on habits at 90° apart were observed, Figure 4.4(a). Since the [001] pole is parallel to two {110} planes at 90° to each other, and not to any {111} planes, those sources are identified immediately as {110} climb sources. Likewise, when viewed in the (111) orientation, three edge-on habits at 60° apart were seen, Figure 4.4(b). Again, since the [111] pole is parallel to three {110} planes at 60° to each other and not to any {111} planes, the sources are identified as climb sources. However, neither of these cases rules out the possibility that other sources seen inclined to the beam in these orientations might be glide sources lying on {111} planes. Therefore, it was necessary to tilt to a {101} orientation. The [101] pole is parallel to two {111} planes at 70.5° and to only one {110} plane. In this orientation, only one habit was ever seen edge-on, as shown in Figure 4.1. There was no evidence that any of the sources found in these foils were glide sources.

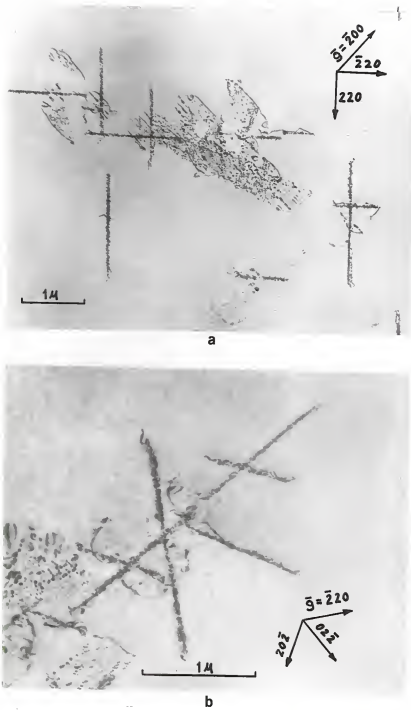

Figure 4.4. (a) Two edge-on habits of climb sources at 90° to each other in an (001)-oriented foil. (b) Three edge-on habits at 60° to each other in a (111)-oriented foil. (Heat treatments: S.T. 1 hour 550°C, quenched to 220°C, aged 5 minutes.)

Occasionally, when viewing edge-on habits in the (001) orientation, it was observed that two different habits did not lie exactly at 90° to one another, although the habits of other sources in the same field of view appeared to be perpendicular, Figure 4.5. It is concluded that climb of the loops is not necessarily confined strictly to the {110} planes. This angular measurement between two adjacent habits is more accurate for determining if the loops lie exactly on {110} planes than are measurements made from the rotation calibration between directions in the diffraction pattern and those in the image.

It has now been established that the dislocation sources in these foils are climb sources. However, the climb of pure-edge dislocations can be either vacancy-annihilating or vacancy-emitting. The former case removes lattice planes from the crystal whereas the latter case adds interstitial planes. It remains to be shown whether the source loops climb by vacancy annihilation or emission, although intuitive arguments favor vacancy-annihilating climb. For instance, it is known that quenching produces large vacancy supersaturations, but negligible concentrations of interstitials. As the temperature drops during quenching, the need for the excess vacancies to diffuse to sinks would promote the growth of vacancy loops and tend to annihilate any interstitial loops. Therefore, one would expect that the large climb sources operate by vacancy annihilation during quenching, but this is not a sufficient proof. In fact, in the past

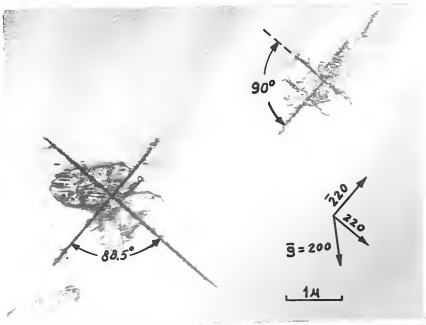

Figure 4.5. Two edge-on habits of climb sources lying slightly off 90° from each other in an (001)-oriented foil. (Heat treatment: S.T. 1 hour 550°C, quench to 220°C, aged 5 minutes.)

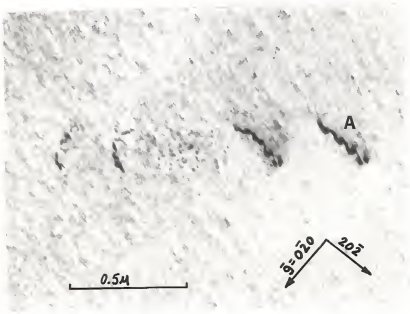

Figure 4.6. Climb source inclined through the foil. Two loops are sectioned leaving dislocation arcs. The arc at A was selected for computer matching to determine its Burgers vector. (Heat treatment: S.T. 1 hour 550°C, quenched to 220°C, aged 4 seconds.)

only intuitive reasoning has been used to show that climb sources in aluminum alloys operate by vacancy-annihilating climb.

In the present work, the technique of computer matching of dislocation images (Head et al., 1973) was employed to establish that these loops climb by vacancy annihilation, thereby removing planes locally from the lattice. This technique is capable of determining unambiguously the Burgers vector of a dislocation line segment, i.e., whether the Burgers vector is $+\vec{b}$ or $-\vec{b}$.

Figure 4.6 shows a climb source in a sample direct-quenched to 220°C and held only four seconds. This source has generated two loops on a {110} habit inclined through the foil, so that each loop is sectioned and leaves two arcs of dislocation. The segment of the outermost loop at A is reasonably straight and was selected for the computer matching experiment (the oscillations in the image are contrast effects arising from the inclination of the dislocation through the foil). From invisibility conditions, the Burgers vectors of these loops were determined to be either a/2[011] or a/2[$0\bar{1}\bar{1}$]. The loops are pure-edge and lie on (011). By stereographic analysis, the line direction of segment A was determined to be very close to [100] in (011), and the foil normal was determined to be [313].

Six experimental images of segment A are shown in Figure 4.7 along with the corresponding computed images for $\vec{b}$=a/2[$0\bar{1}\bar{1}$] and $\vec{b}$=a/2[011]. These six images represent

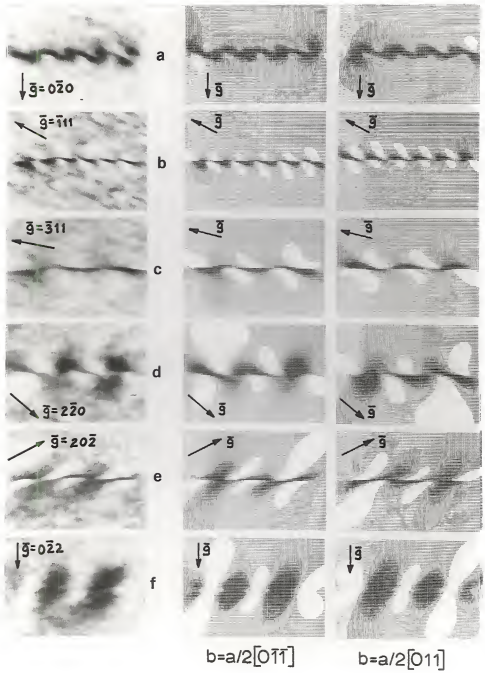

Figure 4.7. Six experimental and computed images of dislocation A in Figure 4.6. The line direction is [100], the foil normal is [313], and the beam direction is close to [101] in (a) and (b), to [112] in (c) and (d), and to [111] in (e) and (f).

reflections from three non-coplanar beam directions, a necessary condition for uniquely identifying a dislocation by computer matching (Head, 1969). From the rotation calibration of the electron microscope, the exact orientation of the $\bar{g}$-vector was marked on each experimental image. Also, from the known geometry of the computer program, the orientation of the $\bar{g}$-vector was marked on each computed image. Thus the direction of the $\bar{g}$-vector serves as a basis for comparison when matching the features of the computed images with those in the experimental images. Now for a given diffraction vector $\bar{g}$, the image of a dislocation with Burgers vector $+\bar{b}$ is identical to that of a dislocation with Burgers vector $-\bar{b}$ after a rotation of 180° (Head *et al.*, 1973, p. 382). Clearly it can be seen from Figure 4.7 that the Burgers vector of Segment A of the loop is $a/2[0\bar{1}\bar{1}]$ and not $a/2[011]$.

By convention, the positive direction of the dislocation line in the computer program is always taken to be acute to the foil normal. Thus for the foil normal [313], the positive direction of Segment A is [100] and not $[\bar{1}00]$. Also, the computer program employs the finish-to-start, right-hand (FS/RH) convention for establishing the direction of the Burgers vector with respect to the positive sense of the dislocation line, Figure 4.8. Thus, from the (FS/RH) convention, and the absolute Burgers vector and positive line direction of Segment A, the geometry of the two loops in Figure 4.6 can be established, and this is illustrated

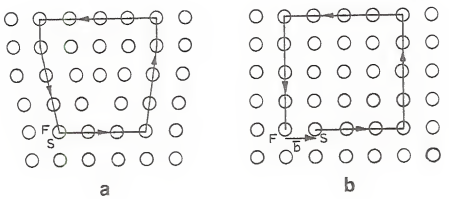

Figure 4.8. Schematic representation of Burgers circuits taken in a cubic lattice around an edge dislocation (a), and in perfect crystal (b), illustrating the FS/RH definition of the Burgers vector. The positive sense of the dislocation line is out of the paper (after Head et al., 1973).

Figure 4.9. The geometry of dislocation climb source loops in Al-Cu as indicated by the absolute sense of the Burgers vector determined from computer matching. The pure-edge loops expand in their habit plane by vacancy-annihilating climb.

schematically in Figure 4.9. Clearly the loops are pure-edge, vacancy loops which climb in their habit plane by vacancy annihilation. It is concluded that these climb sources operate during the quench to act as sinks for the excess, quenched-in vacancies.

Now that it is established that the source loops climb by vacancy-condensation onto the loops, one further experimental observation must be explained. The vacancy-annihilating climb of a/2<110> dislocations in f.c.c. lattices is generally believed to occur easily only on {111} and {110} planes, removing one and two atom planes, respectively (Christian, 1965, p. 363). Stacking faults were never observed within these climb loops, even though the same loops were examined on many different reflections, e.g., Figure 4.3. The stacking of {110} planes in f.c.c. is ABAB (Figure 4.10). Removal of a single {110} plane by vacancy condensation behind a climbing a/2<110> dislocation would create a stacking fault. Two adjacent {110} planes must be eliminated to avoid a stacking fault. It appears, therefore, that the source loops climb by condensation of vacancies onto two adjacent {110} planes. Since the stacking fault energy in dilute aluminum alloys is high, it appears to be energetically favorable for the loops to expand in this manner. A schematic cross-section through a climb source is shown in Figure 4.11.

The nature of the source particles is undetermined. Occasionally, sources were observed that nucleated at very

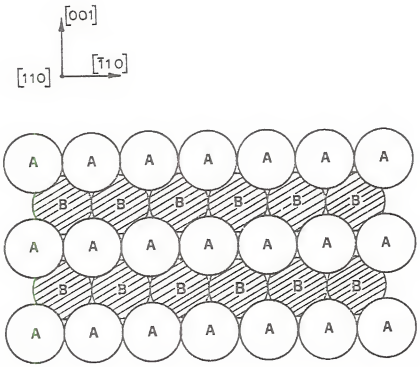

Figure 4.10. Diagram showing the stacking of atoms in {110} planes in a face centered cubic crystal (viewed normal to the planes). Atoms in the third plane down lie in A positions. Removal of a single plane of B atoms creates a stacking fault, A on A.

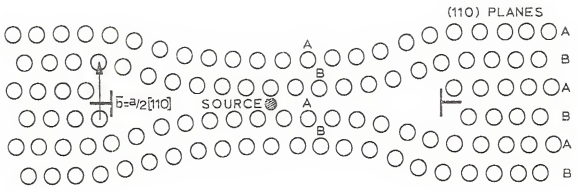

Figure 4.11. Schematic diagram of the cross-section through a climb source loop on (110). The pure-edge loops with b=a/2[110] climb by vacancy condensation onto two adjacent (110) planes, thereby avoiding creation of a stacking fault.

large spheroidized particles (≈1/10 - 1/2μ diameter), Figure 4.12. These particles were large enough to be analyzed on a JEOL 100B Analytical Electron Microscope using a fine-focused electron beam (approximately 1,000Å diameter), and a non-dispersive detection system for fluorescent analysis of the emitted x-rays. The analysis of these large spheroids identified them as pure lead. It is not known how lead entered the sample material. However, such particles were observed in only a few foils and nucleated only a small fraction (<<1%) of the climb sources present. The typical source particle was so small as to be barely visible or not visible at all, Figure 4.2(b). Such particles were too small for the x-ray analysis, but they are most probably not lead. The chemical analysis of the 3.85 wt.% Cu alloy (Section 3.1) showed no appreciable concentration of any single impurity which would suggest a guess at the particle nature.

Although the chemical composition of the source particles is unknown, some observations were made about their distribution. The climb sources were dispersed randomly in most portions of the foils. Occasionally, local high densities of sources were observed. In a few instances, sources were observed evenly spaced in a straight line (Figure 4.13), suggesting that the source particles were part of an impurity stringer produced when the original cast alloy was rolled down.

The density of active climb sources in these foils varied with heat treatment (Section 4.5). In the only other reported

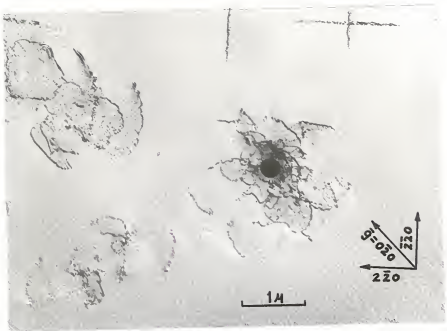

Figure 4.12. Climb sources generated at a large, spherical lead particle. (Heat treatment: S.T. 1 hour 550°C, quench to 220°C, aged 1 minute.)

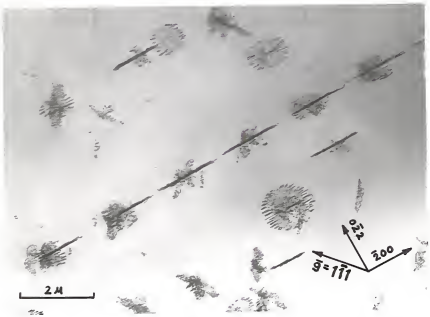

Figure 4.13. Climb sources aligned in a row. (Heat treatment: S.T. 1 hour 550°C, quench to 200°C, aged 5 minutes.)

observation of climb sources in Al-Cu alloys, Boyd and Edington (1971) observed a source density of about three per grain in Al-2.5 wt.% Cu (although it is not stated, most probably measured in the volume of a grain sectioned by the foil; grain size not reported). Source densities many orders of magnitude higher than this were observed in the present foils. The maximum density was produced in a sample quenched from 550°C to 180°C. A micrograph of this foil is shown in Figure 4.49(e). From this micrograph and the average grain size (approximately 250μ diameter), the active source density was estimated to be approximately 6×10^6 sources per grain.

4.2.2. Glide Dislocations Which Climb

In addition to loops generated at climb sources, other dislocations were observed which had climbed during quenching and nucleated precipitate colonies. Examples are shown in Figure 4.14. Generally, these dislocations were long and either smoothly curved or irregular-shaped, depending on their climb paths. The micrographs in this section were taken from foils aged long enough so that the precipitate colonies are readily visible, thereby delineating the climb paths of the dislocations. For the present, it is assumed that the precipitate colonies were nucleated by the climbing dislocations (this will be proven in Section 4.3). In Figure 4.14(a), the dislocation exits the foil surfaces at A and C, and the trailing precipitate colony intersects one foil

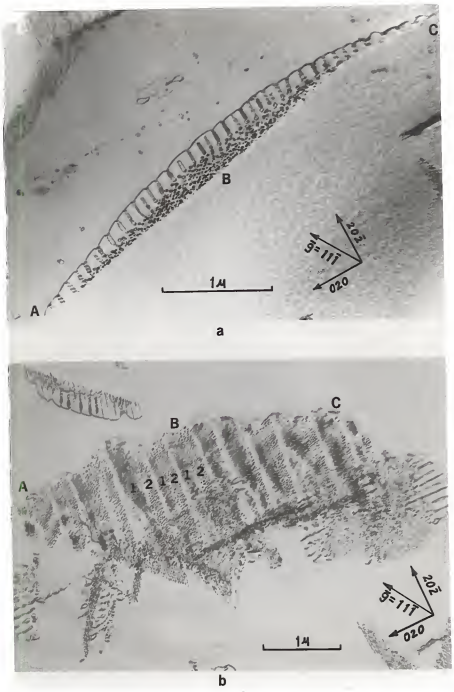

Figure 4.14. Precipitate colonies nucleated at long, climbing dislocations. The dislocation in (b) is out of contrast along ABC. (Heat treatment: S.T. 1 hour 550°C, quenched to 220°C, aged 5 minutes.)

surface along the trace ABC. In Figure 4.14(b), the dislocation lies along ABC at the upper edge of the precipitate colony, where it is "invisible." Some residual contrast can be seen, however. The source of these dislocations is unknown. They could be (1) grown-in dislocations, (2) glide dislocations which existed at the solution treatment temperature prior to quenching, or (3) glide dislocations which were generated at some source, probably grain boundaries, at the onset of quenching. It is thought that most, if not all, fall into categories (2) and (3), i.e., they were a/2<110> glide dislocations on {111} planes prior to climbing.

Figure 4.15, for example, shows two images of a precipitate colony nucleated by one such long dislocation. In (a) the precipitate colony is inclined through the foil. The curved dislocation has been sectioned twice by the foil, leaving two arcs, AB and CD, at the ends of the precipitate colony. The Burgers vector of this dislocation was determined to be $a/2[10\bar{1}]$. The micrograph in (b) was taken after the foil was tilted to the (111) orientation. Here the precipitate colony is viewed edge-on and appears as a curved, dark line. This indicates that the dislocation climbed on an irrational, smoothly curved surface normal to the (111) plane. Since (111) is a glide plane, it is reasonable to assume that it was a curved, glide dislocation on (111) prior to climbing.

Such long glide dislocations were observed often to have climbed on smoothly curved surfaces. This was easily recognized by the curved intersections which the associated

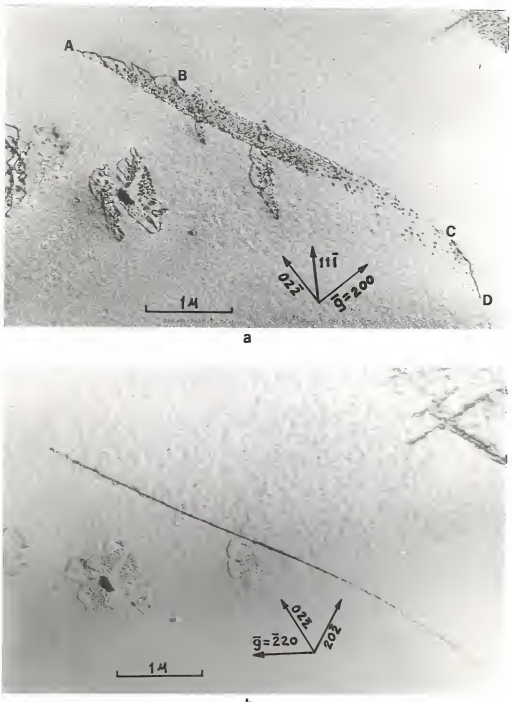

Figure 4.15. Precipitate colony nucleated by climb of a glide dislocation, initially on (111), with $\underline{b}=a/2[10\bar{1}]$. The dislocation has been sectioned twice by the foil, leaving arcs AB and CD in (a). The beam direction is close to [011] in (a) and to [111] in (b). (Heat treatment: S.T. 1 hour 550°C, quenched to 220°C, aged 5 minutes.)

precipitate colonies made with the foil surfaces, Figure 4.16. Similarly, Miekk-oja and Räty (1971) observed repeated nucleation of silver-rich precipitates from solid solutions of silver in copper behind dislocations which were shown to be a/2<110> glide dislocations on {111} planes before climbing. They found that these dislocations subsequently climbed in one of two different ways: (1) off the slip plane on smoothly curved surfaces, similar to that described above, or (2) into a crooked shape so that different segments of the dislocations climbed on different low-index planes intersecting the original slip plane. They further showed that these low index planes were of the types {110} and {111}, i.e., the planes of "easy climb" (Section 2.3.1) on which the chemical climb force, from a subsaturation of vacancies, was the greatest.

In the present research, the shapes of precipitate colonies behind certain glide dislocations suggested that different segments of these dislocations had climbed on separate crystallographic planes also. The term "segmented climb" shall be used here to refer to this mode of climb. Micrographs of precipitate colonies apparently resulting from segmented climb are shown in Figures 4.17 and 4.14(b). In Figure 4.17, the dislocation between AB has climbed through the lattice from left to right. The precipitate colony nucleated by this dislocation is separated into bands of precipitates. This effect is thought to be associated with the climb of adjacent dislocation segments on separate

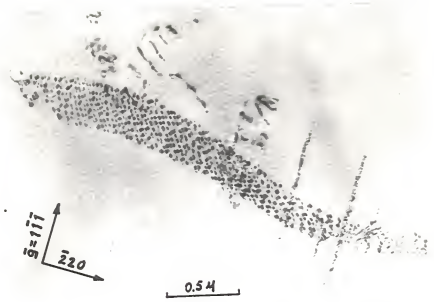

Figure 4.16. Precipitate colony exhibiting curved traces of intersection with the foil surfaces, indicating a curved climb path of the nucleating dislocation. (Heat treatment: S.T. 1 hour 550°C, quenched to 220°C, aged 5 minutes.)

Figure 4.17. Banded precipitate colony nucleated by "segmented climb" of the dislocation AB from left to right through the foil. (Heat treatment: S.T. 1 hour 550°C, quenched to 220°C, aged 5 minutes.)

crystallographic planes. The resultant precipitate colony has a corrugated shape. No precipitation occurred in areas between the bands, e.g., at C. Such precipitate-free areas can also be seen in the climb path of the dislocation in Figure 4.14(b). For some reason the dislocation is ineffective in nucleating precipitates in these regions of its climb path. A possible explanation is that precipitation occurs readily on those segments of the dislocation which climb on the separate crystallographic planes, but not on those curved arcs of the dislocation which bridge the gaps between these planes. This will be discussed further in Section 4.4.6.

The segmented climb of initial glide dislocations was observed only in the Al-3.85 wt.% Cu alloy. An attempt was made to determine the planes upon which segmented climb occurred by trace analysis of the intersections of the precipitate colony with the foil surface, but this proved to be impractical for two reasons. First, as pointed out by Miekk-oja and Räty (1971), the possible planes of easy climb can be numerous, i.e., six {110} and four {111} planes, so that the trace analysis is best accomplished by using single crystals cut to special orientations. Such crystals were not available in this research. Secondly, the traces of the intersections of the bands of precipitates with the foil surfaces were never well defined, a condition which leads to poor accuracy in the stereographic analysis.

There is evidence that the tendency for glide dislocations to climb either on smoothly curved surfaces or to segment and climb on different planes depends upon the line direction of the dislocation before climb began. For example, in Figure 4.18 the curved dislocation along ABC has nucleated a smoothly curved precipitate colony between A and B, and a corrugated colony between B and C. Presumably, the initial line direction of the dislocation segment between B and C was favorable for rapid climb onto the different planes of easy climb.

4.3. Identification and Characterization of the Precipitate Phase

Figure 4.19(a) is a diffraction pattern in the exact (001) matrix orientation taken from the group of precipitates shown in Figure 4.19(b). The image quality in (b) is poor since the exact (001) orientation is a many-beam condition. The geometry in Figure 4.19(b) is as follows. The foil has sectioned three {110} habits of dislocation climb sources, numbered 1, 2 and 3. These habits are viewed edge-on in this orientation. Habits 1 and 2 lie on (110) while habit 3 lies on $(\bar{1}10)$. Small precipitate platelets are dispersed over the three habits. Two orientations of precipitates are present lying parallel to the (100) and (010) matrix planes. The precipitate reflections in the diffraction pattern are streaked in the <100> directions owing to

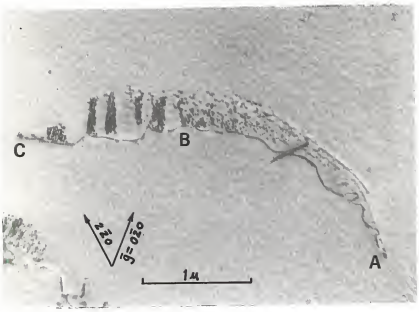

Figure 4.18. A glide dislocation which climbed on a smoothly-curved surface between A and B, and underwent segmented climb between B and C. (Heat treatment: S.T. 1 hour 515°C, quenched to 220°C, aged 5 minutes.)

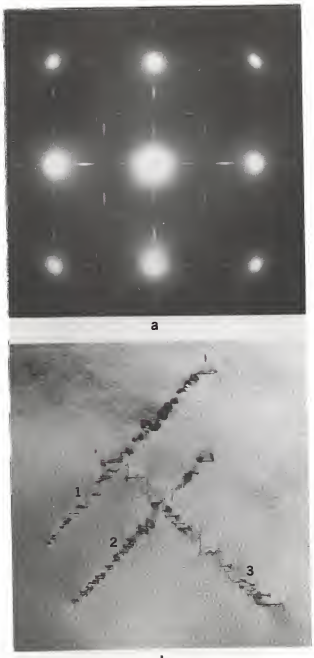

Figure 4.19. (a) (001) diffraction pattern showing precipitate reflections, taken from the area of the foil shown in (b). (Heat treatment: S.T. 1 hour 550°C, quenched to 220°C, aged 30 minutes.)

the relaxation of the Laue condition along the thin dimension of the platelets. The diffraction pattern can be analyzed on the basis of three superimposed patterns shown in Figure 4.20(a)-(c), where we consider only the lower right-hand quadrant of the pattern. The pattern in (a) is the (001) matrix pattern. The pattern in (b) is indexed on the basis of two θ' orientations parallel to (100) and (010) matrix planes, using the lattice parameters of 4.04Å and 5.8Å for θ' (Section 2.2). The remaining reflections in (c) are due to double diffraction from the matrix {200} and {220} beams. Double diffraction is a common occurrence in foils containing precipitates with dimensions much smaller than the foil thickness. The composite pattern, shown in (d), matches the experimental pattern. Thus the precipitates are positively identified as the θ' phase, in agreement with the known fact that θ' is the only metastable phase which nucleates on dislocations in Al-Cu.

In the present research, conditions were chosen to insure that the θ' phase was the only precipitate phase present after heat treatment. Its distribution was always associated with the climbing dislocations.

The appearance of the precipitate colonies at high magnifications is shown in Figure 4.21. These are typical colonies nucleated on dislocation climb sources. The colony in (a) was nucleated on the (101) source habit in the plane of the foil. In (b), five different {110} habits were generated at the same source particle and have nucleated

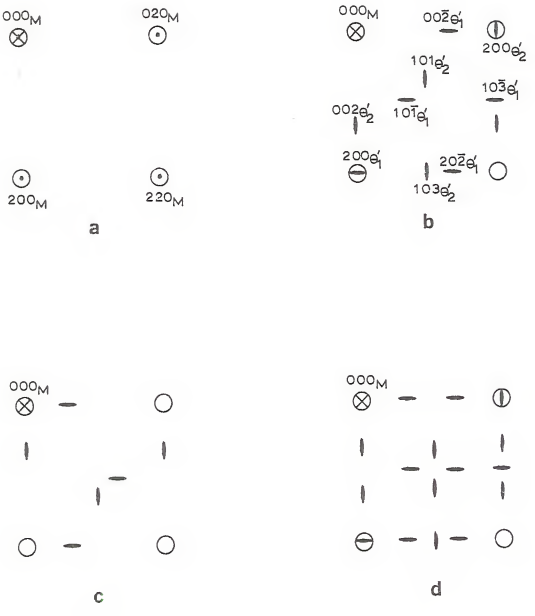

Figure 4.20. Analysis of the lower, right-hand quadrant of the diffraction pattern in Figure 4.14(a). (a) (001) matrix pattern; (b) precipitate reflections from θ' platelets lying parallel to (010) matrix planes (θ'_1), and to (100) matrix planes (θ'_2); (c) double diffraction from matrix 200 and 220 reflections; (d) combination of (a), (b), and (c). Compare with Figure 4.14(a).

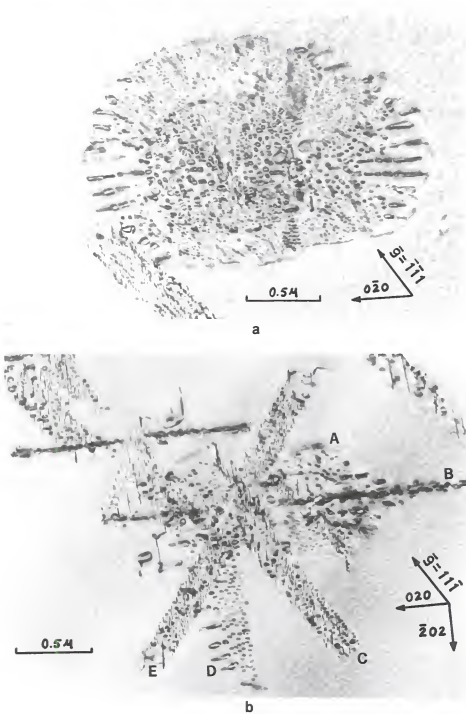

Figure 4.21. (a) and (b) Appearance of typical precipitate colonies generated on the {110} habits of climb sources. (c) and (d) Schematic diagrams illustrating the geometry of the colonies. See text for description. (Heat treatment: S.T. 1 hour 550°C, quenched to 220°C, aged 5 minutes.)

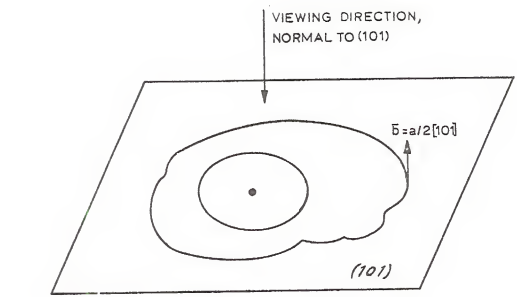

c

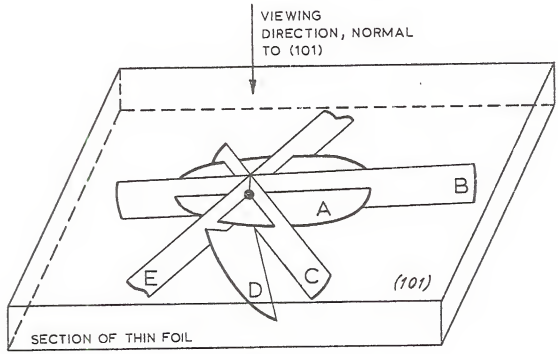

d

Figure 4.21. Continued.

precipitate colonies. One habit lies in the plane of the foil at A, one habit is viewed edge-on at B, and three other habits at C, D and E are inclined through the foil. The geometries of these sources are shown schematically in Figure 4.21(c) and (d).

Often the best condition for imaging the precipitates in a colony was also a condition for "invisibility" of the dislocation loop bounding the colony, e.g., Figure 4.21(a). This was particularly true when examining colonies on dislocation climb sources where the best projected view of a colony was obtained with the beam oriented approximately normal to the colony, and hence to the bounding source loop. However, since the source loops are pure-edge with their Burgers vectors normal to their habit planes, any two-beam reflection selected to view the precipitate colony in this orientation has its $\bar{g}$-vector perpendicular to the Burgers vectors of the loops. Thus the loop will be "invisible" when viewed normal to its habit plane. This is the case in Figure 4.21(a) where $\bar{g}\cdot\bar{b}=0$ for the loop bounding the precipitate colony and only residual contrast due to the pure edge-nature of the loop is detected.

Likewise in Figure 4.21(b), the dislocations bounding the colonies at A, C and D are invisible, whereas the one at E is visible. A consistent interpretation of the geometry of this source array is as follows. The beam direction is close to [101] and $\bar{g}=11\bar{1}$ for this image. Habit A lies on the (101) plane of the foil (see Figure 4.21(d)). The

Burgers vector of its source loop, being pure edge, is a/2[101]. Thus the loop is invisible for $\bar{g}=11\bar{1}$. The source loops bounding the habits C and D are also invisible. These dislocations must have the other two a/2<110> Burgers vectors which cause invisibility for the $11\bar{1}$ reflection, namely, a/2[011] and a/2[$1\bar{1}0$]. Habit B lies on the (101) plane parallel to the beam and is viewed edge-on. The Burgers vector of its source loops must be a/2[$\bar{1}01$]. The source loop bounding habit E must have one of the two remaining a/2<110> Burgers vectors, namely, a/2[110] or a/2[$01\bar{1}$], both of which would be visible for the $11\bar{1}$ reflection. The dislocation is visible at E.

It is difficult to determine whether the smallest precipitates in these colonies are imaged by strain contrast in the matrix or by structure factor contrast (Ashby and Brown, 1963). The larger precipitates in a colony are imaged by the dislocation loops bounding the periphery of the platelets (Section 4.4).

In Section 2.2, it was pointed out that because of dislocation strain effects, only two θ' orientations will nucleate on any given a/2<110> dislocation. The missing orientation has its principal misfit (normal to the plane of the platelet) perpendicular to the Burgers vector of the dislocation so that its strain field is not relieved by the stress field of the dislocation. Careful examination of a number of precipitate colonies at dislocation climb sources revealed that only two θ' orientations were present in any given colony.

The missing orientation was always that {100} orientation whose misfit would be perpendicular to the Burgers vector of the source loop bounding the colony. This is illustrated in Figures 4.21(b), 4.22 and 4.23.

First, Figure 4.22 shows bright and dark field images of several precipitate colonies on climb sources in a foil whose normal was close to [101]. The foil was oriented with the electron beam close to [101]. The dark field image was taken from a precipitate reflection from the (010) θ' orientation parallel to the beam. Climb source A (and its precipitate colony) lies on (101), and its source loops, being pure edge, have Burgers vectors a/2[101]. At B, two other source habits lie on {110} planes inclined to the foil. The Burgers vectors of their source loops were not determined but they cannot be a/2[101]. Now, if all three {100} orientations of θ' were present in the colony at A, the orientation imaged in the dark field would be observed throughout source A as in the sources at B. The misfit of this missing (010) orientation is perpendicular to the a/2[101] Burgers vector of the source loops at A (which are "invisible" in this image). The few precipitates on (010) in the middle of source A in the dark field image were found to lie within small source loops lying on other {110} habits, when this source was examined in another orientation.

Next, in Figure 4.21(b), the source habit at B lies on the $(\bar{1}01)$ plane and is viewed edge-on. The Burgers vectors of its source loops, being pure edge, must be a/2$[\bar{1}01]$.

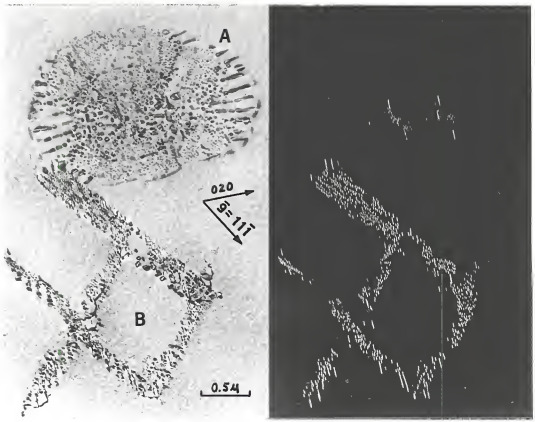

Figure 4.22. Bright-field and dark-field images of precipitate colonies on dislocation climb sources. The colony at A lies in the (101) plane of the foil. The colonies at B are inclined through the foil. The dark-field was taken from a precipitate reflection from the (010) θ' orientation lying parallel to the [101] beam direction. (Heat treatment: S.T. 1 hour 550°C, quenched to 220°C, aged 5 minutes.)

The (010) θ' orientation, which is parallel to the beam direction and also viewed edge-on, is not present in habit B, although it is easily detected in habits C and E. Again, this is the θ' orientation whose misfit is perpendicular to the a/2[$\bar{1}$01] Burgers vector of the source loops bounding habit B.

The fact that θ' platelets lying parallel to the beam can indeed be seen if present in precipitate colonies viewed edge-on is shown in Figure 4.23. This micrograph was taken with the beam oriented near [001]. The two edge-on habits at A and B lie on (110) planes so that the bounding dislocation loops have Burgers vectors a/2[110]. Both the (010) and (100) orientations of θ' platelets can be clearly seen dispersed along the habits. Note that these are the two θ' orientations whose misfits are not perpendicular to the Burgers vector of the bounding dislocation loops and are therefore favored to be nucleated by the loops.

All three θ' orientations were never observed in a given precipitate colony. As pointed out above, the missing orientation was always that whose nucleation is not aided by the stress field of the dislocations bounding the colony. This was true for precipitate colonies generated by both climb sources and glide dislocations which climbed. This evidence leads to the important conclusion that the precipitates must have nucleated in the stress field near the dislocations as they climbed through the lattice, and not at some later time when the influence of the dislocation was no longer present,

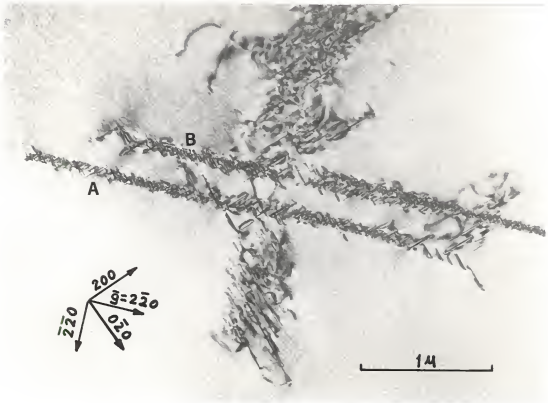

Figure 4.23. θ' precipitate colonies on climb source habits A and B which lie parallel to the beam. Two edge-on orientations of θ' platelets, (100) and (010), are clearly visible in colonies A and B. The beam direction is close to [001]. (Heat treatment: S.T. 1 hour 550°C, quenched to 220°C, aged 30 minutes.)

e.g., during aging. Since the dislocation climb sources are known to have operated during the high-temperature part of the quench, the precipitates must have nucleated during quenching.

Further evidence to support this conclusion was obtained by in situ aging experiments in the electron microscope. The results of these experiments are shown in the micrographs of Figure 4.24. These are images of a foil from a sample solution treated for one hour at 550°C, quenched into oil at 220°C and held only four seconds at 220°C, then water-quenched to room temperature. After electropolishing, the foil was placed in the heating stage of the microscope. The micrographs in Figure 4.24(a) and (b) were taken prior to heating. In (a), a dislocation climb source is viewed normal to its (011) habit of source loops which are "invisible" in this orientation and imaged by residual contrast. Since this is a climb source, we know that these dislocations climbed during quenching. A long, crooked dislocation, which was most probably a glide dislocation prior to quenching, is shown in (b). Its crooked shape is the only indication that it may have climbed during quenching. Now, if nucleation of the θ' precipitates does occur as the dislocations climb through the lattice during quenching, then the precipitates must already be present in the foil in (a) and (b). However, the four-second aging time at 220°C was insufficient to cause the precipitates to grow to visible sizes. The foil was then heated to 230°C in the microscope. After nine minutes at

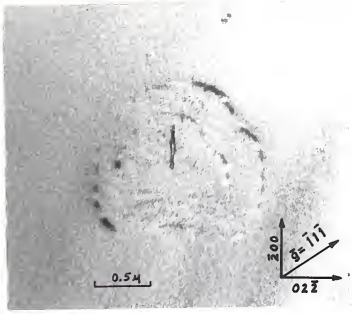

(a)

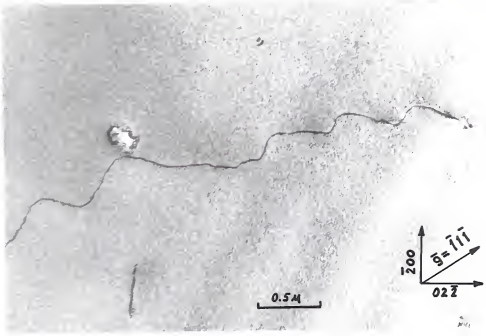

(b)

Figure 4.24. (a) A dislocation climb source, imaged by residual contrast, and (b) a long glide dislocation in a sample quenched from 550°C to 220°C and held only 4 seconds before quenching to room temperature.

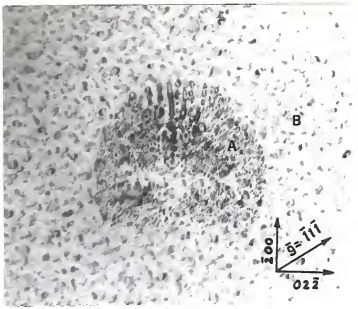

(c)

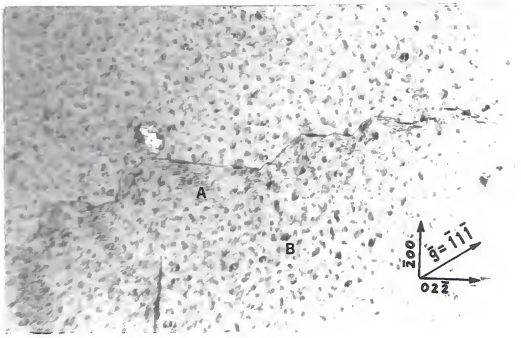

(d)

Figure 4.24. Continued. (c) and (d) Micrographs of the same dislocations in (a) and (b) after aging 9 minutes at 230°C in the electron microscope. The random precipitation at B has occurred at the foil surfaces. The precipitate colonies associated with the dislocations are now clearly visible at A.

230°C, these dislocations were rephotographed and are shown in (c) and (d). Clearly the precipitate colonies existed in the climb paths of the dislocations after quenching, and the nine-minute aging treatment has caused growth to visible sizes, points A in the micrographs. Careful observation is required to see the edge-on θ' platelets at A in the precipitate colony in (d). It is now apparent that this dislocation underwent segmented climb (Section 4.2.2). The random precipitation at points B throughout the micrographs in (c) and (d) results from θ' precipitation on the foil surfaces, an effect which is known to happen when thin foils of Al-Cu alloys are heated in the electron microscope (Thomas and Whelan, 1961).

From the pictures in Figure 4.24 alone, the argument could be made that solute atoms may have segregated to the dislocations and were then left behind when the dislocations climbed away, creating supersaturated layers of copper in the climb paths. Then aging at 230°C caused nucleation and growth of the precipitates from the supersaturated layers. However, if this were the case, all three orientations of θ' should nucleate in a given precipitate colony, and this is inconsistent with the observations discussed above.

4.4. Further Geometric Analyses

The previous two sections established information about the dislocation climb and precipitation which is basic to understanding the details of this section. Included here are (1) descriptions of the various geometrical aspects of the precipitate colonies, (2) explanation of some diffraction effects, and (3) other unusual features of the microstructures, in addition to repeated precipitation, which have not been previously reported. All these descriptions would prove useful to someone examining these types of microstructures for the first time.

4.4.1. Distribution of Precipitates in Colonies at Climb Sources

We consider the distribution of precipitates in a colony on a single {110} habit of a climb source. A typical colony is shown in Figure 4.25. The distribution of precipitates is twofold. First, there is a densely-populated region of small precipitates which covers approximately the central three-fourths of the colony. Secondly, there are two regions marked A on either side of the colony which are comprised of rows of somewhat larger precipitates extending from the outer dislocation loop into the colony. These rows of precipitates shall be referred to as "precipitate stringers." The spacing between stringers is quite uniform. The dense precipitation is not present in the stringer regions. The stringers are always aligned in the <100> direction which is

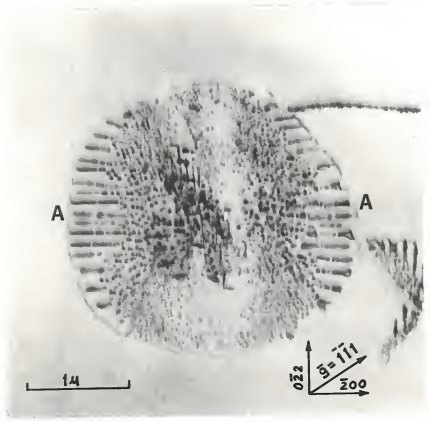

Figure 4.25. A typical precipitate colony on a {110} habit of a climb source exhibiting a central region of dense precipitation, and two regions at A of precipitate stringers aligned along the [100] direction in the plane of the colony.

contained in the {110} plane of the colony. The dislocation loop bounding the colony bows out locally between the stringers and is generally smoothly curved in those regions away from the stringers. The nature of the stringers will be discussed in detail in the next section.

There were five basic shapes of the precipitate colonies on climb source habits observed in these foils. These five shapes are shown schematically, with corresponding micrographs, in Figure 4.26. Shapes I and II were the most commonly observed. The typical colony with shape I was either circular or slightly elliptical in the [001] direction, and the region of dense precipitation was essentially continuous over the center of the colony. Shape II is similar to Shape I, except that there is a figure-eight-shaped region in the center which is void of precipitates. The experimental observations suggest that as the diameter of a colony with Shape I increases, it will tend toward Shape II. At present, there is no satisfactory explanation for the figure-eight-shaped region void of precipitates. Shape III is very elongated in the [001] direction, and the regions of stringers extend out beyond the projected sides of the ellipse. Such colonies were observed only occasionally. In Shape IV, the dislocation loop bounding the colony bows out along $[1\bar{1}0]$ at two points. Narrow precipitate-free zones extend in this direction from the center of the colony to these points. The discussion in Section 4.3.5 may account for the tendency to bow out to points, but there is no satisfactory

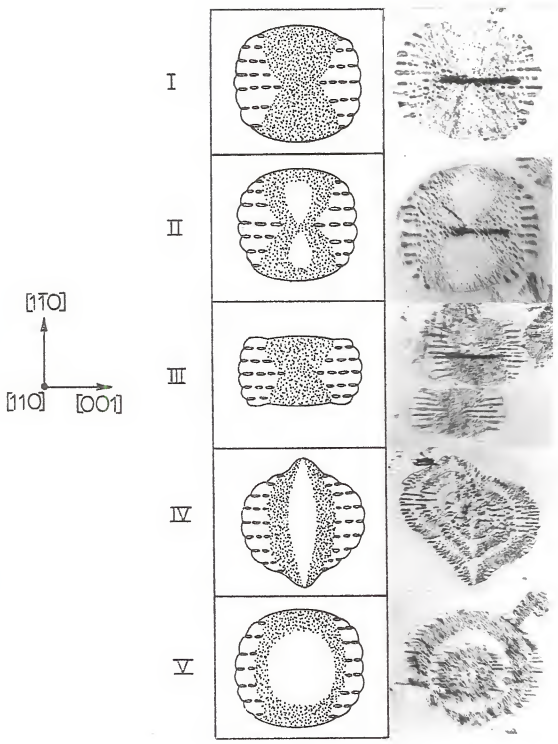

Figure 4.26. Five basic shapes of θ' precipitate colonies nucleated on {110} habits of climb sources in Al-Cu. All are oriented with reference to the crystal directions at left.

explanation for the precipitate-free zones in these directions. In Shape V, there is a well-defined boundary where precipitation begins behind the climbing source loop. Inside this boundary the region is void of precipitates (except where another interior loop has climbed). A possible explanation for this shape is as follows. Different climb sources become active in nucleating loops at different times during quenching. Any climb of the loops which occurred before the temperature passed below the θ' solvus temperature does not nucleate precipitates. Further climb below the θ' solvus temperature generates ring-shaped, precipitate colonies behind the loops.

For the case where several concentric source loops are generated on a given {110} habit, each successive, interior loop nucleates the same basic colony shape on a smaller scale, e.g., Shape IV in Figure 4.26.

4.4.2. Geometry of the Precipitate Stringers

One of the early problems to be solved concerned the identification of the defects in the stringers. The stringers were already visible in samples quenched to the aging temperature and held for very short times (Figure 4.27) although the general precipitate colony was not yet visible. The stringers appear as rows of small dots, so that the contrast cannot be interpreted further at this stage. In samples aged for longer times, the stringers are imaged as rows of small dislocation loops, Figures 4.21 and 4.25.

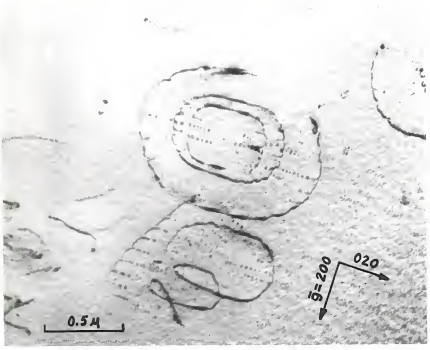

Figure 4.27. Stringers of small dots along [010] in a sample quenched from 550°C to 220°C and aged only 8 seconds.

Three possible mechanisms were considered for the generation of stringers of small loops behind the climbing source loops. These were:

(1) Small loops were pinched off in some regular manner from the climbing source loops.

(2) Vacancy debris was left behind the climbing source loops from some regular arrangement of superjogs or kinks. This debris then coalesced into small loops.

(3) θ' precipitates were nucleated repeatedly in regular rows. The small loops would be misfit loops around the periphery of the platelets.

It is shown in the next section that the Burgers vectors of the small loops in stringers are not the same as those of the climbing source loops. Therefore, they are not pinched-off loops and we can omit possibility (1). For the moment, we disregard possibility (2) and show that the stringers are definitely composed of rows of θ' precipitates.

When foils were viewed along beam directions parallel to {100} planes, θ' platelets were definitely imaged edge-on in some stringers, as at A and B in Figure 4.28(a). This is confirmed in the dark field image, taken from a θ' reflection, in Figure 4.28(b). Other stringers at C contain θ' platelets on another {100} orientation which is not parallel to the beam. In this case, the precipitates are large enough to exhibit displacement fringe contrast (see Section 2.5.3). Another dark field image at high magnification, Figure 4.29(b),

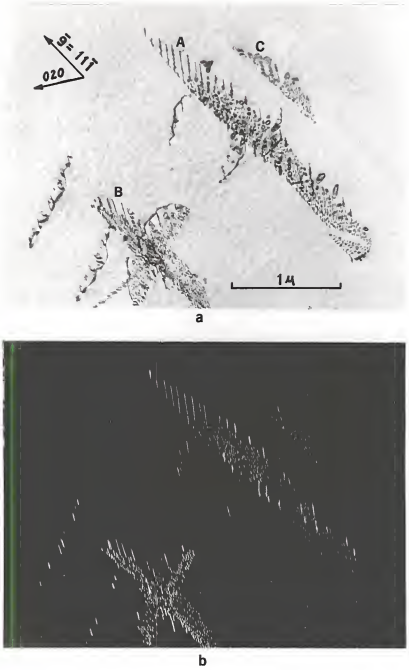

Figure 4.28. (a) Bright-field and (b) dark-field images of a foil oriented so that the stringers at A and B are clearly imaged as θ' platelets viewed edge-on. The precipitates at C are inclined to the beam and exhibit fringes. (Heat treatment: S.T. 1 hour 550°C, quenched to 220°C, aged 5 minutes.)

shows that the stringers contain separate, but closely-spaced, precipitates oriented parallel to the beam. Hence, the stringers are definitely composed of θ' platelets, and the dislocation loops are assumed to be misfit loops at the platelet peripheries (see Section 4.4.3).

Consider now mechanism number (2) above, requiring vacancy debris to be left behind the climbing source loops. Boyd and Edington (1971) observed small dislocation loops lying just inside large, climb source loops in Al-2.5 wt.% Cu. These were analyzed to be prismatic edge-loops with all possible a/2<110> Burgers vectors. They proposed that the small loops were present from condensation of vacancy debris generated by the motion of edge jogs and screw kinks on the climbing source loops. In the present case, such small loops could act as nucleation sites for the precipitate stringers. If this were so, it would be expected that all three θ' orientations could be nucleated since the small loops had all possible a/2<110> Burgers vectors. It was shown earlier that only two of the three possible θ' orientations nucleated in any given precipitate colony. The vacancy debris mechanism therefore does not explain the experimental results. The origin of the precipitate stringers will be discussed in Chapter 5.

As mentioned previously, the stringers in precipitate colonies on climb sources always lie along the <100> direction in the plane of the colony, Figure 4.30. Typically, the boundaries of the two stringer regions are fan-shaped. That

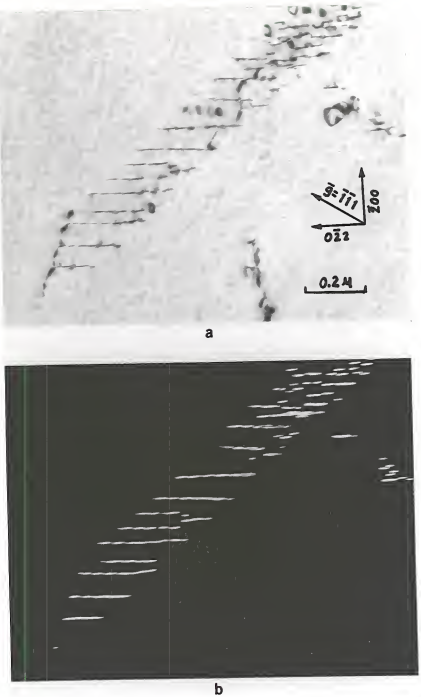

Figure 4.29. (a) Bright-field and (b) dark-field images at high magnification showing that the precipitate stringers are actually composed of separate but closely-spaced θ' platelets. (Heat treatment: S.T. 1 hour 550°C, quenched to 220°C, aged 5 minutes.)

is, the stringers at the center of these regions extend farthest into the middle of the colony, points A in Figure 4.30. The stringers become progressively shorter in going to the ends of the stringer regions, points B.

As aging time at temperature is increased, the precipitates in a stringer grow and probably coalesce, so that stringer geometry evolves through the sequence of shapes shown in Figure 4.31. The outermost precipitate tends to grow into a Y-shape along the bowed-out, climb source loop.

A given source loop always nucleated stringers of the two θ' orientations compatible with its Burgers vector. However, platelets of only one orientation were nucleated in any given stringer, Figure 4.29. Thus, there is some geometrical restriction about the origin of a stringer at or near the dislocation loop which favors repeated nucleation of only one θ' orientation.

Measurements were made of the average spacing between stringers, and the average spacing between precipitates in a stringer. The former were made in precipitate colonies viewed normal to their {110} habits so as to obtain the true projected spacing. The latter were made on the dark field image in Figure 4.29(b). This sample was aged for a short enough time that coalescence of precipitates had not yet begun. The average spacing between stringers, measured normal to the <100> direction was found to be 0.096μ (960Å). The average spacing between precipitates in a stringer was found

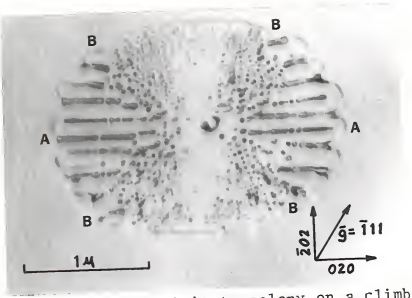

Figure 4.30. Typical precipitate colony on a climb source illustrating the fan-shaped boundaries of the precipitate stringer regions. (Heat treatment: S.T. 1 hour 550°C, quenched to 220°C, aged 5 minutes.)

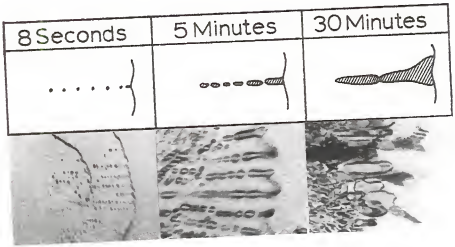

Figure 4.31. Evolution of the geometry of precipitate stringers at climb sources with increasing time at the aging temperature.

to be 0.037μ (370Å), or about one-third of the spacing between stringers.

Precipitate stringers were also observed in θ' colonies nucleated by glide dislocations which climbed, Figure 4.14(a). The average spacing between these stringers was in good agreement with the spacing of stringers at climb sources. Stringers were not present at glide dislocations that underwent segmented climb, Figure 4.14(b).

A further feature of Figure 4.14(a) is that a well-defined boundary exists between stringers and dense precipitation. Since the spacing between stringers is larger than the spacing between precipitates in the region of dense nucleation, it is unlikely that the latter nucleated at the same preferred sites as the stringers. In other words, there has been a change in the mode of nucleation at some point near the end of the quench.

4.4.3. Determination of the Burgers Vectors of Small Loops Within Precipitate Colonies

It was stated previously that the small loops visible in a precipitate colony are loops at the periphery of θ' platelets. It will now be shown that the diffraction contrast at these loops is consistent with this hypothesis, and that these are not loops formed by other possible mechanisms. First, it is known that the misfit between matrix and precipitate planes at the peripheral edge of θ' platelets is accommodated by the presence of a<100> type edge-dislocation

loops around the platelets (Weatherly and Nicholson, 1968; Laird and Aaronson, 1968).

Figure 4.32 shows a precipitate colony generated on a climb source in the (101) plane of the foil. The source loop, being pure-edge, has Burgers vector a/2[101], so that it is invisible for this reflection. Consistent with this Burgers vector, the precipitate colony contains θ' platelets lying on (100) and (001) planes. If some of the platelets are large enough, we should expect to see small loops with Burgers vectors a[100] or a[001] at their peripheries. In Figure 4.32, four stringers of loops are located with arrows and marked either 1 or 2. The Burgers vectors of these loops were determined by invisibility conditions from a number of two-beam images taken for different foil orientations. Selected images are shown in Figure 4.33, and the visibility data are summarized in Table 4.1.

Table 4.1

Summary of Visibility Data for the Images of Figure 4.33

$\bar{g}$=	$1\bar{1}\bar{1}$	$0\bar{2}0$	$\bar{1}\bar{1}1$	$\bar{2}20$	$20\bar{2}$	$02\bar{2}$	$\bar{b}$
Source Loop	I	I	I	V	I	V	a/2[101]
Loops in Stringers 1	V	I	V	I	V	V	a[001]
Loops in Stringers 2	V	I	V	V	V	I	a[100]
Beam Direction	101	101	101	111	111	111	

Note: V = Visible; I = Invisible.

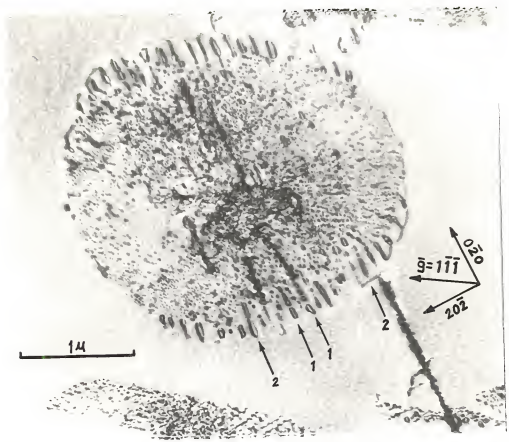

Figure 4.32. Micrograph of a precipitate colony on a climb source showing the location (arrows) of four rows of small dislocation loops whose Burgers vectors were to be determined. (Heat treatment: S.T. 1 hour 550°C, quenched to 220°C, aged 5 minutes.)

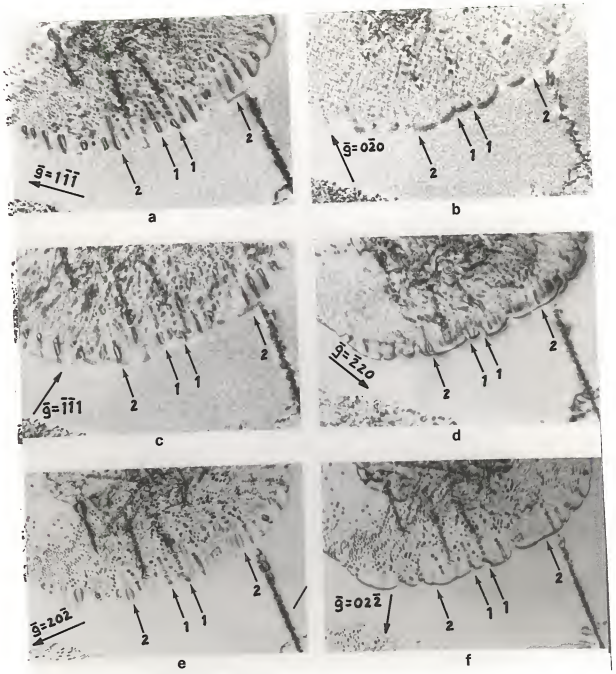

Figure 4.33. Series of micrographs for determining the Burgers vectors of the small dislocation loops in the arrowed rows from invisibility conditions. The invisibility data are summarized in Table 4.1.

The Burgers vectors of the loops in stringers 1 are identified as a[001] and those in stringers 2 as a[100]. These are consistent with the Burgers vectors of the peripheral loops of the two orientations of θ' platelets expected in this colony.

Now it will be shown how the data of Table 4.1 rule out other possible origins for the loops:

(1) It is conceivable that kinks in the climbing source loop could cause portions to trail behind and pinch off, leaving the small loops. However, the small loops would then have the same a/2[101] Burgers vector as the source loop. Table 4.1 shows that the small loops are visible on several reflections where the source loop is invisible. Therefore they cannot be pinched-off loops.

(2) If the θ' platelets form in front of the advancing source loop, the source loop could pinch off around the platelets, reacting with the a<100> peripheral loops around the platelets. Two reactions are possible, depending on the platelet orientation:

$$a/2[101] + a[100] \rightarrow a/2[301] \quad \text{for } \theta' \text{ on } (100),$$

$$a/2[101] + a[001] \rightarrow a/2[103] \quad \text{for } \theta' \text{ on } (001).$$

However, both resultant a/2<103> Burgers vectors can be ruled out since the loops in stringers 1 are invisible for the $\bar{2}20$ reflection.

(3) Frank sessile loops, having a/3<111> Burgers vectors, can form by the collapse of vacancy clusters on {111} planes. Such partial dislocations are invisible for $\vec{g}\cdot\vec{b}=0$

and ±1/3 and visible for all other products (Silcock and Tunstall, 1964; Hirsch et al., 1965). All four possible a/3<111> Burgers vectors can be eliminated by comparing the data in Table 4.1 with these visibility criteria, so that the loops are not Frank loops.

(4) All six possible a/2<110> Burgers vectors can be eliminated by the combinations of visible and invisible images in Table 4.1. Therefore the loops cannot be prismatic loops on {111} with $\vec{b}$=a/2<110>, formed from Frank sessile loops by the passage of a/6<112> Shockley partials over the loops.

(5) The loops cannot be pure-edge, vacancy-condensation loops with b=a/2<110> on {110} planes (of the type observed by Boyd and Edington (1971) lying just within source loops), since all possible a/2<110> Burgers vectors can be ruled out.

Thus, it is concluded that the small loops visible in precipitate colonies have Burgers vectors of the type a<100> and lie at the periphery of the θ' platelets.

4.4.4. "Secondary" Climb Sources

A characteristic grouping of precipitate colonies observed often is shown in Figure 4.34(a). Here a long glide dislocation climbed through the lattice to its final position A-A, where it is out of contrast. In climbing, this dislocation nucleated the large precipitate colony P in its path. At the base of this colony, a number of {110} habits of climb sources have been activated and nucleated their own precipitate

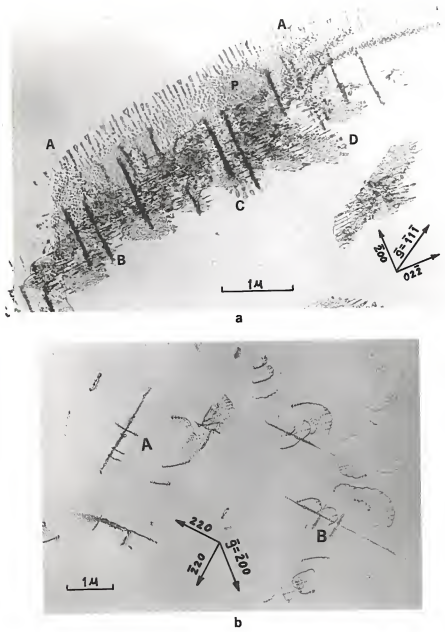

Figure 4.34. (a) Secondary climb sources B, C, and D, generated in the precipitate colony P that was nucleated by climb of the long glide dislocation which is out of contrast between AA. (b) Secondary climb sources A and B generated in the precipitate colonies at primary climb sources (viewed edge-on in this orientation).

colonies. Some of these {110} habits are viewed edge-on (as at B), some lie in the plane of the foil (as at C), and some are inclined through the foil (as at D). A similar configuration was shown in Figure 4.14(b).

It is proposed that these configurations evolved in the following manner. The long glide dislocation began to climb shortly after the onset of quenching. When the sample temperature passed below the θ' solvus, this dislocation began to nucleate θ' precipitates in its climb path. Some of the earliest-nucleated platelets acted as source particles and generated the climb source loops on {110} planes, and these then nucleated their own precipitate colonies.

The term "secondary climb sources" shall be used to distinguish sources nucleated at θ' platelets in this manner from "primary" climb sources nucleated on insoluble particles existing at the solution treatment temperature. This seems an appropriate designation since the secondary sources nucleate only if the θ' precipitation reaction occurs, whereas primary sources operate independent of the precipitation.

From the observation that secondary climb sources were always located at the base of the precipitate colonies generated by the long climbing dislocations, it can be deduced that their nucleation occurs within some limited, time-temperature range just below the θ' solvus when the earliest θ' precipitates formed. The diameters of the largest secondary source loops were never as large as the diameters of the largest primary source loops in the same foil, in

agreement with the conclusion that the latter are nucleated earlier in the quench and consume more vacancies.

Now, if secondary climb sources are indeed nucleated by θ' platelets, they could nucleate in precipitate colonies on primary climb sources as well. Such configurations were also observed, as shown in Figure 4.34(b). In this micrograph, the beam is approximately parallel to [001] so that climb source habits on (110) and ($\bar{1}$10) planes are viewed edge-on as at A and B. The smaller source habits at A and B were obviously nucleated at different sites along the two larger habits. Therefore, they all could not have been nucleated at the original source particle. As they appear to have nucleated in the planes of the larger habits, they were most probably nucleated at θ' precipitates in these planes.

A model will now be presented to illustrate how a θ' platelet could act as a source particle for the nucleation of climb source loops on {110} planes. As discussed in the previous section, the misfit between matrix and precipitate planes at the peripheral edge of θ' platelets is accommodated by the presence of a<001> edge-dislocation loops around the platelets. The extra half-plane must be contained in the precipitate. Furthermore, Laird and Aaronson (1968) have shown that θ' platelets of appreciable size are often octagonal-shaped with their edges lying along the <100> and <110> directions within the plane of the platelet. Consider then such an octagonal-shaped platelet lying parallel to the (001) matrix planes with its c-axis parallel to [001] matrix,

Figure 4.35(a). Two of its eight sides lie parallel to the [100], [010], [110] and [$\bar{1}$10] directions, respectively. For convenience, we assume the thickness of the platelet in its c-direction is such that it has one a[001] dislocation loop at its edge. Now let the two segments of this a[001] loop along [010] between AB, and along [100] between CD dissociate according to the reactions:

$$a[001] \rightarrow a/2[101] + a/2[\bar{1}01] \quad \text{between AB,}$$

$$a[001] \rightarrow a/2[011] + a/2[0\bar{1}1] \quad \text{between CD,}$$

which occur without energy change. The dissociated configuration is shown in Figure 4.35(b). The resultant dislocations are pure-edge segments between AB and CD. Assume further that these segments are free to climb as pure-edge dislocations and that the corners A, B, C and D pin them at these points. These segments of pure-edge dislocations can now operate by climb to produce successive loops on the appropriate {110} planes, as in Figure 4.35(c), in the same manner as the original model of a climb source proposed by Bardeen and Herring (1952). In this way, a given θ' platelet could produce edge-loops on four possible {110} planes.

Since the extra half plane of the original a[100] loop was contained within the precipitate, the initial climb of the dissociated dislocation segments must proceed through a small volume of precipitate before entering the matrix. As the growth of θ' platelets from the matrix generates vacancies within the precipitate (Section 2.2), dislocation climb is aided by the precipitation.

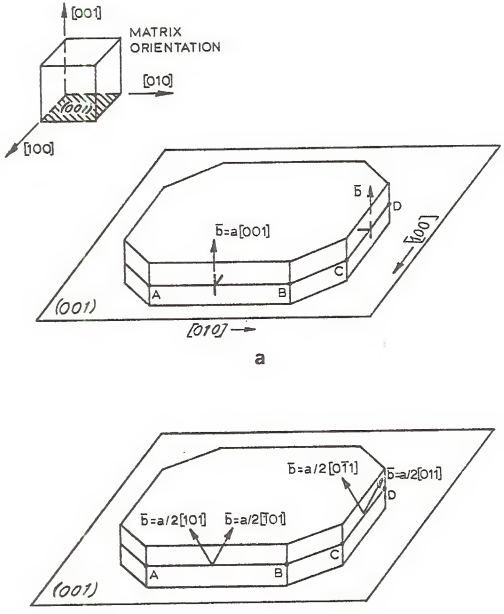

Figure 4.35. Model for the operation of a climb source at a θ' platelet. (a) θ' platelet on (001) with a[100] misfit dislocation loop around its edge. (b) Dissociation of the a[100] loop into total edge dislocations along the portions AB and CD.

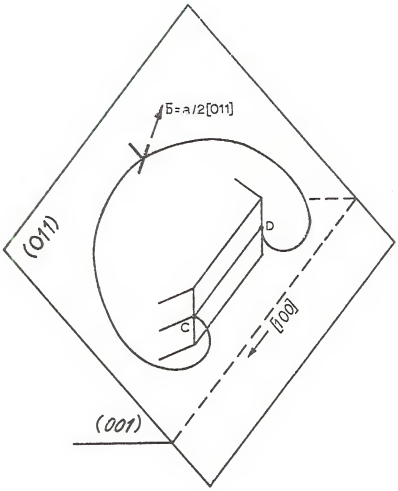

c

Figure 4.35. Continued. (c) The a/2[011] dislocation segment, pinned between C and D, operates as a Bardeen-Herring source by climb on the (011) plane (compare with Figure 2.7).

4.4.5. A Climb Source on (100)

On one occasion, when a foil was being examined in the (001) orientation, a planar, precipitate colony lying on (100) was observed. This colony is shown in Figure 4.36(a) at A. It is different from all other planar colonies observed which were nucleated by dislocation climb sources operating on {110} planes, e.g., at B in Figure 4.36(a). When the foil was tilted away from the (001) orientation, the colony was found to be bounded by an arc of a dislocation loop, Figure 4.36(b). Thus, it had the appearance of a climb source loop and associated precipitate colony, but lying on a (100) plane. This configuration was photographed on different two-beam reflections in several orientations. Selected images are shown in Figure 4.37. Invisibility conditions were used to determine the Burgers vector of the dislocation arc and orientation of the precipitates in the colony. This information is summarized in Table 4.2. The dislocation arc is invisible for $\bar{g}$=020 and 02$\bar{2}$. This eliminates all a<001> and a/2<110> Burgers vectors except a[100] and a/2[011]. Further, it is visible for $\bar{g}$=$\bar{1}\bar{1}$1 and $\bar{3}\bar{1}$1. This eliminates a/2[011] but not a[100]. All partial dislocations with Burgers vector a/3<111> or a/6<112> are eliminated by comparison of the data in Table 4.2 with the visible and invisible criteria for partial dislocations, namely, invisible for $\bar{g}\cdot\bar{b}$=0 or ±1/3 and visible for all other products (Silcock and Tunstall, 1964; Hirsch et al., 1965). It is concluded that the Burgers vector of the dislocation is a[100]. Since it lies on (100), it must

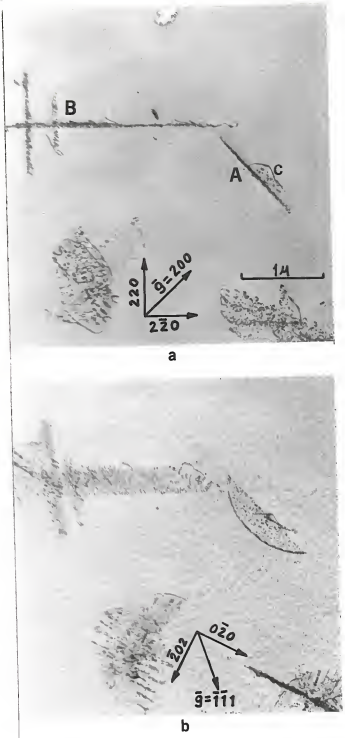

Figure 4.36. Two views of a precipitate colony A which is seen to lie on (100) from its edge-on orientation in (a). The beam direction is close to [001] in (a) and to [101] in (b). (Heat treatment: S.T. 1 hour 550°C, quenched to 220°C, aged 5 minutes.)

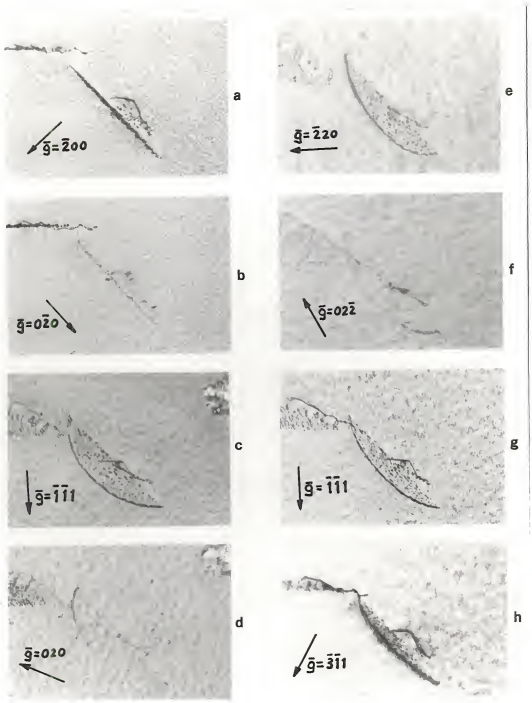

Figure 4.37. Series of micrographs for determining the Burgers vector of the dislocation arc bounding the precipitate colony A in Figure 4.36, and the orientation of θ' precipitates in the colony. The invisibility data are summarized in Table 4.2.

Table 4.2

Summary of Visibility Data for the Images of Figure 4.37

$\bar{g}$=	$\bar{2}00$	$0\bar{2}0$	$\bar{1}\bar{1}1$	020	$\bar{2}20$	$02\bar{2}$	$\bar{1}\bar{1}1$	$\bar{3}\bar{1}1$	Burgers Vector	Ppt. Orient.
Dislocation Arc	V	I	V	I	V	I	V	V	a[100]	
Precipitate Colony	V	I	V	I	V	I	V	V		(100)
Beam Direction	001	001	101	101	111	111	112	103		

Note: V = Visible; I = Invisible.

be an arc of a pure-edge loop. Hence, it can expand in the (100) plane only by climb. The presence of the precipitate colony on (100) indicates that it did indeed climb in this plane. As in the case of climb sources on {110} planes, it is assumed that the precipitate colony was nucleated by the a[100] dislocation as it climbed on (100). Now a dislocation with $\bar{b}$=a[100] favors nucleation of the (100) θ' orientation only. From Table 4.2 we see that the precipitates in the colony are invisible for $\bar{g}$=020 and $02\bar{2}$ and visible for all reflections for which h in (hkl) is non-zero. Since the precipitates are out of contrast only for $\bar{g}$-vectors normal to their misfit, and therefore to their habit plane, the colony must consist of precipitates having only the (100) orientation.

In summary, the configuration has all the characteristics of a climb source operating on (100) with b=a[100], and a precipitate colony of (100) θ' orientation nucleated by the source loop.

As in the case of climb sources on {110}, no stacking fault was observed within this loop. Since the stacking of planes in f.c.c. in the [100] direction is ABAB..., the loop must climb by the condensation of vacancies onto two adjacent (100) planes.

The small partial loop at C in Figure 4.36(a) was also analyzed and found to have $\vec{b}=a/2[10\bar{1}]$. This must be a secondary climb source of the {110}-type that was nucleated at a θ' platelet lying in the precipitate colony on (100).

This observation is the only reported case of a climb source in aluminum alloys operating to produce pure-edge loops on a cube plane. This is not surprising, however, since it was the only (100) source recognized as such among thousands of sources scanned in all these foils.

4.4.6. Nucleation of Preferred θ' Orientations During Segmented Climb

Figures 4.14(b) and 4.17 show corrugated-shaped, precipitate colonies which were nucleated by the segmented climb of glide dislocations on different crystallographic planes. Close examination of such colonies revealed that they consisted of adjacent bands of precipitates, each band containing only one of the two possible θ' orientations favored to be nucleated by the climbing dislocation. This "preferred

nucleation" results in different fringe effects in the bands marked 1 and 2 in Figure 4.14(b). The fringe appearance is a diffraction effect, to be discussed in the next section. This preferred nucleation of only one θ' orientation per band is shown clearly in Figure 4.38, which is a magnified portion of Figure 4.17 on a different reflection. Only the edge-on orientation of θ' is present in the bands marked A. Bands B therefore must contain the other possible θ' orientation favored to be nucleated, which is not parallel to the beam in this orientation. Between some bands are regions where no precipitates were nucleated, e.g., at points C. Depending on the diffracting vector, the misfit of the single θ' orientation in a band can cause the band to go completely out of contrast, as is the case in Figure 4.18 between C and D.

To account for the nucleation of only one θ' orientation in a given band, it is now suggested that a dislocation undergoing segmented climb tries to assume certain line directions on the different crystallographic planes. This is probably due largely to differences in line tension and ease of climb on certain planes. If the local line direction is such that the dislocation is pure edge, nucleation of two orientations is favored. If it is pure screw, no nucleation is favored since there are no tensile or compressive stresses around a screw dislocation. If it is mixed, the resulting stress field could favor the nucleation of one or the other θ' orientation, depending on the line direction and plane on which the dislocation lies. As stated in Section 4.2.2, it was not

Figure 4.38. Micrograph of a precipitate colony at high magnification illustrating that only one θ' orientation is present in different bands A and B which result from segmented climb of a glide dislocation. No precipitates were nucleated in the regions C between bands. (Heat treatment: S.T. 1 hour 550°C, quenched to 220°C, aged 5 minutes.)

possible to determine the different planes on which segmented climb occurred in these foils. However, the vacancy-annihilating climb of a/2<110> dislocation is easiest on {111} and {110} planes (Christian, 1965). Furthermore, Miekk-oja and Räty (1971) were able to show that segmented climb occurred on the {111} and {110} planes in Cu-Ag alloys. Their model for segmented climb on these planes will be used here to suggest how this preferred nucleation could occur and to explain the absence of precipitates between the bands.

Their model is shown in Figure 4.39 for segmented climb of a dislocation with Burgers vector a/2[011] which was initially a glide dislocation in its edge position on $(11\bar{1})$. It quickly deviates from its edge position along XY, so that some of its segments climb on the (011) plane and others climb on the (111) and $(\bar{1}11)$ planes, owing to the large chemical climb forces on these planes. After a short time, the dislocation assumes the multiply curved shape along RS due to line tension effects which are required to mate up the different segments between the planes. The exact curvatures depend on the widths of the segments, the ease of climb on the different planes, and the line tension, all of which are unknown. If it is assumed that this model is valid for segmented climb in Al-Cu, it is possible that the resulting curvatures favor nucleation of one of the two θ' orientations on a certain plane and the other orientation on another plane. If the curvature of the dislocation becomes so great near the plane junctions as to be appreciably screw in orientation,

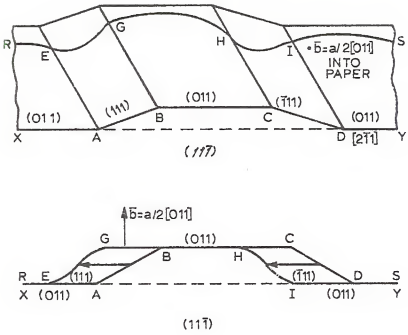

Figure 4.39. Model for segmented climb on the planes of easy climb. The dislocation, initially in its edge position XY on the (111) plane, climbs onto the planes of easy climb and assumes the curved shape RS (after Miekk-oja and Räty, 1971).

then no θ' would nucleate, accounting for the precipitate-free regions between bands in Figure 4.38.

It is interesting to note that Miekk-oja and Räty (1971) observed precipitation during segmented climb but did not report any preferred orientations of the precipitates associated with the climb. In Al-Cu, segmented climb always resulted in this preferred nucleation.

4.4.7. Displacement Fringe Contrast in a Precipitate Colony

Often, fringe effects were observed in the precipitate colonies, Figures 4.38 and 4.40(a). The intensity of the fringes varied with the deviation from the Bragg condition, becoming stronger as the deviation tended toward zero. Sometimes the fringe intensity varied with position over a given colony, appearing to be a function of the local precipitate density. The intensity of fringes increased in areas where the local precipitate density increased. The colony in Figure 4.40(a) has a very dense, but uniform distribution of precipitates so that the fringe intensity is large but uniform.

Similarly, Miekk-oja and Räty (1971) reported fringe effects in precipitate colonies nucleated behind climbing dislocations in Cu-Ag alloys. However, they did not explain the contrast mechanism, but described the effect simply as image contrast variations with foil depth depending strongly on diffraction conditions. It will now be shown that the fringe effect can be explained simply on the basis of

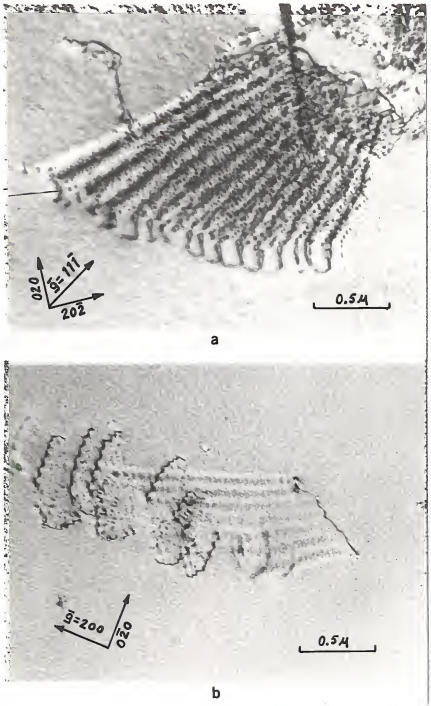

Figure 4.40. Displacement fringe contrast in precipitate colonies in samples quenched from 550°C to 220°C and aged for 5 minutes in (a) and for 1 minute in (b). The dislocation which nucleated the colony in (a) is out of contrast at the bottom of the colony.

displacement fringe contrast (Hirsch et al., 1965, p. 341). In Section 2.5.3, it was shown that displacement fringe contrast arises from abrupt phase changes in the incident and diffracted beams encountering an inclined sheet of precipitate which has displaced the matrix by an amount $\vec{R}$ in opposite directions across the sheet. Figure 4.41 illustrates that a planar, precipitate colony, composed of two orientations of θ' platelets of uniform size, has the resultant effect of a sheet of displacement field which displaces the matrix normal to the colony by a resultant displacement $\vec{R}_1$. Thus, whenever such a precipitate colony is inclined to the electron beam, the displacement fringe effect will be observed. Of course, a colony consisting of only one orientation of θ', whose misfit does not lie in the plane of the colony, would cause a displacement fringe effect also, as seen in Figure 4.38. Similarly, Warren (1974), using the method of Humble (1968), has computed electron micrographs of a plane of dilatation and obtained the displacement fringe effect. An example is shown in Figure 4.42. In addition, Clarebrough (1973) has shown that passage of a unit dislocation through an ordered lattice creates a planar displacement field at the slip plane which causes similar fringe effects in electron micrographs.

Now the intensity of displacement fringes is a function of the magnitude of the normal displacement $\vec{R}$. It can be visualized from Figure 4.41 that, if the density of precipitates varies over the colony, the local resultant displacement, $\vec{R}_1$, varies accordingly. Thus, the fringes will vary

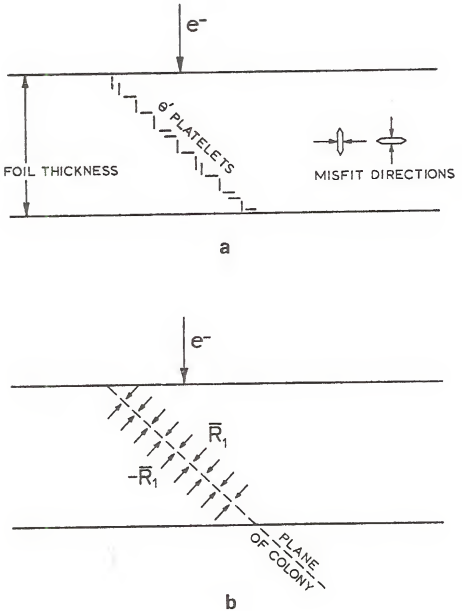

Figure 4.41. Diagram illustrating the origin of fringes in a θ' precipitate colony. (a) A planar colony containing two orientations of θ' platelets of uniform size is inclined through the foil. (b) The combined displacement fields of all the platelets act as an inclined sheet of displacement, $\bar{R}_1$, giving rise to the conditions for displacement fringe contrast.

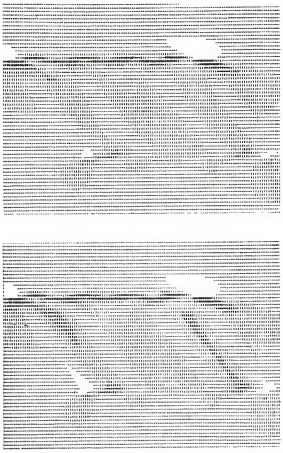

Figure 4.42. Computer-simulated electron micrographs of a plane of dilatation inclined through the foil, illustrating the displacement fringe effect. The fringes lie at about 45° to the horizontal, and there is a horizontal dislocation image at the top of the fringes. The strength of the dilatation increases from the top image to the bottom so that the intensity of the fringes increases (after Warren, 1974).

in intensity in agreement with experimental observation. When the sheet of displacement is not flat, the fringes will not be straight and parallel. Accordingly, the precipitate colony in Figure 4.40(a) has some curvature. Colonies were observed in which the fringes curved as much as 90°, indicating large curvature in the precipitate colony and, therefore, in the climb path of the dislocation.

Figure 4.40(b) shows fringes behind a dislocation in a foil which was quenched to 220°C and aged for only one minute at 220°C. Here the individual precipitates in the colony are not large enough to be visible, but their presence is indicated by the displacement fringes. The intensity of these fringes is less than in those of Figure 4.40(a). This could be due to differences in the deviation from the Bragg condition or by differences in the density of precipitates in the two colonies. A more likely explanation is that the average precipitate thickness is less for the shorter aging time, and therefore the resulting $\bar{R}_1$ is smaller. Such fringes in the absence of visible precipitates were observed often in samples aged for short times. They further support the conclusion that the θ' colonies are nucleated entirely during the quench.

4.4.8. Precipitate Colonies Associated with Subboundary Formation

Dislocation subboundaries were observed in all foils examined in this research, regardless of heat treatment. An example of a subboundary network is shown in Figure 4.43(a).

The dislocations were generated probably at grain boundaries during the quench. Normally, subboundaries are observed in cold-worked metals which have been given recovery anneals. In the present samples, boundary formation was essentially completed during the quench, since well-defined boundaries were observed in foils quenched into liquid nitrogen with no subsequent aging treatment. Both tilt boundaries and twist boundaries were observed, although tilt boundaries were more prevalent.

Figure 4.43(b) shows a junction of three tilt boundaries in a sample direct-quenched to 220°C and aged five minutes. Clearly, the dislocations have nucleated precipitate colonies in the process of climb. The climb paths of all dislocations in a given boundary are in the same direction as indicated by the positions of the precipitate colonies. It cannot be determined from such micrographs if the precipitates were nucleated while the boundaries were forming, or if the boundaries, once formed, climbed in a cooperative manner and nucleated the precipitate colonies. In either case, boundary formation was completed during the quench. Since edge dislocations are potential nucleation sites for θ' precipitates whereas screw dislocations are not, precipitate colonies were always observed to be associated with tilt boundaries, but they were not present at twist boundaries.

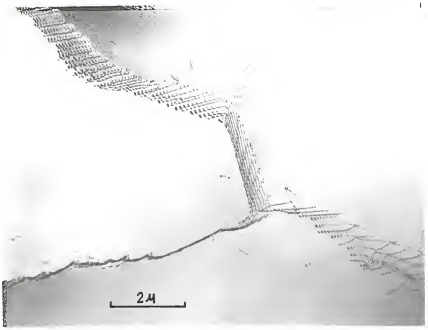

a

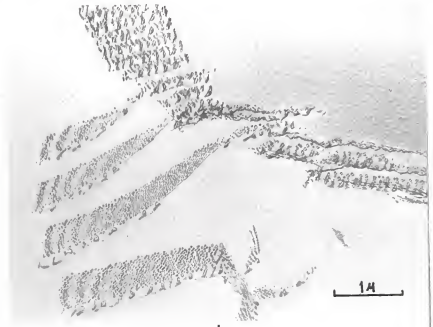

b

Figure 4.43. (a) Dislocation subboundaries in a sample direct-quenched from 550°C to 220°C and held only 8 seconds. (b) Precipitate colonies associated with subboundaries in a sample direct-quenched from 550°C to 220°C and aged 5 minutes.

4.5. Effects of Experimental Variables on Microstructure

Up to this point, evidence has been presented to characterize the nature of repeated precipitation at climbing dislocations. What remains is to determine the mechanisms by which the nucleation events take place. Information towards this objective was obtained by varying independently the following experimental parameters:

(1) time at constant aging temperature after direct-quenching,

(2) solution treatment temperature,

(3) temperature to which samples are direct-quenched,

(4) quench rate, and

(5) solute concentration.

In addition, a clearer picture of the operation of climb sources in Al-Cu alloys during quenching was obtained as well.

4.5.1. Effect of Time at Constant Aging Temperature

In this experiment, samples were solution-treated for one hour at 550°C, direct-quenched in oil at 220°C, and aged for various times. The resulting microstructures after aging for 8 seconds, 1 minute, 5 minutes, 30 minutes, and 2 hours, respectively, are shown in Figure 4.44 at low magnification. After 8 seconds at 220°C, the only visible precipitates are those in the stringers along the $[0\bar{1}0]$ direction. After aging one minute, other precipitates are just visible in the

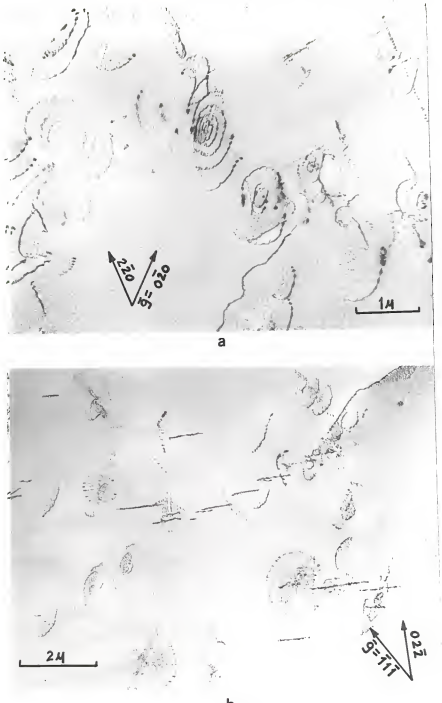

Figure 4.44. Sequence of micrographs showing the effect of time at constant aging temperature on colony growth. Samples were direct-quenched from 550°C and aged for (a) 8 seconds, (b) 1 minute, (c) 5 minutes, (d) 30 minutes, and (e) 2 hours.

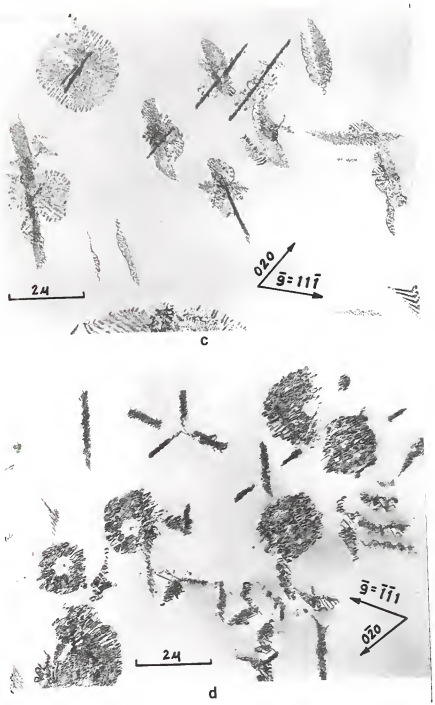

Figure 4.44. Continued.

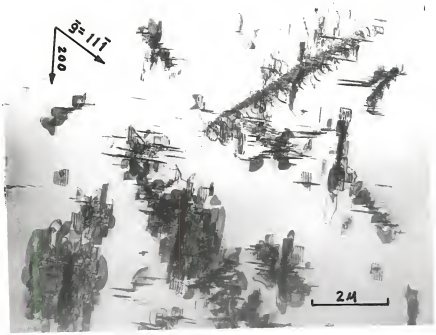

e

Figure 4.44. Continued.

colonies. After 5 minutes' aging, the interiors of the colonies are seen to be densely precipitated. All precipitates in the colonies were present at the start of the aging at 220°C (Section 4.3). After 30 minutes at 220°C, the precipitates are large enough to individually exhibit displacement fringe contrast, but precipitation is still localized within the original colonies. After two hours at 220°C, some scattered precipitates are observed outside the colonies, but the vast majority are still associated with the original colonies.

These results indicate that the density of precipitates generated by repeated nucleation is sufficiently large that aging for long times results essentially only in growth. Since there was no evidence for bands of precipitates spreading out from the colonies, an autocatalytic nucleation mechanism (Section 2.2) can be ruled out. In the original work on autocatalytic nucleation of θ' in Al-Cu, Lorimer (1970) found a uniform distribution of precipitates throughout the foil after aging 35 minutes at 240°C. In the presence of a large precipitate density, generated by repeated nucleation on climbing dislocations, evidently the driving force for autocatalytic nucleation is small, and solute depletion of the supersaturated lattice can be accomplished by growth of existing precipitates.

4.5.2. Effect of Solution Treatment Temperature

Five samples were solution treated for one hour at various temperatures within the solid solution range, then direct-quenched to 220°C and aged for five minutes. The five temperatures employed were 570°, 550°, 530°, 515° and 504°C, covering the range from just below the solidus temperature to just above the $\alpha \rightarrow \theta$ solvus temperature for the 3.85 wt.% Cu alloy (Figure 4.45). The major difference between samples was the quenched-in vacancy supersaturation, which increases exponentially with quenching temperature. However, to a lesser extent, the treatments also differed in quench rate. The resulting microstructures are shown in Figure 4.46 at low magnification.

First, repeated nucleation occurred during quenching in all samples as indicated by the presence of precipitate colonies associated with all dislocations. Therefore repeated nucleation does not appear to depend on the vacancy supersaturation, at least for the range of supersaturations in these direct-quenches. Secondly, both climb sources and glide dislocations which subsequently climbed were present in all samples, although their relative densities varied.

It is not possible to illustrate all the features of these microstructures in one micrograph for each sample in Figure 4.46. Accordingly, descriptions are given here based on observations recorded during examination in the electron microscope.

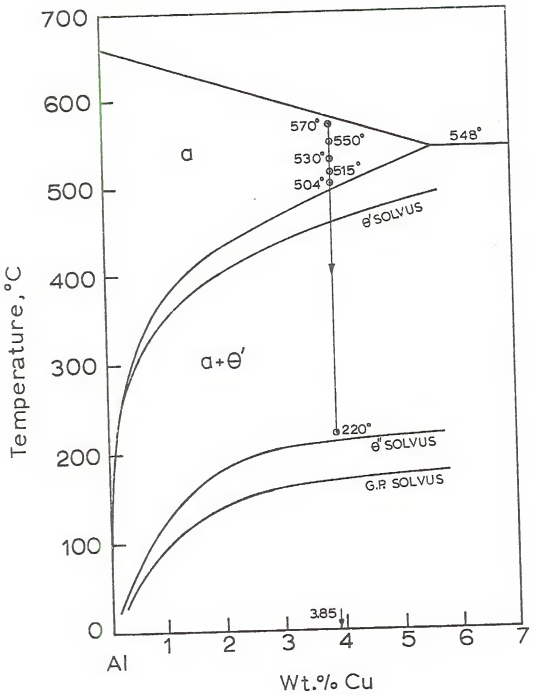

Figure 4.45. Diagram showing the five solution treatment temperatures from which samples were direct-quenched to 220°C and aged.

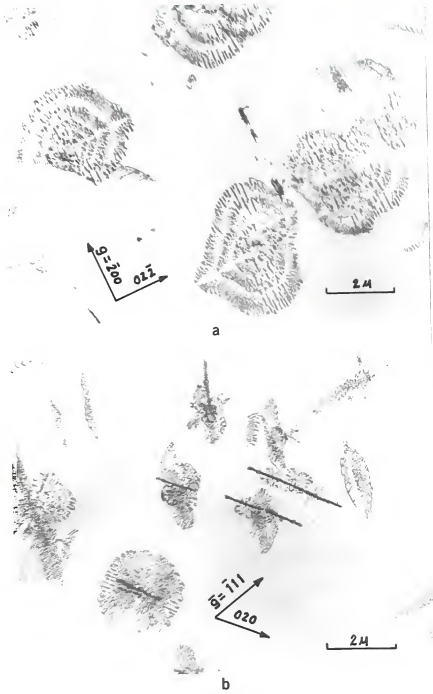

Figure 4.46. Sequence of micrographs showing the effect on microstructure of the solution treatment temperature from which samples were direct-quenched. Samples were solution treated for 1 hour at 570°C in (a), 550°C in (b), 530°C in (c), 515°C in (d), and 504°C in (e), then direct-quenched to 220°C and aged 5 minutes.

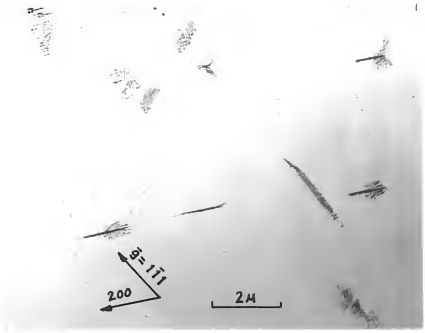

c

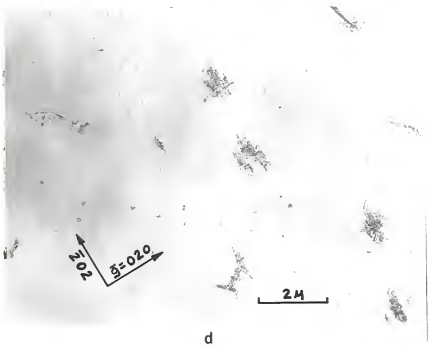

d

Figure 4.46. Continued.

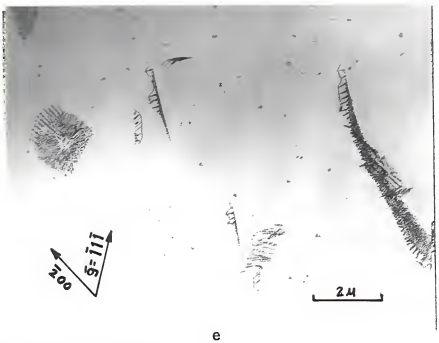

e

Figure 4.46. Continued.

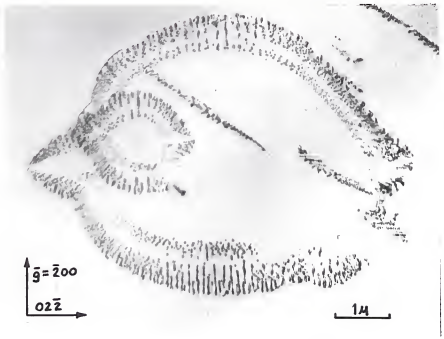

Figure 4.47. Large dislocation climb source in a sample quenched from 570°C to 220°C and aged 5 minutes.

Two observations were made about the effect of quenching temperatures on the operation of climb sources:

(1) The average size of the source loops increased with increasing solution treatment temperature. In the samples quenched from the lowest temperatures, the climb sources were small, with few exceptions. In the sample quenched from 570°C, both small and very large sources (≈5-6μ diameter) were observed, the average size being the largest for all samples. Figure 4.47 shows a very large source in this sample.

(2) The number density of active climb sources was very low for quenching from 504°C, increased with quenching temperature to a maximum for 550°C, then decreased to an intermediate value at 570°C. Insufficient micrographs were obtained to make reliable quantitative measurements of these densities, so that the trend is described only qualitatively here. An important influence on microstructure is that variations in size and density of climb sources are reflected in the density of precipitates which nucleate during quenching.

The above observations can be explained as follows. The vacancy supersaturation increases exponentially with quenching temperature so that the average distance a source loop will climb increases. Secondly, if nucleating sites for climb sources are indeed particles, the particle solubility will tend to increase with temperature. Thus, as the solution treatment temperature was increased, a trade-off between increasing vacancy supersaturation and a decreasing density

of undissolved source particles could lead to the observed maximum density of sources in the sample quenched from 550°C. That is, at 570°C, there would be a minimum number of undissolved source particles, and a maximum vacancy concentration. Upon quenching fewer sources would generate much larger source loops compared to the structure quenched from 550°C. At 504°C, the undissolved particle density would be a maximum, but the vacancy concentration is a minimum. Upon quenching only a minimum operation of climb sources is required to provide sinks for vacancy annihilation.

In the sample quenched from 570°C, repeated nucleation of θ' occurred within a limited band, approximately one micron wide, immediately behind the final position of the dislocations (Figures 4.46(a) and 4.47). As this sample was quenched from the highest temperature and contained the largest vacancy supersaturation, it is believed that appreciable dislocation climb occurred above the θ' solvus temperature, where no θ' could nucleate. The well-defined boundary where precipitation begins indicates that the concept of a θ' solvus temperature is a very effective and sensitive barrier to nucleation during quenching. In addition, the slope of the θ' solvus at the composition 3.85 wt.% Cu is small, causing a large driving force for nucleation immediately below it.

4.5.3. Effect of Temperature to Which Samples Are Direct-Quenched

In this experiment, five samples were solution treated for one hour at 550°C, direct-quenched into oil at various temperatures above the G.P. zone solvus, and aged (Figure 4.48). Therefore, the basic difference between samples was the quenching rate. The temperatures were 180°C, just above the G.P. zone solvus; 200° and 220°C, just below and above the θ'' solvus; 250° and 300°C, increasing temperatures in the α+θ' region. The oil bath was limited to 300°C. The temperature to which each sample was quenched shall be referred to as the aging temperature, Ta. With decreasing Ta, the samples were aged for longer times so that the θ' precipitates would be visible. The resulting microstructures are shown at low magnification in Figure 4.49.

In general, θ' nucleated repeatedly on climbing dislocations during quenching in all samples, although only to a small degree in the sample quenched to 300°C (Figure 4.49(a)). Furthermore, both glide dislocations which climbed and climb sources were observed in all samples. Whereas the density of glide dislocations varied little from sample to sample, the density of climb sources varied greatly.

The sequence of micrographs in Figure 4.49 shows that decreasing Ta increases the number of active climb sources and decreases the average source loop diameter. The maximum source density occurred for Ta=180°C and was about 6×10^6 per grain (Section 4.2.1).

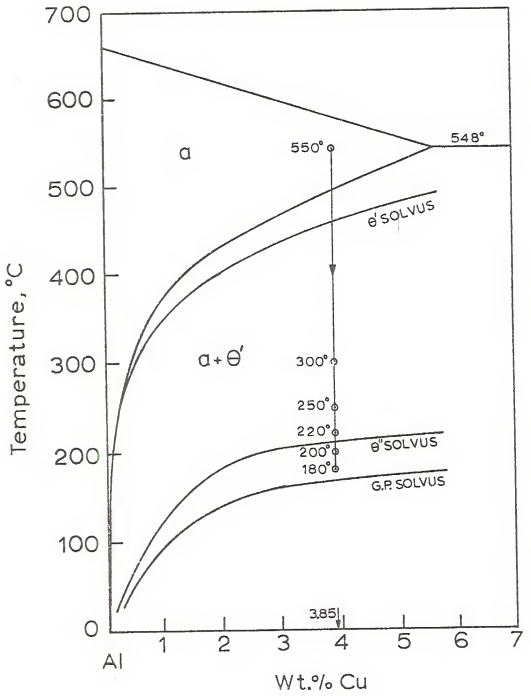

Figure 4.48. Diagram showing the five temperatures above the G.P. solvus to which samples were direct-quenched from 550°C and aged.

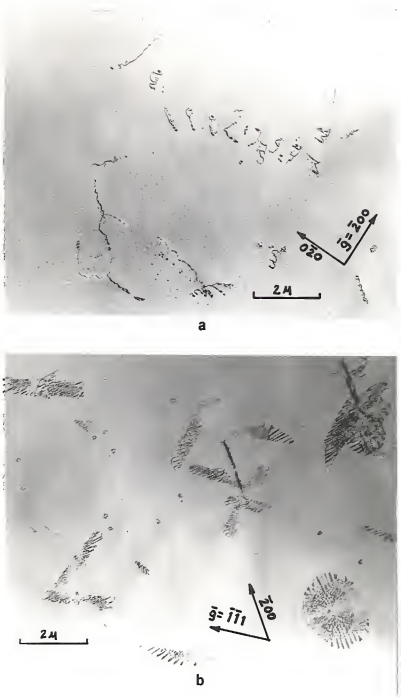

Figure 4.49. Sequence of micrographs showing the effect on microstructure of the temperature to which samples were direct-quenched from 550°C and aged. The samples were quenched to (a) 300°C and aged 15 seconds, (b) 250°C and aged 1 minute, (c) 220°C and aged 5 minutes, (d) 200°C and aged 30 minutes, and (e) 180°C and aged 1 hour.

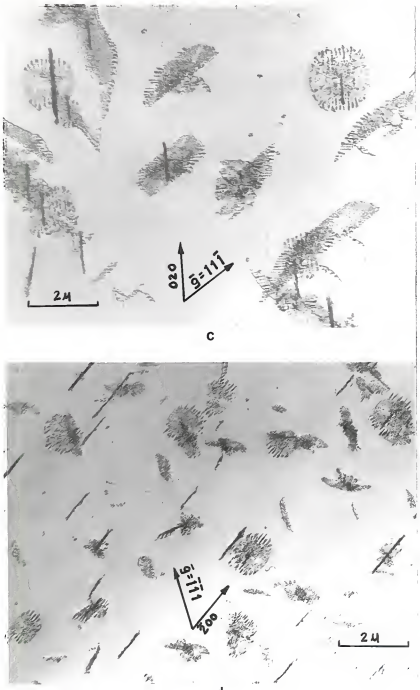

Figure 4.49. Continued.

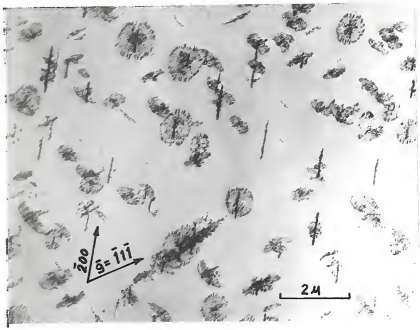

e

Figure 4.49. Continued.

These observations can be explained if two factors are accounted for. First, Figure 4.50 shows typical cooling curves for identical samples quenched at two different rates. Clearly, the sample quenched at the slower rate, R_2, takes longer to reach a given temperature, T_1, than a sample quenched at a faster rate, R_1. The former also spends longer within any given temperature increment, ΔT. Secondly, the variation in active source density can be treated as a problem analogous to the nucleation of precipitates over a distribution of favorable sites at different aging temperatures. It is assumed only that some particles will be more favorable sites for nucleating loops than others.

First consider the sample with the slowest quench rate (Ta=300°C). Shortly after the onset of quenching, source loops nucleate only at the most favorable particles. Since this sample spends a maximum time at high temperatures, the diffusion distance for vacancies is large. The first loops to nucleate can grow to be large, depleting the matrix of vacancies, and thereby suppressing the nucleation of other loops in nearby regions. As a result, this sample should have the lowest active source density, but the largest average loop size, in agreement with experiment (Figure 4.49(a)). As the quench rate increases (i.e., as Ta decreases), the time spent at high temperatures decreases and the diffusion distance for vacancies decreases. The first loops to nucleate can no longer grow as large before other loops nucleate on the next most favored particles (Figure 4.49(b)). Carried

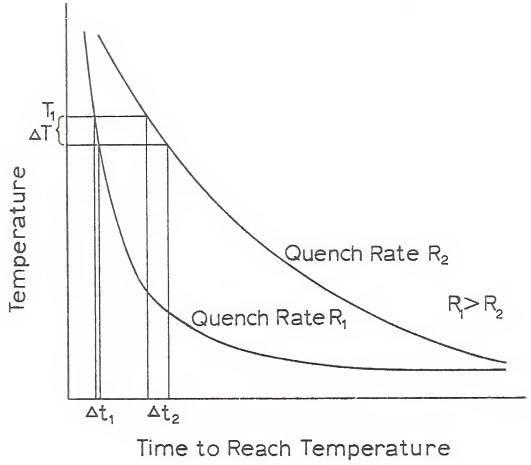

Figure 4.50. Diagram showing the differences in the time to reach a given temperature T_1, and the time spent in a given temperature range ΔT, for two different quench rates.

still further, the sample with the fastest quench rate (Ta= 180°C) should contain the maximum density of active sources with the smallest average loop size, again in agreement with experimental observations (Figure 4.49(e)).

An additional feature of the sample quenched to 300°C was that repeated nucleation occurred for only short distances behind the climbing dislocations and resulted in a low density of precipitates, Figure 4.49(e). This effect can be explained also using Figure 4.50. Given the slowest quench rate, this sample stayed longest at temperatures above the θ' solvus, thus causing maximum dislocation climb and the maximum depletion of vacancies before any precipitates nucleate. Also, the sample remained longest at high temperatures just below the θ' solvus. Therefore only a few precipitates nucleate and these grow rapidly (Figure 4.49(a)). This sample was aged only 15 seconds at 300°C so that the precipitate size is still small.

In the two samples quenched to 200° and 180°C (temperatures below the θ'' solvus, Figure 4.48), θ'' did not form as predicted from the metastable phase diagram. This is in agreement with observations that θ'' nucleates only on previously-formed G.P. zones (Lorimer and Nicholson, 1969; Lorimer, 1970).

4.5.4. Effect of Quench Rate

The previous section described results of changing the quench rate by direct-quenching to various aging temperatures. However, direct-quenching is, in general, a slow quench. The

purpose of the following experiments was to determine if repeated nucleation could be eliminated, or suppressed, by faster quenching. The quench rate was changed by varying the quenching medium.

Samples were solution treated for one hour and quenched into:

(1) air,

(2) liquid nitrogen,

(3) oil at room temperature, and

(4) water at room temperature.

The quench rates were not measured, but it is believed they increased in the order given above. After quenching, the samples were up-quenched into oil at 220°C and aged for five minutes in order to grow any θ' precipitates present to visible sizes. The air-cooled sample was held for approximately six seconds to insure complete cooling before up-quenching to 220°C. All other samples were up-quenched within about two seconds after down-quenching.

It was found that repeated nucleation of θ' had occurred on climbing dislocations during all quenches listed above. However, dislocation configurations varied widely as a result of the different quench rates so that each treatment will be discussed separately.

Air quench

Air quenching generated approximately the same density of glide dislocations as did direct-quenching into oil. All

had climbed during quenching and had nucleated precipitate colonies, Figure 4.51(a). Climb sources were found only occasionally, but they had nucleated precipitate colonies with the same general appearance as those in direct-quenched specimens. A small group of sources is shown in Figure 4.51(b).

Liquid nitrogen quench

The structure of this sample was similar to that of the air-cooled sample. The density of glide dislocations was approximately twice that in the air-cooled sample. Both small and large climb sources were present and all had nucleated precipitate colonies, Figure 4.52(b).

Room-temperature oil quench

The dislocation structure changed abruptly in going to a room-temperature oil quench. The resulting microstructure is shown in Figure 4.53 at low magnification. The foil is full of small dislocation loops. In addition, there were some glide dislocations present which had climbed during quenching and had nucleated precipitate colonies (Figure 4.53 at A and B). Note that the density of small loops is reduced in the vicinity of the glide dislocations. Some climb sources were observed, but their density was much lower than in the samples direct-quenched into oil at the aging temperature. Figure 4.54 shows an area where a number of climb sources are grouped together. The density of small loops was low in the regions adjacent to climb sources.

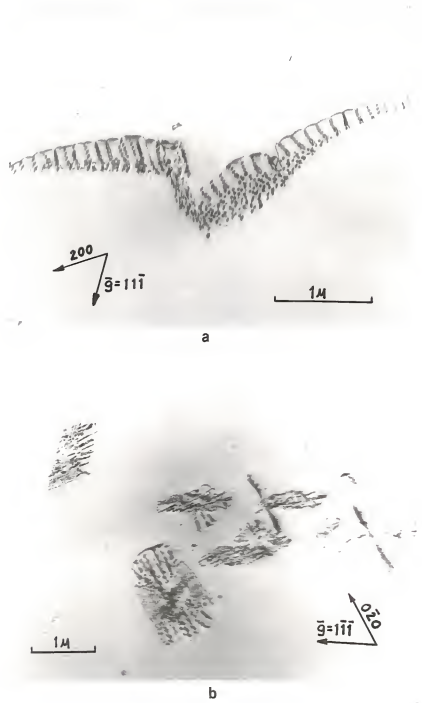

Figure 4.51. Precipitate colonies nucleated on (a) an initial glide dislocation, and (b) climb sources in a sample air-quenched from 550°C, then up-quenched in oil to 220°C and aged 5 minutes.

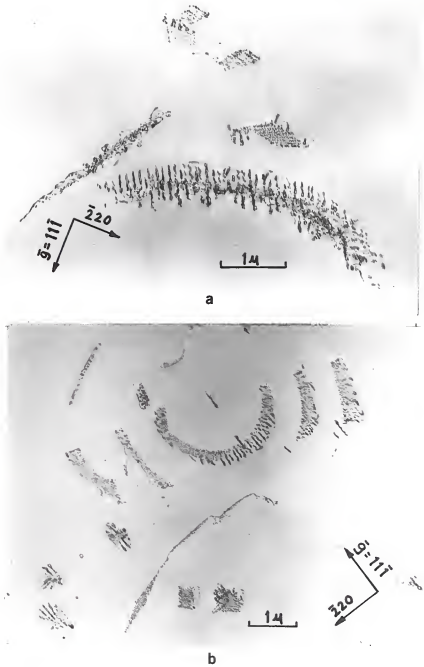

Figure 4.52. Precipitate colonies nucleated on (a) initial glide dislocations, and (b) climb sources in a sample quenched from 550°C into liquid nitrogen, then up-quenched to 220°C and aged 5 minutes.

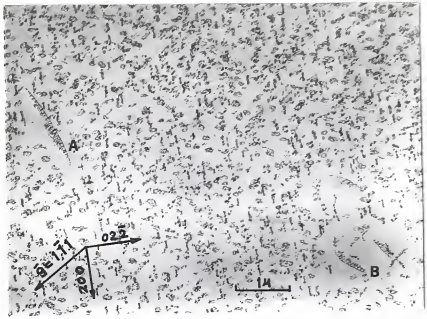

Figure 4.53. Microstructure of a sample quenched from 550°C into room temperature oil, then up-quenched to 220°C and aged 5 minutes, showing a high density of small dislocation loops and several glide dislocations which climbed (at points A).

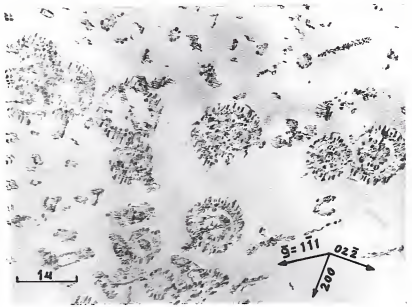

Figure 4.54. Dislocation climb sources and associated precipitate colonies in the sample quenched into room-temperature oil, then up-quenched to 220°C and aged 5 minutes.

The small loops are shown at high magnification in Figure 4.55. The interior of the loops are precipitated in much the same manner as the interior of the climb source loops shown in previous micrographs. For example, the loops and associated precipitate colonies at points A have the same appearance, but on a smaller scale, as climb source loops and their associated precipitate colonies viewed normal to their {110} habits. The small loops encircling the precipitates at A are invisible in this image, and in place of precipitate stringers in the <100> directions, they have single larger precipitates at the interior edges of the loops.

The small loops were found to lie on {110} planes as illustrated by the edge-on habits at B in Figure 4.55. Their Burgers vectors were determined from invisibility conditions to be a/2<110> types normal to the loop planes. Thus, they are prismatic edge-loops on {110} with $\vec{b}$=a/2<110>. It is assumed that they formed by collapse of vacancy clusters onto {110} planes. Similar prismatic loops on {110} have been observed in quenched Al-2.5 wt.% Cu (Boyd and Edington, 1971) and in quenched Al-Mg alloys (Embury and Nicholson, 1963). Once the loops form, they grow by climb from further vacancy condensation. In so doing, they nucleate the small precipitate colonies. In fact, apart from their origin and size, there is probably no difference in the mechanism of repeated nucleation during the growth of these small loops and during the growth of climb source loops.

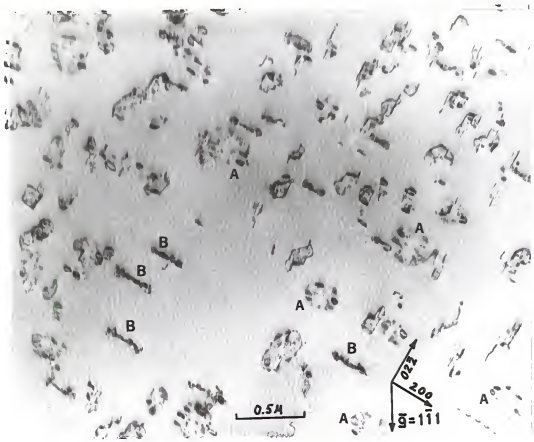

Figure 4.55. Higher magnification of the structure in Figure 4.53 showing that the interiors of the small dislocation loops contain precipitate colonies. Loops at B are viewed edge-on, while loops at A are out of contrast around their precipitate colonies.

The high density of small loops in this structure can be explained as follows. The room temperature oil quench is a moderately fast quench achieving a much larger supersaturation of vacancies than direct-quenching to the aging temperature. Most vacancies do not have time to diffuse to active climb sources or to glide dislocations which are climbing. They therefore cluster rapidly and collapse into loops which grow by further vacancy condensation.

If the origin of these small loops is neglected, this microstructure can be thought of as an extension of the structures described in the previous section, where direct-quenching into oil at progressively lower temperatures increased the density of active climb sources and decreased their average diameter.

From Figure 4.53, the density of small loops was estimated to be $2.2 \times 10^{13}/cm^3$. Their average diameter was measured from Figure 4.55 and found to be approximately 0.25μ. From these estimates, and assuming that each loop climbs by removing two adjacent {110} planes to avoid a stacking fault, the quenched-in vacancy concentration was estimated as 3×10^{-4}. This value is a slight overestimate since it neglects any vacancy contribution from the growing θ' platelets, which have a smaller atomic volume than the matrix.

However, this estimate is in good agreement with a value of approximately 2.5×10^{-4} for the equilibrium concentration of vacancies in pure aluminum at the 550° solution treatment temperature (Simmons and Balluffi, 1960; Guerard et al., 1974).

Room-temperature water quench

The structure of this sample was similar to that of the sample quenched into room-temperature oil. Figure 4.56(a) shows the microstructure to be full of small loops. Occasional glide dislocations were observed which had climbed and nucleated θ' colonies (Figure 4.56(a) at point A). The edge-on orientations of the small loops indicated that they lie on {110} planes. As in the oil quenched sample, their Burgers vectors were found to be a/2<110> normal to the loop planes. These are prismatic edge-loops and, as before, it is assumed that they formed by collapse of vacancy clusters onto {110}. When viewed at high magnification (Figure 4.56(b)), the interiors of the loops appear to contain small precipitate colonies. It is assumed that the loops nucleated θ' in the process of growth by climb.

Two features were observed in the microstructure of this sample that were not present in the sample quenched into room-temperature oil. First, in isolated areas, helical dislocations were observed which had partially broken up into loops, e.g., Figure 4.57. This is in agreement with the work of Thomas (1959), who showed that helical dislocations were present in Al-4 wt.% Cu quenched from low temperatures in the solid solution range. In the present case, the solution treatment at 550°C was sufficiently high that the structure consists mainly of vacancy-condensation loops with occasional helical dislocations.

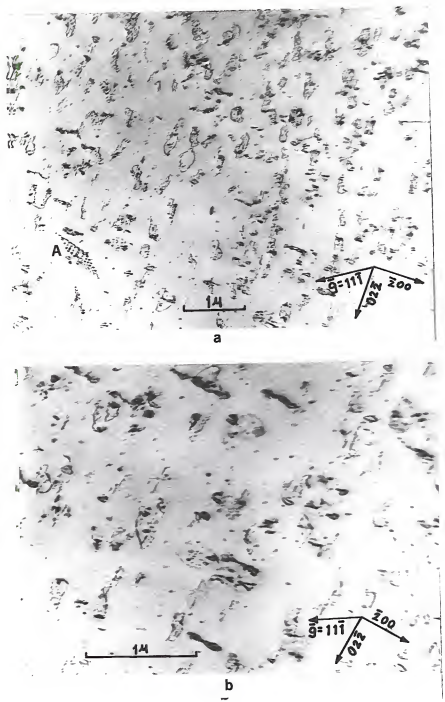

Figure 4.56. (a) Low and (b) high magnification of microstructure of sample quenched from 550°C into room temperature water, then up-quenched to 221°C and aged 5 minutes. The foil contains a high density of irregular-shaped loops which are internally precipitated.

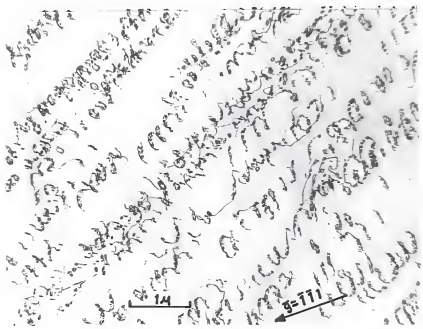

Figure 4.57. Helical dislocations in the sample quenched from 550°C into room temperature water, then up-quenched to 220°C and aged 5 minutes.

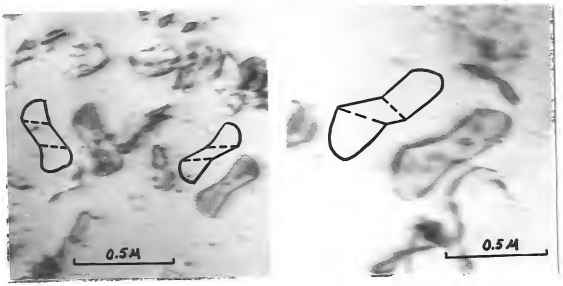

Figure 4.58. Loops which have partially moved off their habit planes in the sample quenched from 550°C into room temperature water, then up-quenched to 220°C and aged 5 minutes.

Secondly, it was found that portions of many small loops had moved off their {110} habits. Examples are shown in Figure 4.58. Since the original {110} habit is the most favorable climb plane for these edge loops (Miekk-oja and Räty, 1971), it is unlikely that they would move off by climb. They have most probably slipped onto intersecting {111} planes under the quenching stresses.

4.5.5. Effect of Copper Concentration

Samples with decreasing copper content were given direct-quenching treatments to determine if solute concentration played an important role in the repeated nucleation mechanism. The copper concentrations of the samples were nominally 1.96 wt.%, 1.0 wt.%, and 0.5 wt.%, respectively (evidence for repeated nucleation in the 3.85 wt.% Cu alloy has already been discussed in great detail). The samples were solution treated for one hour at 545°C, direct-quenched into oil at 210°C, and aged at that temperature. These temperatures are shown in relation to the θ' and θ'' solvus lines in Figure 4.59. Samples of the 1.96 wt.% Cu alloy were aged for either 30 minutes or one hour at 210°C. Samples of the 1 wt.% Cu alloy were aged for either three seconds, one hour, or 24 hours at 210°C. Samples of the 0.5 wt.% Cu alloy were aged for either three seconds, one hour, or 7-1/2 hours at 210°C.

It was found that repeated nucleation of θ' occurred extensively in the 1.96 wt.% alloy, but did not occur at all in the 1.0 and 0.5 wt.% Cu alloys. Appreciable dislocation

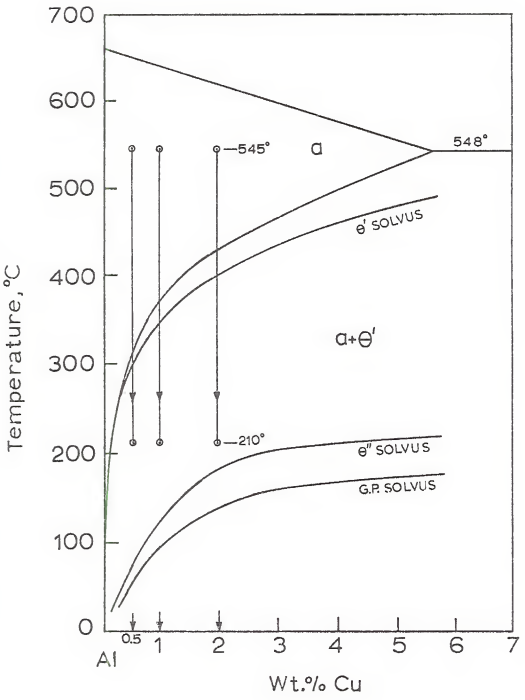

Figure 4.59. Diagram showing the solution treatment and aging temperatures used for direct-quenching the 2, 1, and 1/2 wt.% copper alloys.

climb occurred during quenching in all three alloys. Thus, copper concentration is an important variable in the repeated nucleation process, tending to suppress the mechanism altogether below some critical concentration between 1.96 and 1 wt.% Cu. The microstructures in these samples are discussed separately below.

1.96 wt.% copper

Many glide dislocations were observed which had climbed and nucleated precipitate colonies. An example is shown in Figure 4.60(a), where the dislocation is invisible along AB. All the precipitate stringers have coalesced into long platelets due to the one-hour aging treatment at 210°C. Many climb sources were observed which had nucleated precipitate colonies during quenching, Figure 4.60(b).

1.0 wt.% copper

Again both glide dislocations and dislocation climb sources were present in this alloy, Figure 4.61. However, no evidence for repeated nucleation of precipitates was observed and only a few precipitates were found near dislocations after aging up to 24 hours. All climb source loops had the Class IV shape of Figure 4.26, e.g., the source sectioned by the foil in Figure 4.61(b).

0.5 wt.% copper

As before, both climb sources and glide dislocations were present after direct-quenching this alloy. In addition,

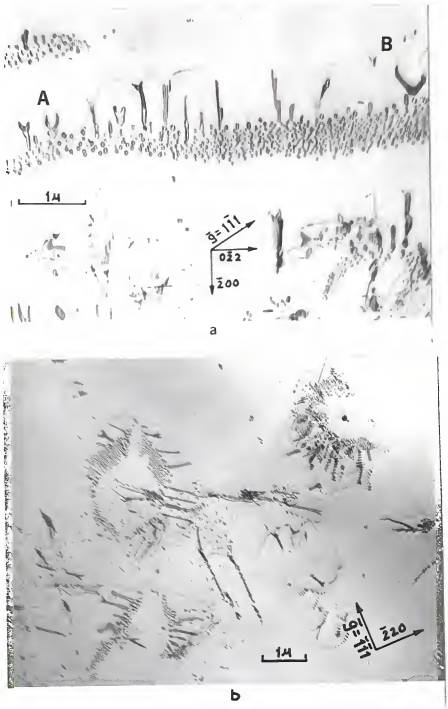

Figure 4.60. Precipitate colonies nucleated on (a) a long glide dislocation which is out of contrast between AB, and (b) dislocation climb sources in the Al-2 wt.% Cu alloy. (Heat treatment: S.T. 1 hour 545°C, quenched to 210°C, aged 1 hour.)

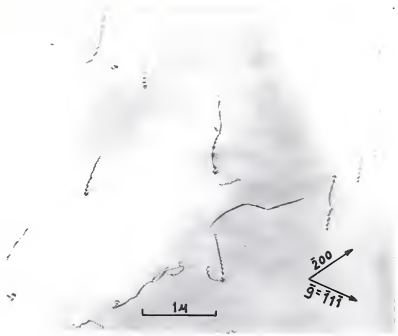

(a)

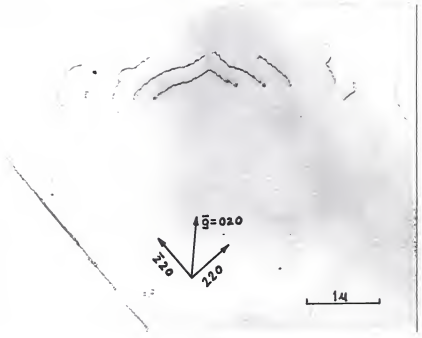

(b)

Figure 4.61. Micrographs of Al-1 wt.% Cu alloy quenched from 545°C to 210°C and aged 1 hour, showing that no repeated nucleation of θ' occurred during quenching. (a) Glide dislocations; (b) climb sources.

bands of small dislocation loops were present throughout the microstructure of the sample aged only three seconds at 210°C, Figure 4.62. These small loops exhibit stacking fault contrast and are assumed to be Frank loops formed by the collapse of vacancy clusters. After aging one hour at 210°C, no such loops were observed and it is assumed that they annealed out. No evidence for repeated precipitation was observed in this alloy, even after aging for 7-1/2 hours at 210°C. In fact, no precipitates at all were detected in this alloy, although it was aged in the two-phase $\alpha+\theta'$ region (Figure 4.59).

The shape of climb source loops changed appreciably in going to the 0.5 wt.% Cu alloy. After direct-quenching and aging for three seconds at 210°C, some climb source loops had the Class IV shape of Figure 4.26, but most had the shape of nearly perfect rhombuses. After aging for one hour at 210°C, all source loops, without exception, had the shape of nearly perfect rhombuses (Figure 4.63). The long axis of the rhombus is close to the <100> direction in the {110} habit of the loops. The loop sides lie along <112> directions to within about 5%. These <112> directions are the lines of intersection of the two {111} planes perpendicular to the {110} plane of the loops, i.e., these are the two slip planes containing the a/2<110> Burgers vectors of the loops. This is the same geometry of climb source loops observed in Al-Mg alloys by Embury and Nicholson (1963).

It is now apparent that, as the copper content of the alloy decreases from 3.85 wt.% to 0.5 wt.%, the typical climb

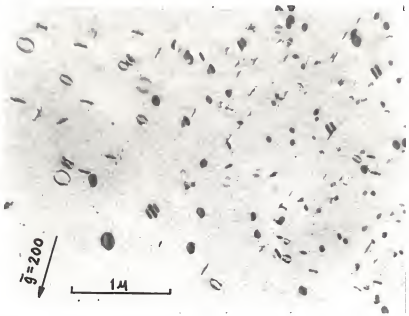

Figure 4.62. Band of small prismatic dislocation loops in Al-0.5 wt.% Cu quenched from 545°C to 210°C and aged only 3 seconds.

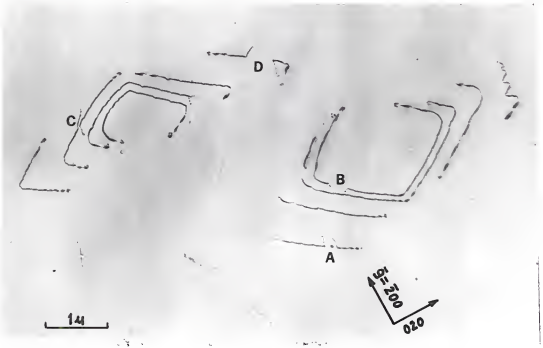

Figure 4.63. Rhombus-shaped climb sources in Al-0.5 wt.% Cu quenched from 550°C to 210°C and aged 1 hour. Local segments at A, B, C, and D appear to have slipped out of the climb plane.

source loop changes in shape from slightly elliptical in the [100] direction to a rhombus elongated in the [100] direction, as shown schematically in Figure 4.64.

Close examination of the sides of the rhombus loops in the sample aged for one hour at 210°C showed that they contained a very regular spacing of kinks or jogs, Figure 4.65. It is suggested that these are kinks caused by slip in the {111} planes normal to the loops. In fact, it was observed often that short segments of the loops had undergone extensive slip out of the plane of the loops, e.g., at A, B, C, and D in Figure 4.65. The kinks were not resolvable (if present) in climb source loops in the sample aged for only three seconds.

The average spacing of the kinks was measured normal to the <100> direction in the loop plane and found to be about 0.1μ. This is almost exactly the same as the measured spacing (0.096μ) between precipitate stringers in the colonies on climb sources in the 3.85 wt.% Cu alloy (Section 4.4.2). Therefore, it is suggested that the origin of the precipitate stringers in the alloys of higher copper concentration is associated with a regular spacing of kinks out of the climb plane of the source loops.

Examination of the lines of intersection of concentric rhombus loops at a climb source with the foil surfaces revealed that these intersections were not parallel, Figure 4.63. This indicates that the planes of successive loops are rotated with respect to each other. In addition, it was

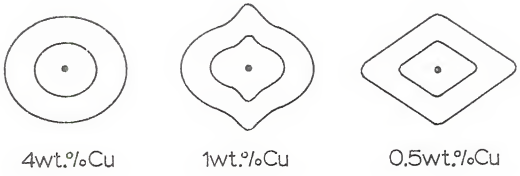

Figure 4.64. Diagram showing the change in shape of the typical climb source in Al-Cu with decreasing copper concentration.

Figure 4.65. High magnification of climb source loops in Al-0.5 wt.% Cu quenched from 545°C to 210°C and aged 1 hour, revealing a regular spacing of kinks along the dislocations.

often observed that, where a large outer loop intersected both foil surfaces, the two lines of intersection were not parallel, indicating that the loops themselves are not strictly planar. These observations could be explained only if the loops are allowed to slip or climb locally out of their habit planes in varying step heights.

4.6. Summary

The results in this chapter may be summarized as follows:

(1) The θ' phase nucleated repeatedly on climbing dislocations during quenching, creating precipitate colonies along the climb paths. The precipitate density thus generated was sufficiently large to suppress autocatalytic nucleation during long aging.

(2) The dislocations climb during the quench by annihilation of quenched-in vacancies. These dislocations fall into three categories according to origin:

(a) pure-edge loops on {110} planes, generated at dislocation climb sources,

(b) glide dislocations on {111} planes, and

(c) prismatic edge-loops on {110} formed by collapse of vacancy clusters.

The dislocation density in each category varied with heat treatment. Categories (a) and (b) were found in all samples. Category (c) was found only in samples quenched into oil or water at room temperature.

(3) Glide dislocations climb in one of two ways:

(a) on smoothly curved surfaces, nucleating precipitate colonies containing two θ' orientations, or

(b) on corrugated-shaped surfaces, nucleating bands containing only one θ' orientation in each band.

(4) Only the two θ' orientations compatible with the Burgers vector of the climbing dislocation are nucleated in a given colony. This suggests that the precipitates were nucleated during quenching in the wake of the climbing dislocations. In situ aging treatments in the TEM support this conclusion.

(5) Precipitate colonies generated on climb sources contain a region of dense precipitation and regions of precipitate stringers in <100> directions. The stringers are associated with a regular spacing of kinks on the climbing source loops. Only one θ' orientation is nucleated in a given stringer.

(6) The number density and average size of active climb sources are functions of the quench rate and vacancy supersaturation for direct-quenches. The typical shape of a climb source loop changes from an ellipse to a rhombus, with decreasing copper concentration.

(7) Repeated nucleation does not occur in alloys with copper concentration below some critical value between 1.96 and 1 wt.% copper.

CHAPTER 5

THE REPEATED NUCLEATION MECHANISM

In the previous chapter, it was convenient to include some discussion and analysis in each section. Hence, the discussion in this chapter will be limited to aspects of the mechanism of repeated nucleation of θ' in Al-Cu.

5.1. Nucleation of θ' Near Edge Dislocations

The α→θ' transformation occurs with a 3.95% volume contraction in the lattice (Section 2.2). The resulting misfit strain energy is sufficient to suppress nucleation except at dislocations whose stress fields reduce this strain energy. The observation that just two θ' orientations nucleate in each colony (Section 4.3) provides insight as to where the nucleation events occur about the dislocation. One θ' orientation does not nucleate because its misfit is perpendicular to the Burgers vector. Hence, its strain field is not relieved by the stress field of the dislocation (Section 2.2). The other two orientations nucleate because their misfits lie at 45° to the Burgers vector, so that their strain fields are partially relieved by the stress field of the dislocation. Since the α→θ' transformation is a volume contraction, the

resulting strain puts the surrounding matrix in tension. Thus, this strain can be relieved only if the θ' platelet forms on the compressive side of the dislocation. In order to determine how close to the dislocation it forms, one must solve the elastic interaction problem discussed in Section 2.1. In the case of the pure-edge loops generated at climb sources in these alloys, the compressive region lies in front of the expanding loops, Figure 5.1(a). Hence, nucleation occurs in advance of the climbing dislocations, Figure 5.1(b). Since essentially all the visible precipitates in a colony on a climb source lie within the loops (e.g., Figure 4.30), the loops must climb through or by the particles, or pinch off around them in order to continue expanding. Now θ' forms parallel to {100} with a<100> peripheral misfit loops, so that the climbing dislocation with a/2<110> Burgers vector cannot comprise a part of the platelet edge. And as discussed in Section 4.3.3, there was no evidence that the climbing dislocations pinched off around the platelets. If a nucleus forms above or below the climb plane, the climbing dislocation can pass by more easily than if the nucleus forms along the climb plane (or grows to intersect it). In the latter case, the dislocation must either cut through the precipitate or, if the stresses involved are too high, glide locally around it.

Occasionally a large precipitate was observed outside a source loop which bent locally around the precipitate, Figure 5.2. It is assumed that such precipitates were the last to

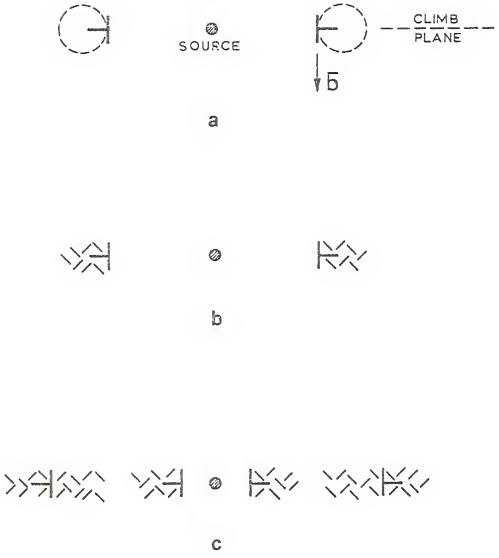

Figure 5.1. (a) Schematic cross-section through a climb source particle and one loop showing regions of compression (dashed) in advance of the loop. (b) Nucleation in the compressive regions. (c) After further climb and generation of another source loop.

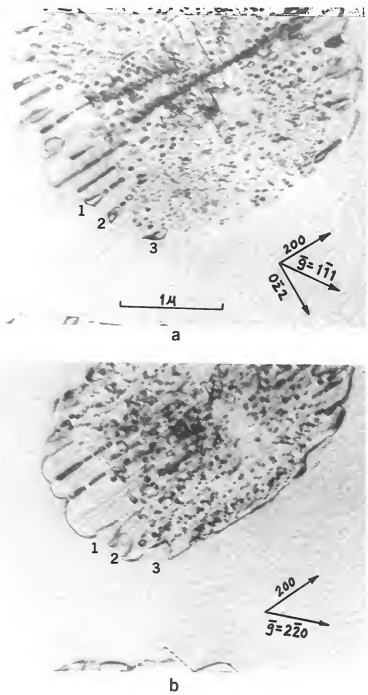

Figure 5.2. Two images of a precipitate colony on a climb source showing that the precipitates 1, 2, and 3 lie outside the outermost loop. The source loop is out of contrast in (a), and the three precipitates are out of contrast in (b). The beam direction is close to [011] in (a), and to [001] in (b).

nucleate near the end of the quench when the dislocation climb rate had dropped to a low value. Thus, these precipitates had time to grow large enough to retard the passage of the climbing dislocation.

5.2. Comparison with Previous Repeated Nucleation Mechanisms

The fundamentals of the repeated nucleation mechanism proposed by Nes (1974) were reviewed in Section 2.4. This mechanism reportedly accounts for the phenomenon in all systems in which it has been observed to date, but in all these cases the transformed phase has had a larger atomic volume than the matrix. The Nes model will now be compared with repeated nucleation of θ' in Al-Cu. The fundamentals of the Nes mechanism are:

(1) Vacancies must be supplied to the transforming particle in order to reduce the particle/matrix mismatch.

(2) The subsequent particle growth provides the driving force for the vacancy-emitting climb of the dislocation.

(3) The sequence between repeated nucleations is controlled by balancing the rate of vacancy consumption by the precipitates with the rate of vacancy emission by the climbing dislocation.

(4) The particle is dragged some distance by the dislocation before unpinning occurs.

(5) The parameters controlling colony growth are either (a) the atomic diffusion of solute, or (b) the core self-diffusion, whichever has the highest activation energy.

We now compare each of the above with the evidence in Al-Cu.

(1) The $\alpha \rightarrow \theta'$ transformation involves a 3.95% volume contraction.

Thus, if anything, the precipitates generate a few vacancies instead of consuming them.

(2) The dislocation climb is essentially independent of the precipitation reaction.

Evidence for this is as follows. First, it was shown in Section 4.2.1 that the dislocation climb is definitely vacancy-annihilating instead of emitting. As climb occurs during quenching, it is concluded that the driving force is the annihilation of the quenched-in vacancy supersaturation. If any vacancies produced by the transformation contribute to climb, the experimental evidence suggests that this contribution is small. For example, depending on quench rate and vacancy supersaturation, the dislocations often climbed over large distances before precipitation began, e.g., Figures 4.47 and 4.52(b). And as evidenced by Figures 4.25 and 4.44(a-d), the dislocations undergo little, if any, additional climb during aging, while the precipitates grow orders of

magnitude in size.

(3) There is no vacancy balance required between precipitate and dislocation in Al-Cu.

This conclusion is based on (1) and (2) above.

(4) Particle dragging was not observed in Al-Cu. There was no visual evidence that the particles had been dragged by the dislocations during θ' colony growth. If in fact it did occur, the dragging distances involved must be smaller than the resolution limit of a small particle near a dislocation image. This is estimated to be less than 100Å.

(5) Colony growth in Al-Cu is controlled by the dislocation climb rate.

It is suggested that the rate of colony growth is primarily controlled by the rate at which the dislocation climbs through the lattice after the sample temperature passes below the θ' solvus. This in turn is controlled by the rate at which excess vacancies reach the dislocation and depends, therefore, on the self-diffusion coefficient. In addition, it is influenced by the degree of vacancy supersaturation below the θ' solvus which depends on the solution treatment temperature and the quench rate (Sections 4.5.2-4.5.4).

5.3. The Mechanism in Al-Cu

In light of the discussion above, it is clear that repeated nucleation of θ' in Al-Cu cannot be explained by the

mechanism of Nes (1974). It does not involve a vacancy flux problem between growing precipitate and climbing dislocation. Rather it appears to be a basic heterogeneous nucleation problem, requiring that the dislocation stress field be present long enough for nucleation to occur. The mechanism of repeated nucleation in Al-Cu apparently involves three essential factors:

(1) Nucleation occurs because the dislocation stress field is present to help overcome the energy barrier.

(2) Repeated nucleation is possible because the dislocation climbs under a driving force independent of the precipitation process, namely the quenched-in vacancy supersaturation. This assures that the dislocation advances to act as a catalyst at successive positions along the climb surface.

(3) The climb rate is apparently slow enough to allow nucleation, but rapid enough to move the dislocation past the newly-formed precipitates before they grow large enough to pin it.

Factor (3) could be a self-regulating effect in that the initial precipitate size may be limited by the strain field of the dislocation. Growth after nucleation relies principally on long-range bulk-diffusion of solute and may not be fast enough to pin the climbing dislocation.

5.3.1. Local Solute Buildup

The matrix is a random distribution of 2-4 wt.% Cu (∿1-2 atomic%) in the aluminum lattice. For nucleation to occur repeatedly, it is necessary that concentration buildups occur at the moving dislocation which can provide for the high copper content of the θ' nuclei (∿33 atomic%). It is suggested that the necessary concentration changes probably do not come about by long-range bulk-diffusion of copper. Prior to nucleation there is no concentration gradient to promote long-range copper diffusion to the dislocation. There is, though, a drift force on the copper to diffuse to the dislocation and lower the associated strain energy. However, since nucleation occurs rapidly during quenching, it is unlikely that bulk-diffusion due to the drift force is rapid enough to cause the necessary copper buildups.

In the absence of a sufficient contribution from long-range bulk-diffusion, we consider two possibilities whereby the copper concentration can be enhanced locally at the moving dislocation.

(1) There is indirect evidence from resistivity measurements that copper atoms cluster during quenching of Al-Cu alloys (Perry, 1966). Clusters located at or very near the climb plane would provide copper-rich regions that might transform to θ' as the dislocation stress field passes. It is not valid to assume that a cluster will automatically transform to θ' if it contains more copper atoms than are required for the critical nucleus size in the presence of the

dislocation. The nucleation event still involves a statistical probability that the correct combination of copper and aluminum atoms rearrange into the correct structure with sufficient size and shape (i.e., the critical nucleus size and shape). It is valid, however, to assume that the probability that this event will occur is higher in a copper-rich cluster than elsewhere in the matrix. In addition, it is generally believed that clusters can trap vacancies with a binding energy characteristic of the alloy (Federighi and Thomas, 1961). Such trapped vacancies could aid in the local atomic rearrangements involved in forming the critical nucleus structure. However, without available information on cluster sizes and densities, it is not possible to estimate if clustering alone could provide enough solute buildup for nucleation in these samples.

(2) If it is assumed that the dislocation acts as a highly efficient sink for the copper atoms it encounters along the climb surface, then rapid pipe diffusion along the core to a nearby growing nucleus can provide sufficient copper locally for θ' precipitation. Assuming that thermal fluctuations create growing embryos of the new phase at various locations along the dislocation (a basic assumption of nucleation theory), then adjacent portions of the climbing dislocation could collect and transport solute to these growing embryos. Since dislocation pipe diffusion is much faster than bulk diffusion, the frequency of atoms joining the critical nucleus (the term β in Equation 2.1) is increased over

that for bulk diffusion. This provides an advantage for nucleation at the dislocation in addition to that gained from the strain field. To test if this model could provide sufficient solute for the observed repeated nucleation, a calculation was made to determine if there was enough copper over the climb surface to account for the density of precipitates generated in a colony. The density of precipitates per unit area, measured from Figure 5.3, was found to be approximately $6.4 \times 10^{10}/(cm)^2$. It is assumed that the density of visible precipitates at this stage is the same as the density of nuclei which form initially. As discussed in Section 4.2.1, an a/2[110] dislocation climbing by vacancy annihilation on a {110} plane in f.c.c. removes two adjacent planes of atoms. Initially, it was assumed that the dislocation could collect easily all the solute on these two planes and each plane on either side of it, or all copper atoms on a total of four adjacent {110} planes. Assuming 2 atomic% copper (4 wt.% Cu) on these {110} planes, the dislocation collects 5.8×10^5 copper atoms in climbing over a square micron area. If by pipe diffusion, the dislocation can distribute this amount of solute to the 640 embryos per square micron, then on the average there would be 900 copper atoms available to each embryo. There are two copper atoms per unit cell of θ' so this amounts to enough solute for 450 unit cells/embryo. An estimate of the critical nucleus size must now be made to determine if this is enough solute to form stable nuclei. This was done on the basis of a plate-like nucleus on (100),

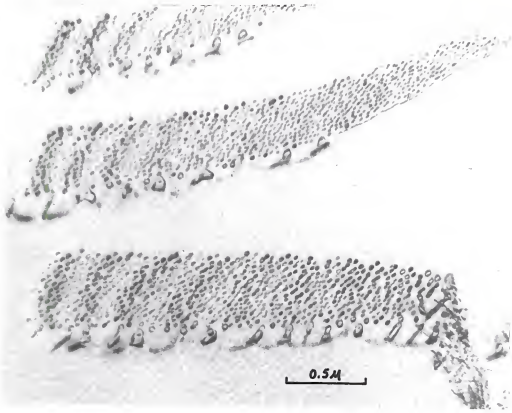

Figure 5.3. Micrograph from which a measurement was made of the number density of precipitates in a colony. (Heat treatment: S.T. 1 hour 550°C, quenched to 220°C, aged 5 minutes.)

a thickness sufficient to nucleate one a[100] misfit dislocation around its edge (≈2 unit cells thick), and a diameter slightly less than the resolution limit of the electron microscope (≈30Å maximum). Such a critical nucleus would contain about 90 unit cells. Hence, this model can supply more than enough solute to nucleate the precipitate density observed, so that it is not required for the dislocation to collect all the solute in its climb path.

It is suggested that the pipe diffusion model provides the primary means for locally enhancing the solute concentration for repeated nucleation. However, it is likely that there is at least some contribution, however small, from bulk-diffusion to the surface of the growing embryos. The importance of clustering cannot be accurately assessed, but it is not a necessary condition. It would be helpful, of course, in attaining local concentration enhancement.

5.3.2. Precipitate Stringer Formation

All the above considerations would predict a random distribution of θ' nucleated by a passing dislocation. This could account for the regions of uniform precipitation observed behind the climbing dislocations, but not for the regions of straight and uniformly-spaced precipitate stringers which always form along <100> directions on climb sources, Figure 4.30. We now consider a possible mechanism for this stringer formation, and we limit the discussion to stringers produced in precipitate colonies on climb sources.

It was shown in Section 4.5.5 that the spacing between stringers (about 0.1μ) is the same as the spacing of visible superkinks on climb source loops. It is assumed that the origin of the precipitate stringers is related to the movement of such superkinks. According to Balluffi (1969) the climb of a dislocation which is rotated out of its pure edge orientation introduces kinks in the dislocation line. The spacing of kinks depends on the magnitude of the rotation and is equal to $\overline{b}/\tan(90°-\alpha)$, where $\overline{b}$ is the Burgers vector and represents the kink height, and α is the angle between the Burgers vector and the dislocation line direction. It is now assumed that the climb source loops are rotated slightly off their {110} habit about an axis parallel to the <001> direction in the habit plane. Such rotations could result from local slip out of the climb plane due to the stress fields of the precipitates forming in advance of the climbing loops. A kink spacing of 0.1μ implies a rotation of only 0.13° for kinks of one Burgers vector in height. Such kinks would not be resolved in the electron microscope, as are those in Figure 4.65. Rather, it is assumed that the rotation is on the order of several degrees, creating numerous kinks. It is further assumed that at the high temperatures where climb occurs, the kinks are mobile and coalesce into visible superkinks with an equilibrium spacing of 0.1μ. Then each time a source loop expands and increases its line length by an amount 0.1μ (projected normal to <001>), a new superkink becomes stable. It is assumed that the precipitate

nucleation process associated with the kink then becomes active and continues as the loop expands. This process of forming successive superkinks and trailing precipitates behind them as the loop expands is illustrated in Figure 5.4. For clarity, the precipitate stringers are shown to be continuous. The shape in Figure 5.4 compares favorably with the shape of precipitate colonies observed on climb sources, e.g., Figure 4.50.

Several further aspects of the above model are now considered. First, the fact that the superkink configuration is apparently a favored nucleation site is probably a function of the stress field set up around it. In addition, pipe diffusion of solute along the dislocation is most probably slowed at these superkinks. Thus, solute builds up at the kinks providing both a solute-rich environment for nucleation and a continuing supply of solute for growth. Next, we consider why superkinks and their trailing precipitate stringers are confined in their motion to the <100> direction in the loop habit. It may be that only one nucleation event occurs near the kink in advance of the climbing loop. Then, as the dislocation climbs by (or through), pipe diffusion to the kink continues to supply solute so that a long, thin ribbon of θ' trails behind the advancing kink. It can be seen from Figure 5.5 that the two possible {100} orientations of θ' which nucleate on a given loop could be extended from such superkinks only along the <100> direction contained in the loop habit, provided the loop continues to expand macroscopically

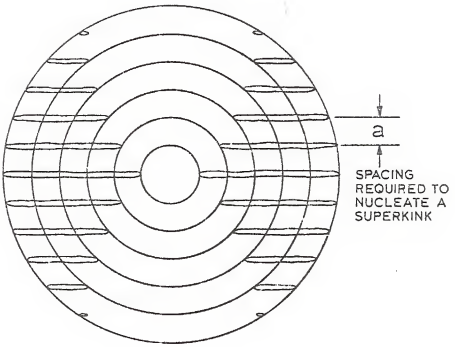

Figure 5.4. Diagram illustrating the shape of precipitate stringer regions which would result from successive nucleation of superkinks of spacing a, as a circular climb source loop expands. The precipitate stringers are shown continuous for clarity.

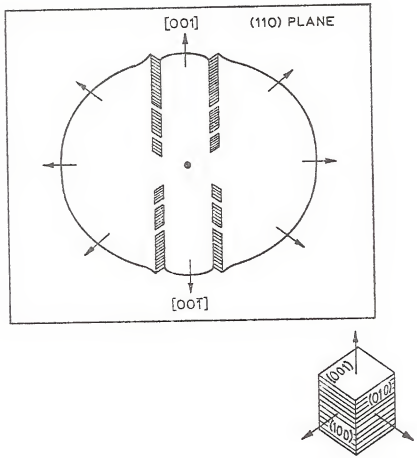

Figure 5.5. Diagram of an expanding climb source loop on ($1\bar{1}0$) with Burgers vector a/2[110]. The two θ' orientations, (100) and (010), which nucleate on this dislocation, can be extended in continuous ribbons from moving superkinks only along the [100] direction.

in its habit plane. This is in agreement with the fact that the stringers are always aligned along <100>.

This model predicts a thin, continuous ribbon of precipitate, but it was shown in Figure 4.27 that the stringers are composed of separate, small particles when they are first visible after quenching. It is probable that immediately after a thin ribbon forms, surface energy effects cause it to pinch off into small platelets, in a manner similar to the initial rapid spheroidization of eutectoid platelets upon annealing. Further aging would then cause these platelets to grow and coalesce as shown in Figure 4.31. This continuous ribbon model is consistent with the observation that platelets of only one θ' orientation exist in any given stringer (Section 4.4.2). In fact, it is difficult to imagine a more logical interpretation.

It is suggested that initial rapid growth of the precipitates in these stringers, enhanced by pipe diffusion along the dislocation, creates a sufficient concentration gradient in the matrix such that this is the only mechanism which continues to operate once it begins. This could account for the fact that uniform nucleation of precipitates does not occur in the regions where the stringer mechanism operates (Figure 4.30).

5.4. Criteria for Repeated Nucleation in Al-Cu and Application to Other Systems

Based on the results reported herein, the following criteria may be established for repeated nucleation in this system:

(1) a phase which nucleates easily on dislocations, namely the θ' phase;

(2) a source or sources of dislocations during the quench, namely dislocation climb sources and glide dislocations generated during quenching;

(3) a driving force for dislocation climb which is independent of the precipitate reaction, namely the annihilation of quenched-in vacancies; and

(4) a climb rate which is sufficiently slow to permit nucleation, but sufficiently fast so that the precipitates do not grow so large as to effectively pin the dislocations.

These criteria are far simpler than those required by the mechanism of Nes (1974), and might well apply to other systems in which dislocation-nucleated transformations occur. (2) and (3) above apply to most aluminum alloys. In particular, Al-Mg and certain Al-Mg ternary alloys have mestable phases which nucleate on dislocations, and appreciable dislocation climb occurs when these alloys are quenched. Unlike copper in Al-Cu, the magnesium atom is larger than the aluminum atom and it is unclear what effect this may have. The Al_2CuMg phase nucleates easily as laths on dislocations in

the Al-Cu-Mg system and might be a candidate for repeated nucleation. In steels, the Ni_3Ti phase nucleates easily on dislocations in austenitic stainless steel. This transformation, like θ' in Al-Cu, involves a net volume contraction and could be a candidate for repeated nucleation.

CHAPTER 6
CONCLUSIONS AND SUGGESTIONS FOR FUTURE WORK

This research has shown that the $\alpha \rightarrow \theta'$ transformation in Al-Cu can initiate and propagate during quenching by the mechanism of repeated nucleation on climbing dislocations. The dislocations are generated and climb during quenching by annihilation of the quenched-in vacancies. Densely populated colonies of θ' precipitates nucleate in the passing stress fields of the climbing dislocations. The distribution of the entire volume fraction of θ' is thus determined during the quenching step ($\leq 10^{-1}$ seconds). Therefore, autocatalytic nucleation is not required to propagate the reaction during aging.

The goals of this research were twofold: (1) to characterize the microstructures resulting from repeated nucleation, and (2) to establish the repeated nucleation mechanism in this system. Pertaining to microstructure, the following conclusions were drawn:

(1) The dislocations which climb during quenching fall into three categories according to origin:

a. pure-edge loops on {110} planes with a/2<110> Burgers vectors, generated at dislocation climb sources.

b. a/2<110> glide dislocations on {111} planes.

c. prismatic edge-loops on {110} with $\vec{b}$=a/2<110>, formed by the collapse of vacancy clusters.

The dislocation density in each category varied with heat treatment. Categories (a) and (b) were found in all samples regardless of quench procedure. Category (c) was found only in samples quenched into oil or water at room temperature.

(2) Glide dislocations climb either (a) on smoothly curved surfaces, nucleating precipitate colonies containing two θ' orientations, or (b) on corrugated-shaped surfaces, nucleating precipitate bands containing only one θ' orientation per band.

(3) Only the two θ' orientations compatible with the Burgers vector of the climbing dislocation are nucleated in a given colony (with the exception of 2(b) above).

(4) Precipitate colonies generated on climb sources exhibit a central region of uniform precipitation, and two regions of precipitate stringers aligned in <100> directions. The origin of the stringers is probably associated with the movement of regularly spaced superkinks on the climbing source loops. Only one θ' orientation is nucleated in a given stringer.

(5) θ' platelets nucleated by repeated precipitation can serve as source particles for generation of "secondary" climb sources which nucleate more precipitates. In a sense, this is a form of autocatalytic propagation of the reaction.

(6) The number density and the average size of active climb sources are functions of the quench rate and vacancy supersaturation for direct-quenches. The typical shape of a source loop changes from an ellipse to a rhombus with decreasing copper concentration.

(7) Repeated nucleation of θ' does not occur in alloys with copper concentration below some value between 1.96 and 1.0 wt.%.

The morphologies resulting from repeated nucleation contained many fascinating features which had not been previously reported, and it is certain that further investigation of these microstructures would reveal even more details not disclosed by this initial work.

The mechanism of repeated nucleation of θ' in Al-Cu is different from other previously reported mechanisms. The vacancy-annihilating dislocation climb appears to be independent of the precipitation process. Repeated nucleation is possible simply because the climb rate is slow enough to permit nucleation in advance of the moving dislocation, but rapid enough to permit the dislocation to pass before particle growth can result in effective pinning. The fact that the phenomenon occurs during quenching assures that there is a continuous supply of non-equilibrium vacancies to move the dislocation along and present fresh sites for further nucleation. The criteria for repeated nucleation by this mechanism are:

(1) a phase which nucleates easily on dislocations,

(2) a source of dislocations during quenching,

(3) a driving force for dislocation climb which is independent of the precipitation process,

(4) a climb rate slow enough to permit nucleation but rapid enough to move the dislocation past the stable precipitates.

This research has provided a basic understanding of the phenomenon in Al-Cu, but it is by no means complete. Several topics for further investigation are suggested:

(a) If a dislocation can climb through the lattice at elevated temperatures and provide the catalyst for repeated nucleation, then perhaps a gliding dislocation can also. It would be instructive to examine samples deformed either at temperatures slightly below the θ' solvus or during quenching from the solution treatment temperature for evidence of repeated nucleation during glide.

(b) It is suggested that a small-angle x-ray investigation at temperatures near the θ' solvus would provide direct evidence for copper clustering if it exists. If so, a determination of the density and size distribution of clusters would help resolve whether or not clustering could be involved in the repeated nucleation mechanism.

(c) Trace element additions are known to alter the kinetics of the $\alpha \rightarrow \theta'$ transformation, presumably by segregating to the particle interface where they can change both the interfacial energy and, to some extent, the misfit strain. It would be of interest to determine if trace additions of

such elements as Cd, In, or Sn could either enhance or eliminate repeated nucleation during quenching.

(d) An item, examined to some extent here, which needs further investigation is the nature of the segmented climb of glide dislocations in this system. In particular it would be of interest to understand more completely why this mode of climb nucleates precipitate bands containing only one θ' orientation instead of two.

(e) As a by-product, this investigation has established a good understanding of the operation of dislocation climb sources in Al-Cu alloys, but some questions remain to be answered. First, the nature of the source particles is still unknown. The capability of the new breed of scanning transmission electron microscopes (STEMs) to focus the electron beam to diameters on the order of 15Å, and to thereby obtain microdiffraction patterns and/or x-ray chemical analysis from very small particles, might be employed to solve this problem. Secondly, further work is required to understand the dependence of the shape of source loops on solute concentration.

(f) It is suggested that a calculation of the interaction energy between a θ' nucleus and an edge dislocation would reveal the location of the nucleation events around the dislocation. The method outlined by Larché (1974) for a coherent nucleus at an edge dislocation should be modified for the known geometry of a θ' platelet on {100} at an edge dislocation on (110). The position which maximizes the interaction energy (more negative) should be sought.

(g) Finally, the criteria for repeated nucleation in Al-Cu are relatively simple and probably exist in a number of other systems. It may be that the effect has not been observed in some alloys that have phases which nucleate on dislocations, simply because slow quenches are not normally employed in laboratory investigations. Commercial quenching practice is often a different situation though, where thick-section parts almost certainly receive relatively slow quenches. It is suggested that other aluminum alloys, which meet the criteria above, should be investigated to determine if the mechanism has broader application than the Al-Cu system. Al-Mg or Al-Mg ternary alloys should receive first consideration.

BIBLIOGRAPHY

Aaronson, H. I., Kinsman, K. R., and Russell, K. C. (1970), Scripta Met., 4, 101.

Ashby, M. F., and Brown, L. M. (1963), Phil. Mag., 8, 1649.

Balluffi, R. W. (1969), Phys. Stat. Sol., 31, 443.

Balluffi, R. W., and Thomson, R. M. (1962), J. Appl. Phys., 33, 817.

Bardeen, J., and Herring, C. (1952), Imperfections in Nearly Perfect Crystals, Wiley and Sons, p. 261.

Barnett, D. M. (1971), Scripta Met., 5, 261.

Barnett, D. M. (1973), private communication.

Beton, R. H., and Rollason, E. C. (1957-58), J. Inst. Metals, 86, 77.

Boyd, J. D., and Edington, J. W. (1971), Phil. Mag., 23, 633.

Bullough, R., and Newman, R. C. (1959), Proc. Royal Soc. London, A249, 427.

Cahn, J. W. (1957), Acta Met., 5, 169.

Christian, J. W. (1965), The Theory of Phase Transformations in Metals and Alloys, Pergamon Press, p. 363.

Clarebrough, L. M. (1973), Phys. Stat. Sol.(a), 18, 427.

Darwin, C. G. (1914), Phil. Mag., 27, 315, 675.

Dollins, C. C. (1970), Acta Met., 18, 1209.

Edington, J. W., and West, D. R. (1966), J. Appl. Phys., 37, 3904.

Embury, J. D. (1963), Ph.D. Dissertation, University of Cambridge.

Embury, J. D., and Nicholson, R. B. (1963), Acta Met., 11, 347.

Eshelby, J. D. (1957), Proc. Royal Soc. London, A241, 376.

Eshelby, J. D. (1961), Progress in Solid Mechanics, Sneddon and Hill, eds., North-Holland, p. 89.

Federighi, T., and Thomas, G. (1961), Phil. Mag., 6, 127.

Frank, F. C., and Read, W. T. (1950), Phys. Review, 79, 722.

Friedel, J. (1964), Dislocations, Addison-Wesley.

Guerard, B. von, Peisl, H., and Zitzmann, R. (1974), Appl. Phys., 3, 37.

Guinier, A. (1938), Nature, 142, 569.

Guinier, A. (1939), Ann. Physique, 12, 161.

Guinier, A. (1942), J. Phys. Radium, 3, 129.

Guinier, A. (1950), Compt. Rend., 231, 655.

Guinier, A. (1952), Acta Cryst., 5, 121.

Gulden, M. E., and Nix, W. D. (1968), Phil. Mag., 18, 217.

Head, A. K. (1969), Aust. J. Phys., 22, 43.

Head, A. K., Humble, P., Clarebrough, L. M., Morton, A. J., and Forwood, C. T. (1973), Computed Electron Micrographs and Defect Identification, Amelinckx, S., Gevers, R., and Nihoul, J., eds., North-Holland.

Hirsch, P. B., Howie, A., Nicholson, R. B., Pashley, D. W., and Whelan, M. J. (1965), Electron Microscopy of Thin Crystals, Butterworths.

Hirth, J. P., and Lothe, J. (1968), Theory of Dislocations, McGraw-Hill.

Hornbogen, G. (1967), Aluminum, 3, 163.

Hosford, W. F., and Agrawal, S. P. (1974), paper presented at the 6th Annual Spring Meeting of A.I.M.E., Pittsburgh, Pa.

Howie, A., and Whelan, M. J. (1961), Proc. Royal Soc. London, A263, 217.

Howie, A., and Whelan, M. J. (1962), Proc. Royal Soc. London, A267, 206.

Humble, P. (1968), Aust. J. Phys., 21, 325.

Kelly, A., and Nicholson, R. B. (1963), Progress in Materials Science, 3, Chalmers, B., ed., Pergamon Press, p. 149.

Laird, C., and Aaronson, H. I. (1968), Trans. AIME, 242, 1393.

Larché, F. C. (1974), chapter to be published in book by Nabarro, F.R.N.

Lorimer, G. W. (1968), paper presented at the Fourth European Regional Conference on Electron Microscopy, Rome, Italy.

Lorimer, G. W. (1970), Fizika, 2, Suppl. 2, p. 33.1.

Lorimer, G. W., and Nicholson, R. B. (1969), The Mechanism of Phase Transformations in Crystalline Solids, Inst. of Metals, p. 36.

Lothe, J. (1960), J. Appl. Phys., 31, 1077.

Lyubov, B. Y., and Solov'Yev, V. A. (1965), Fiz. Metal. Metalloved., 19, 333.

Marshall, G. W., and Brittain, J. O. (1974), paper presented at the 6th Annual Spring Meeting of A.I.M.E., Pittsburgh, Pa.

Miekk-oja, H. M., and Räty, R. (1971), Phil. Mag., 24, 1197.

Nes, E. (1974), Acta Met., 22, 81.

Nicholson, R. B. (1970), Phase Transformations, American Society for Metals, p. 269.

Nicholson, R. B., and Nutting, J. (1958), Phil. Mag., 3, 531.

Passoja, D. E., and Ansell, G. S. (1971), Acta Met., 19, 1253.

Perry, A. J. (1966), Acta Met., 14, 305.

Preston, G. D. (1938a), Nature, 142, 570.

Preston, G. D. (1938b), Proc. Royal Soc. London, A167, 526.

Preston, G. D. (1938c), Phil. Mag., 26, 855.

Ramírez, R. G., and Pound, G. M. (1973), Met. Trans., 4, 1563.

Reed-Hill, R. E. (1973), Physical Metallurgy Principles, Van Nostrand, p. 170.

Ravi, K. V. (1971), Met. Trans., 3, 1311.

Seidman, D. N., and Balluffi, R. W. (1968), Lattice Defects and Their Interactions, Hasiguti, R. R., ed., Gordon and Breach, p. 913.

Servi, I. S., and Turnbull, D. (1966), Acta Met., 14, 161.

Silcock, J. M., Heal, T. J., and Hardy, H. K. (1953-54), J. Inst. Metals, 82, 239.

Silcock, J. M., and Tunstall, W. J. (1964), Phil. Mag., 10, 361.

Simmons, R. O., and Balluffi, R. W. (1960), Phys. Review, 52, 117.

Thomas, G. (1959), Phil. Mag., 4, 1213.

Thomas, G., and Nutting, J. (1956), The Mechanism of Phase Transformations in Metals, Institute of Metals, p. 57.

Thomas, G., and Whelan, M. J. (1961), Phil. Mag., 6, 1103.

Thomson, R. M., and Balluffi, R. W. (1962), J. Appl. Phys., 33, 803.

Warren, J. B. (1974), Ph.D. research in progress.

Weatherly, G. C., and Nicholson, R. B. (1968), Phil. Mag., 17, 801.

Westmacott, K. H., Hull, D., and Barnes, R. S. (1959), Phil. Mag., 4, 1089.

Westmacott, K. H., Barnes, R. S., and Smallman, R. E. (1962), Phil. Mag., 7, 1585.

Whelan, M. J., and Hirsch, P. B. (1957), Phil. Mag., 2, 1121.

Wilsdorf, H., and Kuhlmann-Wilsdorf, D. (1955), Defects in Crystalline Solids, Physical Society, p. 175.

BIOGRAPHICAL SKETCH

Thomas Jeffrey Headley was born June 22, 1943, at Sheffield, Alabama. In June, 1961, he was graduated from Coffee High School, Florence, Alabama. In June, 1965, he was graduated from Virginia Polytechnic Institute with the degree of Bachelor of Science in Metallurgical Engineering. In June, 1967, he was graduated from Virginia Polytechnic Institute with the degree of Master of Science in Metallurgical Engineering. He worked, first as an Engineer, and then as an Associate Scientist for the Lockheed-Georgia Company, Marietta, Georgia, from July, 1967, to April, 1970. He entered graduate school at the University of Florida in April, 1970. Since that date, he has worked as a graduate research assistant in the Materials Science and Engineering Department while pursuing the degree of Doctor of Philosophy.

Thomas Jeffrey Headley is married to the former Lynn Lancaster Moore and is the father of two children. He is a member of the American Institute of Mining, Metallurgical, and Petroleum Engineers, the American Society for Metals, Alpha Sigma Mu, and the Society of Sigma Xi.

I certify that I have read this study and that in my opinion it conforms to acceptable standards of scholarly presentation and is fully adequate, in scope and quality, as a dissertation for the degree of Doctor of Philosophy.

John J. Hren, Chairman
Professor of Materials Science
and Engineering

I certify that I have read this study and that in my opinion it conforms to acceptable standards of scholarly presentation and is fully adequate, in scope and quality, as a dissertation for the degree of Doctor of Philosophy.

F. N. Rhines
Professor of Materials Science
and Engineering

I certify that I have read this study and that in my opinion it conforms to acceptable standards of scholarly presentation and is fully adequate, in scope and quality, as a dissertation for the degree of Doctor of Philosophy.

R. E. Reed-Hill
Professor of Materials Science
and Engineering

I certify that I have read this study and that in my opinion it conforms to acceptable standards of scholarly presentation and is fully adequate, in scope and quality, as a dissertation for the degree of Doctor of Philosophy.

R. T. DeHoff
Professor of Materials Science
and Engineering

I certify that I have read this study and that in my opinion it conforms to acceptable standards of scholarly presentation and is fully adequate, in scope and quality, as a dissertation for the degree of Doctor of Philosophy.

C. S. Hartley
Associate Professor of Materials Science and Engineering

I certify that I have read this study and that in my opinion it conforms to acceptable standards of scholarly presentation and is fully adequate, in scope and quality, as a dissertation for the degree of Doctor of Philosophy.

M. A. Eisenberg
Associate Professor of Engineering Science and Mechanics and Aerospace Engineering

This dissertation was submitted to the Graduate Faculty of the College of Engineering and to the Graduate Council, and was accepted as partial fulfillment of the requirements for the degree of Doctor of Philosophy.

August, 1974

Dean, College of Engineering

Dean, Graduate School